An investigation of cell turnover in the planarian epidermis

Dissertation
for the award of the degree
“Doctor of Philosophy”
Division of Mathematics and Natural Sciences
of the Georg-August-Universität Göttingen

within the doctoral program *(Genes in Development, Disease and Evolution)*
of the Georg-August University School of Science (GAUSS)

submitted by

Jun-Ru Lee

from Taiwan
Göttingen 2023

Thesis Advisory Committee:

Prof. Dr. Jochen Rink, Department of Tissue Dynamics and Regeneration, Max Planck Institute for Multidisciplinary Sciences

Prof. Dr. Ernst Wimmer, Department of Developmental Biology, Georg-August-University Göttingen

Prof. Dr. Herbert Jäckle, Department of Molecular Developmental Biology, Max Planck Institute for Multidisciplinary Sciences

Members of the Examination Board:

Referee: Prof. Dr. Jochen Rink, Department of Tissue Dynamics and Regeneration, Max Planck Institute for Multidisciplinary Sciences

2nd Referee: Prof. Dr. Ernst Wimmer, Department of Developmental Biology, Georg-August-University Göttingen

Further members of the Examination Board:

Prof. Dr. Herbert Jäckle, Department of Molecular Developmental Biology, Max Planck Institute for Multidisciplinary Sciences

Prof. Dr. Daniel Jackson, Department of Geobiology, Georg-August-University Göttingen

Dr. Peter Lénárt, Research Group Cytoskeletal Dynamics in Oocytes, Max Planck Institute for Multidisciplinary Sciences

Dr. Gerd Vorbrüggen, Research Group Molecular Cell Dynamics, Max Planck Institute for Multidisciplinary Sciences

Date of oral examination: 27.02.2024

Abstract

Cell turnover is an important biological process for maintaining tissue homeostasis. During cell turnover, newly generated cells replace unwanted cells to balance the number of cells and ensure the functionality of a tissue. Failure of cell turnover can lead to physiological complications. Therefore, it is of high interest to understand the mechanistic basis of cell turnover. Planarian flatworms, with their unique biology, can serve as a model to study cell turnover: Planarians undergo cell turnover on an organismal scale, continuously replacing all cells throughout their lifetime. In this process, adult pluripotent stem cells serve as the only source for generating new cells. Third, their flexible body size contributes to the dynamic maintenance of tissue homeostasis. Despite the interesting biology of planarian cell turnover, our knowledge of this process is limited due to the limited tools available.

To deepen our knowledge about this process, I developed two imaging assays to investigate cell turnover in planarians. In Chapter 2, I established a pulse-chase dye labeling assay to quantify the turnover rate of epidermal cells. The results show that the ventral epidermis is a very dynamic tissue with a half-life of 4.5 days. Interestingly, differences in turnover rates were observed between dorsal and ventral epidermis and between anterior and posterior epidermis. In Chapter 4, I developed a live imaging protocol to directly observe cell removal in the planarian epidermis. The results show that epidermal cells were eliminated by basal extrusion and entered the interior of the animal. In this process, basally extruded epidermal cells relocated to the intestine.

In summary, the imaging assays developed in this thesis allow for the quantification of the epidermal cell turnover rate and observation of the elimination of these cells. The findings show that cell turnover in the planarian epidermis involves basal extrusion and subsequent

intestinal digestion, suggesting that extruded epidermal cells are recycled as an energy resource.

Table of Contents

List of Figures and Tables

Chapter 1: Introduction

1.1 Cell turnover in the biological system

In multicellular organisms, maintaining a balance of cell numbers is essential for proper tissue function. Aging or unwanted cells in tissues are replaced by newly differentiated cells derived from stem cells, a process called cell turnover, in which cell proliferation, cell differentiation and cell death are coordinated to maintain tissues in a homeotic state (Banjac et al., 2023; Pellettieri & Alvarado, 2007). Dysregulation of any of these processes leads to physiological defects in the tissue. For example, excessive stem cell proliferation or failure of cell death leads to the overcrowding of the tissue and accumulation of unfit cells. On the other hand, excessive cell death or insufficient supply of new cells from stem cells can lead to a shortage of differentiated cells. Therefore, it is important understand the mechanisms that regulate cell turnover during tissue homeostasis. In many animals, some tissues, such as the gastrointestinal epithelia and skin, are frequently renewed. It is estimated that about $4.0*10^{11}$ gastrointestinal epithelial cells and $3.3*10^{9}$ skin cells are replaced daily in humans (Sender & Milo, 2021) and they are therefore popular models to study cell turnover (Bianconi et al., 2013). In this section, I will discuss examples from different biological systems to illustrate how cell turnover maintains tissue homeostasis including the epithelial tissues and the hematopoietic tissue.

1.1.1 Tissue turnover in different biological systems

Skin and intestinal epithelial tissues form barriers between internal organs and the external environment (Arwert et al., 2012) and they have long been models for studying tissue turnover due to their rapid turnover rate resulting from constant external chemical

or physical stimuli from the outside (Bianconi et al., 2013). In skin tissue, epidermal stem cells, located in the deeper layer undergo asymmetric division and produce one daughter cell whose fate is committed and one daughter stem cell (Lechler & Fuchs, 2005) **(Figure 1)**. The committed epidermal cells then migrate outward, pass through various tissue layers and eventually integrate into the outermost layer to replace old cells that were previously shed outward (Dai & Segre, 2004; Watt, 1998). Similarly, in the intestinal epithelium, old intestinal cells undergo apoptosis and are extruded at the tip of a villus (Hall et al., 1994; Potten, 1992, 1997). At the same time, stem cells residing in a crypt proliferate and become transit amplifying cells that migrate toward the villus and give rise to mature cells (Barker, 2014; Beumer & Clevers, 2021; Crosnier et al., 2006; Marshman et al., 2002) **(Figure 2)**. Therefore, the cell loss in the villus is compensated by new cells from the crypt. Both the epithelial tissues in skin and intestine serve as examples of how cell turnover maintains tissue homeostasis.

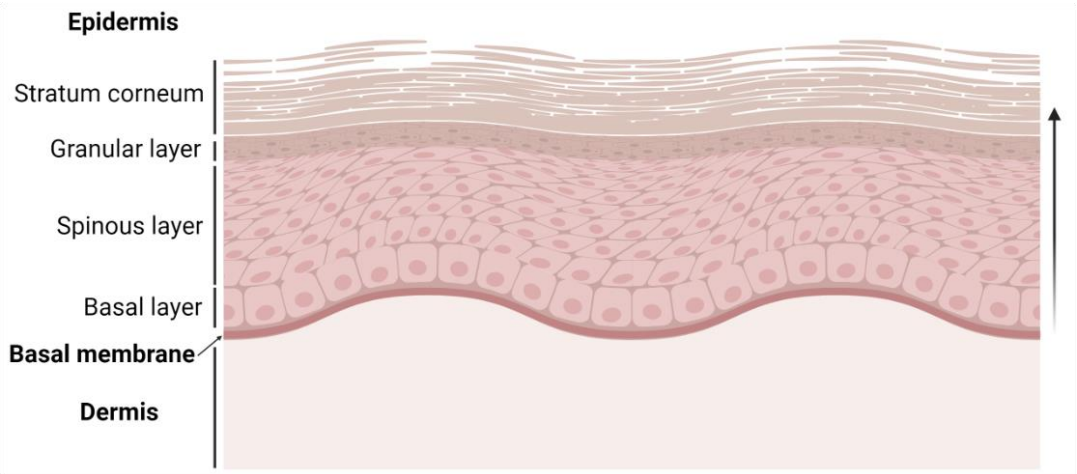

Figure 1. Cell turnover and anatomy of skin tissue.

The Skin consists of epidermis and dermis, that are separated by the basal membrane. The epidermis consists of the basal layer, spinous layer, granular layer, and stratum corneum (from basal to apical). The arrow on the right indicates the direction of migration of newly generated cells in the basal layer. The epidermal cell progenitors pass through the different layers and become mature epidermis in the stratum corneum. This figure was Created with BioRender.com.

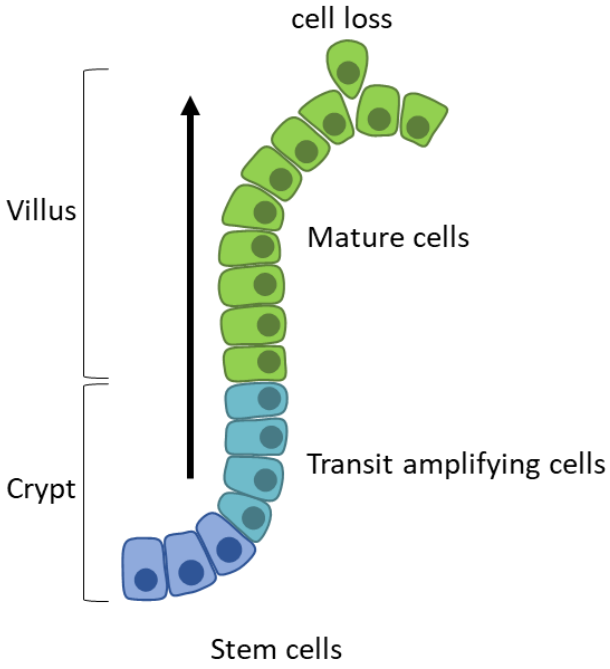

Figure 2. Cell turnover in the intestinal epithelium.

The intestinal epithelial tissue contains the crypt protruding toward the luminal side and villus invaginating into connective tissues. Stem cells in the crypt generate transit amplifying cells, which then migrate toward the villus to differentiate into mature epithelial cells. Old cells are extruded apically and shed into the lumen. The arrow indicates the direction of new cell migration.

In addition to the epithelial tissues of the skin and intestines, hematopoietic tissues also undergo constant cell turnover. Hematopoietic cells comprise several cell types that are responsible for many important physiological functions. Hematopoietic stem cells located in the bone marrow are multipotent (Bonnet, 2002). They can self-renew and produce new cells that give rise to all blood cells to compensate for the loss of short-lived hematopoietic cells. The dead or damaged hematopoietic cells circulating in the body are then eliminated by immune cells (Borges & Sesti-Costa, 2022). In summary, the generation of new cells, the removal of old or damaged cells and the clearance of dead cell bodies work together to maintain the dynamic balance in hematopoietic tissue.

Cell turnover is not only necessary to maintain the homeostatic state of tissues, but

it is also important for animal development. For example, cell replacement is required during metamorphosis in *Drosophila*. During metamorphosis, larval epidermal cells in the abdomen must be replaced by adult epidermal cells (Nakajima et al., 2011; Ninov et al., 2007). During this replacement, the death of larval epidermal cells and the generation of adult epidermal cells from progenitor cells must be coordinated. Larval epidermal cells first migrate dorsally and undergo apoptosis, followed by the delamination in the animals (Bischoff, 2012). Simultaneously, adult epidermal cells migrate towards the ventral midline and close the gap. Blocking larval epidermal cell apoptosis resulted in the accumulation of larval epidermal cells at the ventral midline and the failure of ventral closure (Ninov et al., 2007). Similar phenomena have also been observed during dorsal closure in *Drosophila* embryos. During dorsal closure, the leading edges of lateral cells migrate toward the dorsal midline and undergo zipping to close the gap previously occupied by extraembryonic tissue (amnioserosa) (Kiehart et al., 2000; Peralta et al., 2007). Amnioserosa cells undergo apoptosis and delamination during the closure of the dorsal epidermis. Blocking apoptosis in amnioserosa cells caused dorsal closure defects (Toyama et al., 2008), indicating that the removal of amnioserosa cells is important for dorsal closure. Furthermore, unlike skin and intestinal epithelial tissues, where epithelia are eliminated by shedding to outside, cells in the amnioserosa and abdomen migrate inward in *Drosophila*. These cells are then scavenged by circulating hemocytes (Ninov et al., 2007). In summary, the death of old cells, the clearance of dead cells, their clearance, and the migration and generation of new cells are critical steps during animal development

1.1.2 Tissue turnover and diseases

Defects in maintaining tissue homeostasis have long been thought to be associated with disease. Firstly, stem cell incapacity leads to an inadequate supply of new cells,

affecting the functions of specific tissues. The most common way in which stem cells become less capable is through stem cell aging (Goodell & Rando, 2015). For example, stem cell aging in skin cells leads to skin atrophy and hair loss (Liu et al., 2022). Furthermore, aging of intestinal stem cells leads to reduced regenerative capacity and changes in intestinal structure (Jasper, 2020). Second, aberrant stem cell proliferation or defects in cell death can lead to cancer. For example, mutations in p53, a damage-sensor gene, have been found in many cancer cells (Junttila & Evan, 2009; Labi & Erlacher, 2015). These cells can escape apoptosis in the presence of DNA damage and become malignant. In addition, stem cell hyperactivity is another way in which cancer can develop. For example, when cells receive excessive growth factors, downstream signaling pathways can be over-activated, leading to hyperactive proliferation and cancer formation (Hanahan & Weinberg, 2011). Third, the inability to eliminate dead cells is associated with autoimmune diseases. For example, systemic lupus erythematosus is an autoimmune disease that results from inefficient clearance of dead cells by macrophages (Nagata et al., 2010). DNA and cell corpses can be found in patients, leading to the appearance of autoantibodies that can attack their own tissues (Rumore & Steinman, 1990). In summary, the maintenance of cell turnover is critical for physiological functions in animals.

1.1.3 Summary

Cell turnover is important for maintaining tissue homeostasis in both adult and developing animals. During cell replacement, the generation of new cells, the proliferation of stem cells and the loss of unwanted cells must be perfectly coordinated to balance the number cells in the system. Failure in any of these processes can have physiological or developmental consequences: If the eliminated cells remain in the system, such as the cases in hematopoietic tissue and in animals undergoing metamorphosis, clearance mechanisms are required to recycle dead cells. In the

following section, I will focus on the how cell death is regulated during cell turnover and how dead cells are removed during tissue homeostasis.

1.2 Cell removal mechanisms during tissue homeostasis

1.2.1 Cell death

Several forms of cell death have been identified, including autophagic cell death, necrosis and apoptosis. Autophagic cell death is mediated by the formation of autophagosomes, a double-membrane structure used for degrading intracellular contents, in dying cells (Jung et al., 2020). It has been shown to be required for the regression of salivary glands during *Drosophila* metamorphosis (Baehrecke, 2003; Berry & Baehrecke, 2007). Necrosis occurs when cells are exposed to extreme conditions, resulting in the disruption of cell integrity and the leakage of cytoplasm outside the cell (Green & Llambi, 2015). Finally, apoptosis, also known as programmed cell death, is the best characterized form of cell death. Apoptosis is an important mechanism in both tissue homeostasis and animal development. One of the classic examples was observed in *C. elegans*, where the term "programmed cell death" originated from the observation of cell death in somatic cells during *C. elegans* development (Horvitz, 1999). During apoptosis, cell shrinkage, membrane blebbing, nuclear condensation, and DNA fragmentation occur, followed by the formation of apoptotic bodies consisting of packed organelles and DNA fragments with an intact cell membrane (Kerr et al., 1972).

1.2.2 Initiation and regulation of apoptosis

In general, there are two pathways that initiate apoptosis in cells: the extrinsic pathway and the intrinsic pathway (Elmore, 2007) **(Figure 3)**. The extrinsic pathway is initiated by the binding of death ligands from the extracellular matrix to death receptors, such as tumor necrosis factor (TNF), on the cell membrane (Locksley et al., 2001). The cytoplasmic domains of the death receptors then recruit adaptor proteins, such as FADD

and TRADD, which contain death domains. Subsequently, the adaptor proteins associate with procaspase-8 to form the death-inducing signaling complex (Kischkel et al., 1995). The intrinsic pathway, also known as the mitochondrial pathway, is mainly driven by intrinsic factors, such as DNA damage, ER stress and replication stress (Galluzzi et al., 2018). This involves the activation of pro-apoptotic proteins, such as BAX and BAK, which create pores in the mitochondrial membranes and lead to a change in mitochondrial permeability, followed by the release of cytochrome C into the cytoplasm (Dewson & Kluck, 2009; Peña-Blanco & García-Sáez, 2018). Cytochrome C then binds to Apaf-1 and procaspase-9, forming apoptosomes that trigger the downstream caspase cascade (Chinnaiyan, 1999; Saelens et al., 2004). For both the extrinsic and intrinsic pathways, activation of the caspase cascades is the final step in the execution of downstream proteolytic reactions (Slee et al., 2001).

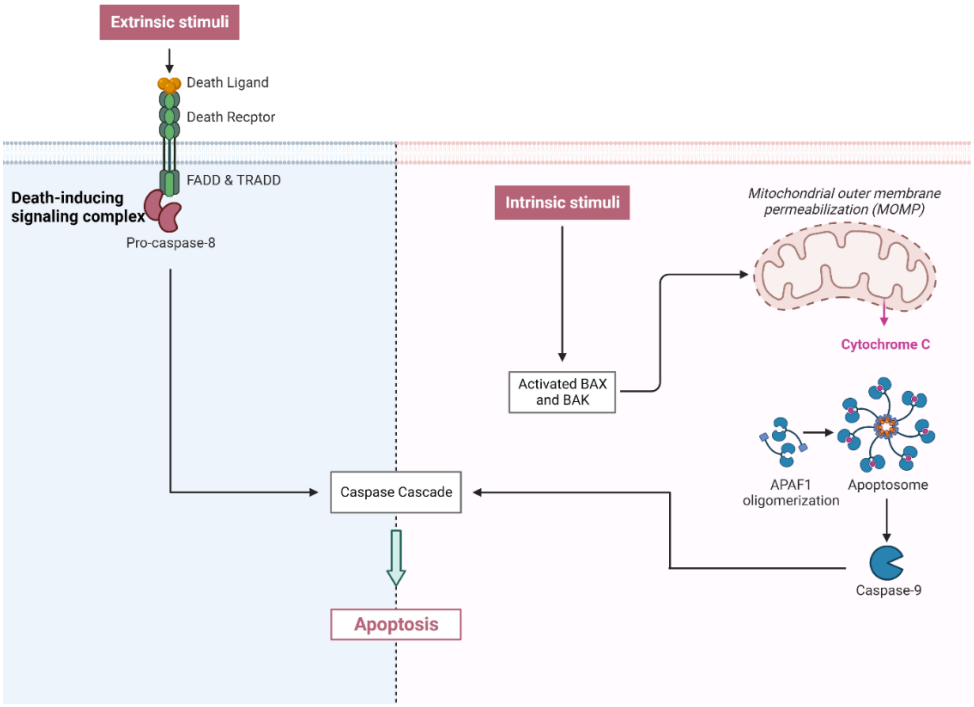

Figure 3. The extrinsic and intrinsic pathways of apoptosis.

The extrinsic pathway (left) is initiated when death ligands bind to death receptors. The formation of the death-inducing signaling complex triggers the caspase cascade and executes apoptosis. The intrinsic pathway (right) is triggered by internal stimuli. The pro-apoptotic proteins are activated and cause the transfer of cytochrome C from the mitochondria to the cytoplasm. Cytochrome C then forms the apoptosomes with APAF-1 and initiates the downstream caspase cascade. This figure was created with BioRender.com.

1.2.3 Ways of cell removal in tissue homeostasis

How dying cells are removed from the tissue is an interesting question and has been well studied in epithelial tissues. Epithelial tissues form the boundary between the external environment and the internal tissues. Due to the constant external stimuli, epithelial tissues have a high turnover rate compared to other tissues. To maintain the barrier function of epithelia, it is important to maintain their integrity. Therefore, epithelial cells undergo a process called extrusion, in which the extruded cells are squeezed out by neighboring cells to fill the gaps left by exiting cells (Rosenblatt et al., 2001). Previous studies by the Rosenblatt group have identified the cellular and molecular

mechanisms of cell extrusion: First, an epithelial cell undergoing apoptosis releases Sphingosine 1 Phosphate (S1P) and the G protein-coupled receptor Sphingosine-1-Phosphate Receptor 2 ($S1P_2$) in neighboring cells senses the ligands. Ligand binding activates the small GTPase, Rho, which in turns causes the formation of actomyosin rings in the neighboring cells (Gu et al., 2011; Gudipaty & Rosenblatt, 2017; Slattum et al., 2009). Subsequent contraction of the actomyosin ring squeezes out the apoptotic cell and seals the gap between the neighboring cells (Gu et al., 2011). Failure of cell extrusion causes cell mass formation in epithelial tissues (Eisenhoffer et al., 2012).

1.2.4 Direction of epithelial cell extrusion

Based on the direction of cell extrusion, cell extrusion can be divided into two modes: apical extrusion and basal extrusion **(Figure 4)**. In apical extrusion, cells are extruded toward the apical direction and enter the extracellular lumen or exit the organism. Most adult epithelial tissues perform this process to prevent extruded cells from entering the interior of the animal. For example, in intestinal epithelia, cells are extruded apically in intestinal epithelia and enter the intestinal lumen (Potten, 1992, 1997). In contrast, basal extrusion occurs when epidermal cells are extruded toward the basal membrane, mainly during embryonic development or metamorphosis. For example, epithelial cells in the *Drosophila* imaginal disc, notum and larval epidermal cells undergo basal extrusion (Ninov et al., 2007; Pastor-Pareja et al., 2004; Toyama et al., 2008). In addition, basal extrusion is also involved in some pathological contexts. For example, mutation of the tumor suppressor gene, adenomatous polyposis coli (APC), disrupts cytoskeletal dynamics, which in turn leads to a change in the direction of cell extrusion toward the basal membrane (Marshall et al., 2011). Similarly, expression of oncogenic K-Ras induced basal extrusion and basally extruded cells were able to invade other tissues (Slattum et al., 2014; Slattum & Rosenblatt, 2014).

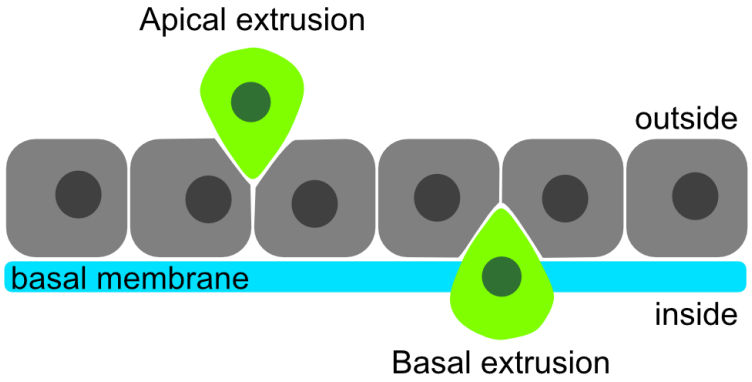

Figure 4. Two modes of cell extrusion in epithelial cells.

The first mode is apical extrusion. The unwanted cell is extruded apically by the surrounding cells and falls into the lumen or the outside environment. The second mode is basal extrusion, where the unwanted cell is extruded basally and migrates toward the basement membrane.

1.2.5 Upstream control of epithelial cell extrusion

There are two main stimuli for cell extrusion. The first are apoptotic signals. Damaged or unsuitable cells undergo apoptosis and the apoptotic signals then generate the S1P and activate the S1P-$S1P_2$-Rho signaling pathway to extrude the apoptotic cells (Andrade & Rosenblatt, 2011; Gu et al., 2011). Blocking apoptotic signals led to the failure of apoptotic cell extrusion (Andrade & Rosenblatt, 2011). The second stimulus is mechanical strain. Previous studies have found that crowding induced cell extrusion in different models such as *Drosophila*, zebrafish, and epithelial tissue culture (Eisenhoffer et al., 2012; Eisenhoffer & Rosenblatt, 2013; Marinari et al., 2012). In contrast to apoptotic cell extrusion, cells are extruded while still alive and then die. Piezo-1, an ion channel protein, acts as a stretch sensor. Crowding activates Piezo-1, which subsequently triggers the activation of the downstream S1P-$S1P_2$-Rho signaling pathway and executes cell extrusion (Eisenhoffer et al., 2012). Both stimuli help to maintain the epithelial cell numbers by eliminating the unwanted cells or cells in the crowded area.

1.3 Clearance of dead cells during tissue turnover

1.3.1 Cellular mechanisms

When dead cells remain in the body, which is the case in most situations except for cell loss in the skin tissue or apical extrusion in epithelia, it is crucial to remove them in a timely manner. Failure to clear dead cells from the body is associated with some diseases, such as autoimmune diseases (Hanayama et al., 2004; Nagata et al., 2010). Previous studies have identified the mechanisms of dead cell clearance by immune cells. Apoptotic cells release “find me” signals, including nucleotides, the chemokine fractalkine, and lipids, to attract nearby phagocytes. Phagocytes then engulf the dead cells depending on the recognition of the “eat me” signals (Arandjelovic & Ravichandran, 2015). The lipid phosphatidylserine (PtdSer) is the best characterized “eat me” signal. Exposure of PtdSer in the outer leaflet of the plasma membrane of apoptotic cells is recognized by engulfment receptors present in the phagocyte membrane (Fadok et al., 1992). Subsequently, downstream signaling is activated to induce actin polymerization, which facilitates phagocytosis (Park et al., 2007). Following phagocytosis, phagosomes are formed within cells. Phagosomes mature via progressive membrane remodeling (Hochreiter-Hufford & Ravichandran, 2013; Kinchen & Ravichandran, 2008). During the maturation process, the pH value inside phagosomes gradually decreases. Finally, phagosomes fuse with lysosomes to degrade the apoptotic cells. The process of clearance of apoptotic cells is shown in **(Figure 5)**.

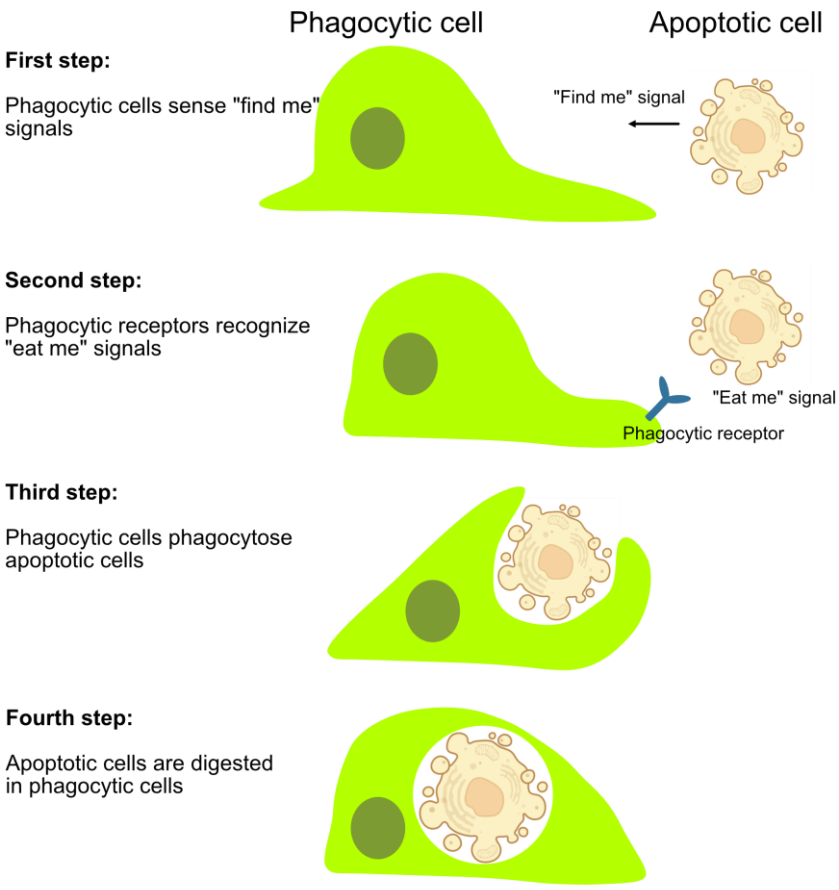

Figure 5. Illustration of how a phagocytic cell clears an apoptotic cell.

First, the apoptotic cell releases “find me” signals to attract phagocytic cells. Second, the apoptotic cell displays “eat me” signals such as phosphatidylserine (PtdSer) on the plasma membrane and the phagocytic cell detects the signals via its receptor. Third, the phagocytic cell undergoes phagocytosis and engulfs the apoptotic cells. Finally, the engulfed cell is digested in the phagocytic cell. The figures were created with BioRender.com and modified from (Hochreiter-Hufford & Ravichandran, 2013).

1.3.2 Examples of dead cell clearance

Previous studies have identified several types of phagocytes responsible for removing of dead cells in different organs. For example, Kupffer cells in the liver are able to remove old erythrocytes (Dini et al., 2002) and alveolar macrophages remove the apoptotic cells in the lung (Monks et al., 2005). In addition to specialized phagocytes, some studies have identified several non-phagocytes cells that are also able to phagocytose dead cells in the tissues. This often happens in tissues where there are not

enough phagocytes nearby. For example, the zebrafish surface epithelial cells are able to phagocytose dead epithelial cells during embryonic development (Hoijman et al., 2021), and hepatocytes have also been found to engulf apoptotic cells in the liver (Dini et al., 2002). Another study in zebrafishes showed that dead cells are removed by migrating neural crest cells during neural development (Zhu et al., 2019). In summary, different mechanism have evolved for the clearance of dead cells and cell clearance is important to maintain tissue homeostasis in both developmental and adult stages.

1.4 Planarian flatworms

As described in previous sections, cell turnover relies on the successful coordination of cell proliferation, cell elimination and clearance of dead cells. I would like to focus on the mechanistic underpinnings of cell turnover in my thesis and I chose planarian flatworms as the animal model because of their unique biology in cell turnover which will be introduced in the following sections.

1.4.1 General information

Planarians are flatworms belonging to the phylum Platyhelminthes, order Tricladida. Planarians have flattened bodies that are bilaterally symmetrical. Despite the relatively simple body structure, planarians are thought to have tissues derived of the three germ layers, including neurons, muscles and intestines (Agata et al., 1998; Elliott & Sanchez Alvarado, 2013; Ivankovic et al., 2019; Reddien & Alvarado, 2004; Saló, 2006). The name Tricladida ("tri-" = three; "clad" = branch) derives from the three intestinal branches, with one located in the anterior and two in the posterior (Forsthoefel et al., 2011; Orii et al., 2002) **(Figure 6A)**. The pharynx, which is responsible for ingestion and defecation, is the only connection for the blind-ended intestinal tracts to the outside **(Figure 6A)**. Apart from the digestive system, planarians have a nervous system with a brain and a pair of eyes in the anterior and two ventral nerve chords along the body (Agata et al., 1998) **(Figure 6B)**. The rudimentary eyes contain photoreceptors with axons projecting to the brain (Agata et al., 1998; Okamoto et al., 2005). The planarian excretory system is comprised of protonephridia that are responsible for regulating osmolarity and removing wastes, which are functionally similar to the vertebrate kidneys (King & Newmark, 2013; Rink et al., 2011; Vu et al., 2015) **(Figure 6C)**. On the surface of theses worms is covered by an epidermis. The epidermis consists of different types of epithelial cells, including

multiciliated cells that are used for locomotion and small numbers of sensory or secretory cells (McGee et al., 1997; Pedersen, 1976; Rompolas et al., 2010) **(Figure 7)**. Furthermore, planarians are acoelomates, which means that they do not have body cavities for the visceral organs. Between the body wall surface and the intestine lies the loosely connected cell mass of the mesenchymal tissue **(Figure 8A)**. Within the mesenchyme, the pluripotent stem cells, known as neoblasts, are widely distributed except in the pharynx and anterior tip of animals (Orii et al., 2005) **(Figure 8B)**.

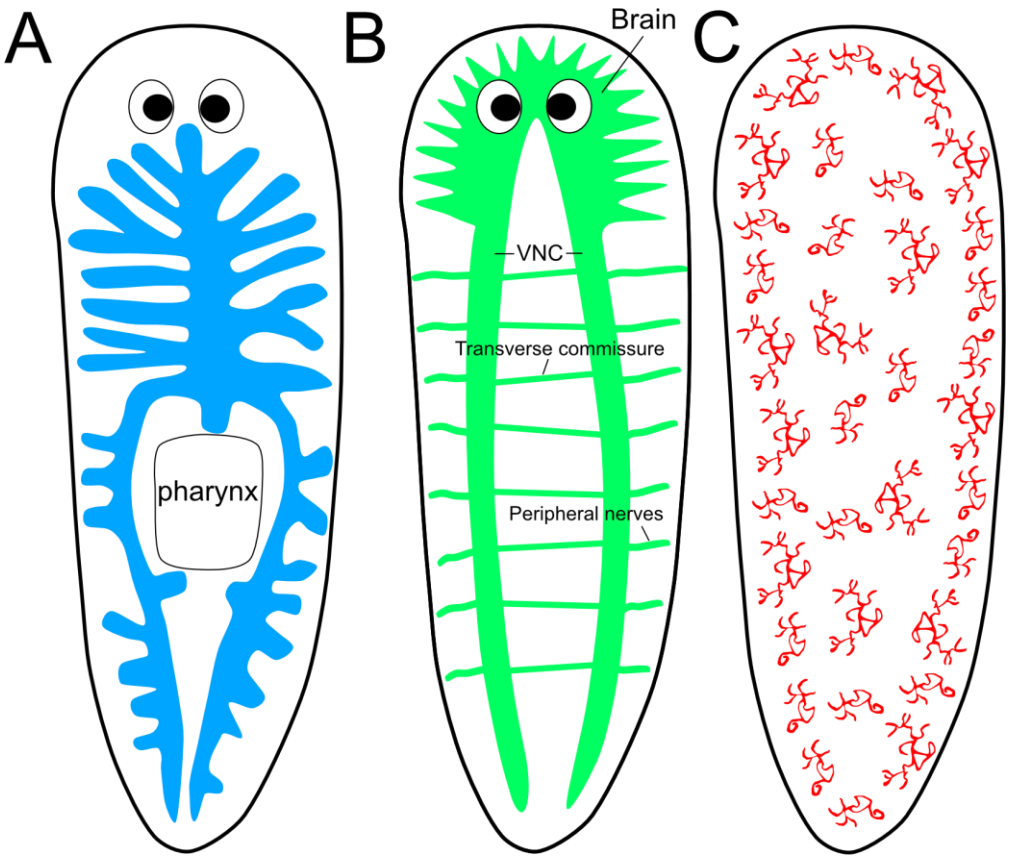

Figure 6. Anatomy of planarians.

(A) The digestive system of a planarian. The blue color shows the intestine with one anterior branch and two posterior branches. The pharynx is located between the two posterior branches. (B) The nervous system of a planarian includes central nervous system and peripheral nerve net. The central nervous system consists of a bilobed brain, a pair of eyes in the head and a pair of ventral nerve chords (VNC). (C) Protonephridia (red) are widely distributed in planarians and are responsible for osmoregulation and waste

removal. This figure was modified from (Vu et al., 2015).

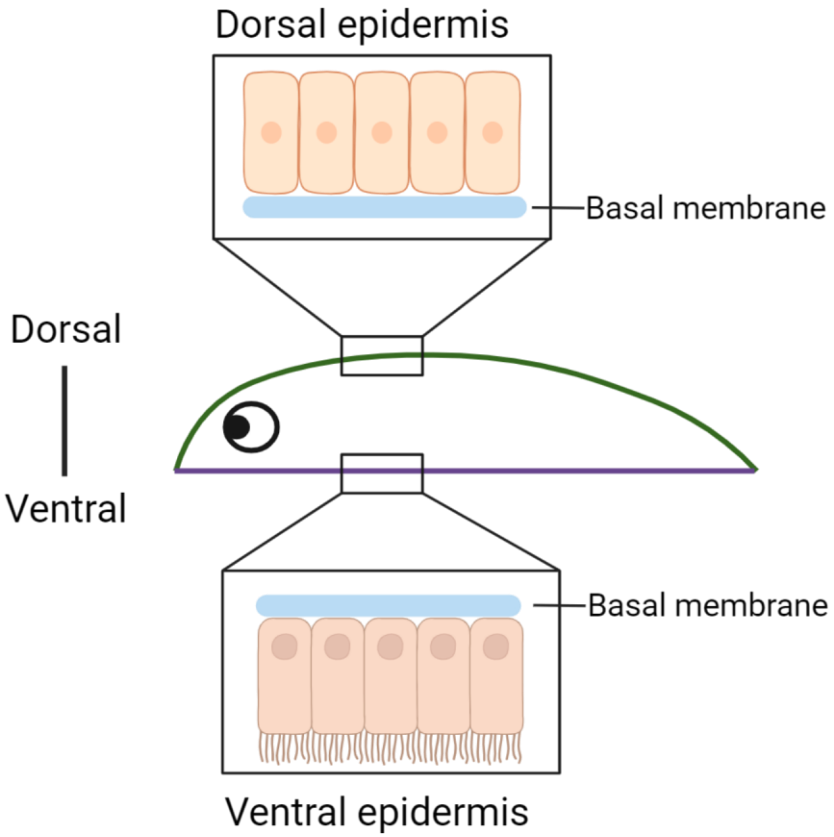

Figure 7. Anatomy of the planarian epidermis.

The planarian epidermis is comprised of columnar cells, which on the ventral surface are densely ciliated and responsible for the gliding motility of planarians. The dorsal epidermal cells are less densely ciliated and interspersed with the projections of sensory neurons at the dorsal midline.

The figure was created with BioRender.com.

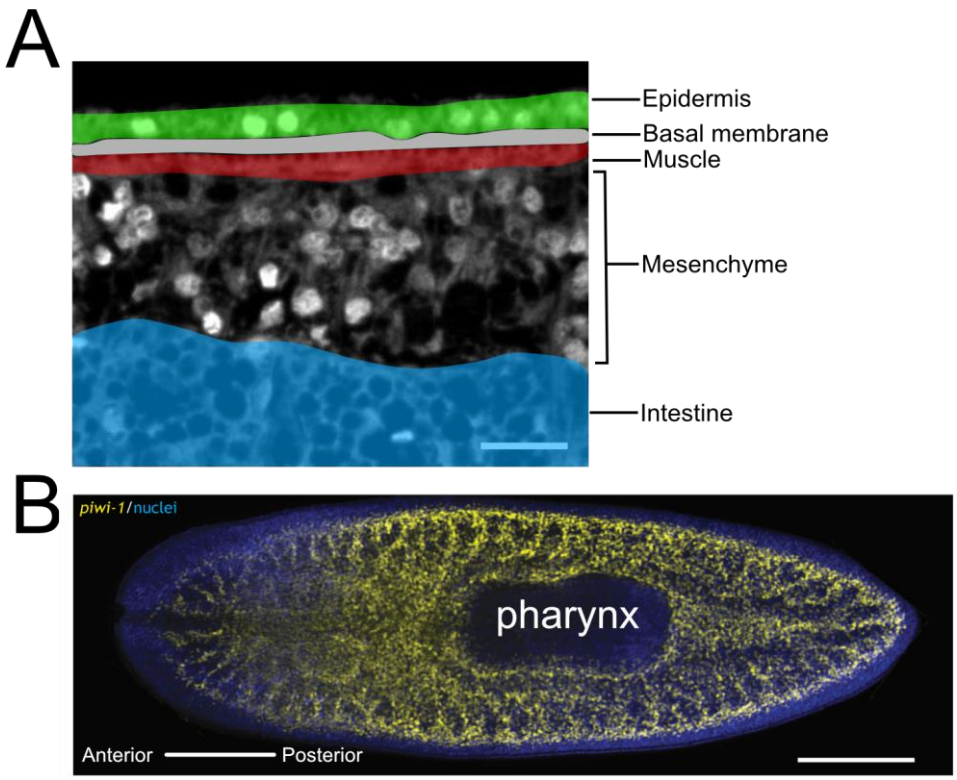

Figure 8. A sagittal section of the internal structures of a planarian and the distribution of neoblasts. (A) A DAPI-labeled sagittal section image. The structures from outside to inside are as follows: epidermis, basal membrane, body wall muscles, mesenchyme and intestine. The loosely populated mesenchymal tissue is located between the intestine and the body wall muscle layer. Scale bar: 20 µm (sample courtesy of Maria Ina Moroni) (B) *in situ* hybridization of the neoblast marker gene, *piwi-1*. Neoblasts are widely distributed in a planarian, with the exception of the pharynx and in the anterior tip end. Scale bar: 500 µm. The nuclei were visualized using DAPI staining. This image was adapted from (Ivankovic et al., 2019).

1.4.2 Unique biology of planarians

Masters of regeneration

Planarians are known for their remarkable regenerative ability. T. H. Morgan's experiments more than 120 years ago demonstrated that when a planarian was cut into several pieces, each fragment could regenerate into a fully functional organism (Morgan, 1898). In recent decades, some planarian species, such as *Schmidtea mediterranea* and *Dugesia japonica* (Agata & Watanabe, 1999; Reddien & Alvarado, 2004), have emerged

as the model organisms for regeneration studies. Studies have shown that adult pluripotent stem cells (neoblasts) play a crucial role in the planarian regeneration (Baguñà, 2012). Increased proliferation of neoblasts was observed within 6 hours of amputation (Wenemoser & Reddien, 2010), followed by the accumulation of neoblasts and their progeny near the wound. A blastema, an unpigmented structure, formed 2 to 3 days after amputation and gave rise to the missing body parts (Reddien & Alvarado, 2004).

Flexible body size

Unlike many animals that reach a fixed adult body size, adult planarians maintain a flexible body size depending on nutritional status (Baguna et al., 1990; Thommen et al., 2019) **(Figure 9)**. Planarians grow when food is abundant and gradually shrink when food is scarce. Previous observations have shown that changes in cell number account for variations in body size (Baguna & Romero, 1981; Thommen et al., 2019). In the model organism *Schmidtea mediterrannea*, body length ranges from 2 mm to 20 mm and total cell number ranges from a minimum of 7000 cells to a maximum of 7 million cells (Thommen et al., 2019). Therefore, cell proliferation and cell loss must play an important role during growth and degrowth. Theoretically, cell proliferation should increase and cell death should decrease during growth, and the opposite scenario should apply during degrowth. Previous observations have shown a dramatic increase in the number of mitotic cells 24 hours after feeding by detecting phosphorylated histone H3 (H3P), a marker of cells in metaphase (Gonzalez-Estevez et al., 2012). The level of cell proliferation remains constant during starvation (Gonzalez-Estevez et al., 2012). On the other hand, the question of whether cell death is modulated during growth and degrowth is still inconclusive due to a lack of suitable assays.

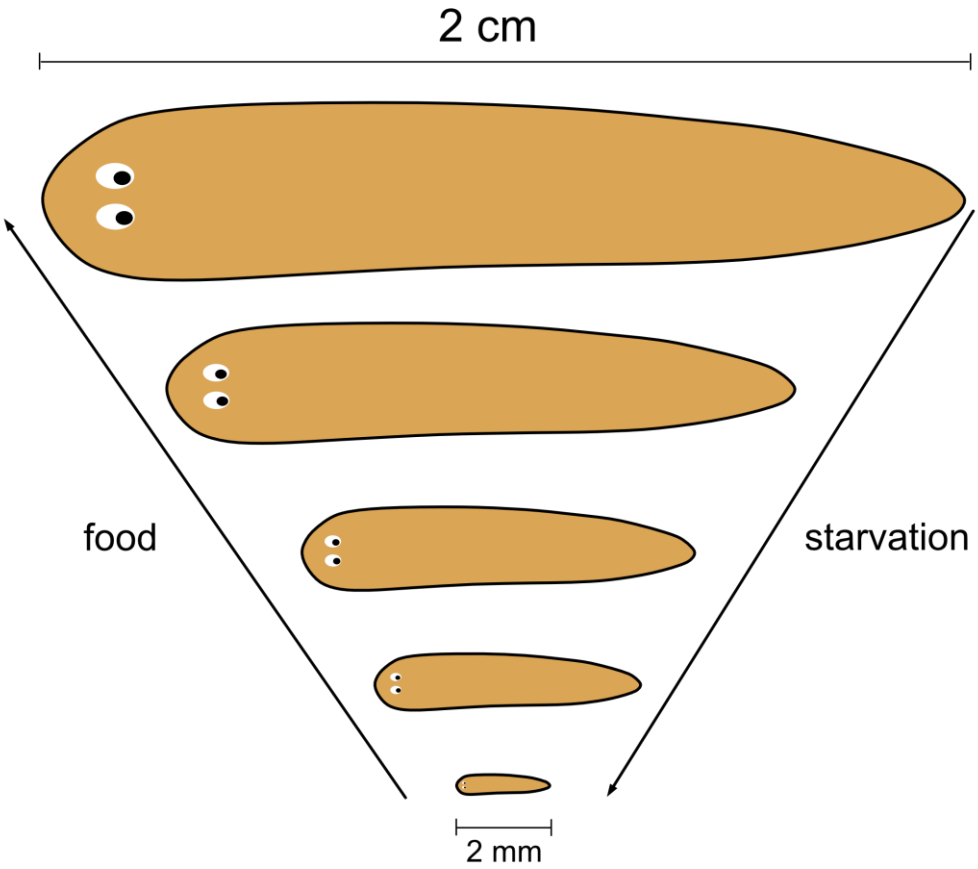

Figure 9. Flexible body size of the planarian *Schmidtea mediterranea*.

The size of the planarian increases after feeding and decreases during starvation. Lengths range from approximately 2 mm to 2 cm. This figure is adapted from (Thommen et al., 2019).

Unique system for cell turnover

The planarian is a unique model for studying cell turnover for several reasons. First, unlike the tissue-specific stem cell system in vertebrates, planarians have pluripotent stem cells called neoblasts that are widely distributed in the mesenchymal tissues of the body (Baguna, 2012; Ivankovic et al., 2019; Newmark & Alvarado, 2000; Orii et al., 2005) and these cells are capable of giving rise to all cell types in planarians (Baguna et al., 1989; Wagner et al., 2011). The progeny of neoblasts migrate and differentiate into specialized mature cells (Adler et al., 2014; Eisenhoffer et al., 2008; Tu et al., 2015). Second, cell

turnover occurs on an organismal scale in planarians. Ablation of neoblasts by irradiation resulted in a rapid cessation of cell division within 24 hours and progressive regression of planarians (Bardeen & Baetjer, 1904; Eisenhoffer et al., 2008; Reddien, Bermange, et al., 2005; Wolff & Dubois, 1947). In addition, transplantation of a single donor neoblast into an irradiated host with ablated neoblasts showed that the donor neoblast gradually colonized the host (Wagner et al., 2011), indicating that neoblasts are capable of giving rise to all cell types in planarians. From the irradiation and single cell transplantation experiments, it can be concluded that all tissues are continuously replaced by the newly generated cells from neoblasts. Lastly, due to the flexible body size of planarians, there is no steady state for tissue homeostasis during its lifetime, indicating that the total cell number is constantly changing. It can therefore serve as a unique platform to study how cell proliferation and cell death are coordinated in such a dynamic system. These three biological features make planarians a fascinating model for studying cell turnover.

1.4.3 Cell turnover in planarians

Generation and differentiation of neoblast progeny

In planarians, all dividing cells express the *piwi-1* gene, encoding a protein belonging to the Argonaute protein family (Carmell et al., 2007; Cox et al., 1998) and neoblasts are believed to be the only cell types outside the germ line that are capable of undergoing proliferation (Baguna et al., 1989; Newmark & Alvarado, 2000; Reddien & Alvarado, 2004). The *piwi-1*$^{+}$ cells constitute a heterogeneous cell population with distinct gene expression signatures (Fincher et al., 2018; Raz et al., 2021; van Wolfswinkel et al., 2014; Zeng et al., 2018). Among these neoblasts, some are specialized and contribute to the generation of different cell types. Currently, two models are proposed for the lineage specification of neoblasts. The first is the hierarchical model. This model proposes that specialized

neoblasts are derived from “truly pluripotent” neoblasts, and that specialized neoblasts are fate determined and cannot transform into other lineages (Zeng et al., 2018). The other hypothesis is the non-hierarchical model. This model proposes that specialized neoblasts can transition to another lineage when they enter the next cell cycle (Pearson, 2022; Raz et al., 2021). It is important to note that these hypotheses are based on indirect evidence due to the current limitations of lineage tracing techniques, e.g. the lack of genetic labeling tools, in planarians.

The maturation process of progenitors has been identified in some specific tissues of planarians. Among these, the maturation process of the epidermal lineage has been best characterized, with zeta-neoblasts expressing the zinc finger protein (zfp-1) identified as epidermal progenitors (van Wolfswinkel et al., 2014). An epidermal progenitor located deep in the mesenchyme undergoes differentiation and migrates to the surface of planarians **(Figure 10)**. During differentiation, an epidermal progenitor passes through early and late stages and at each stage expresses specific marker genes **(Figure 10)** (Eisenhoffer et al., 2008; Tu et al., 2015; van Wolfswinkel et al., 2014). The planarian epidermis consists of ventral multiciliated epithelia and dorsal epithelia that are less densely ciliated (McGee et al., 1997; Pedersen, 1976; Rompolas et al., 2010). Notably, already early dorsal epidermal progenitors exhibit distinct gene expression signatures, which are specified by the dorsally expressed morphogen BMP, which may therefore program the final epithelial cell fate of the progenitors (Wurtzel et al., 2017).

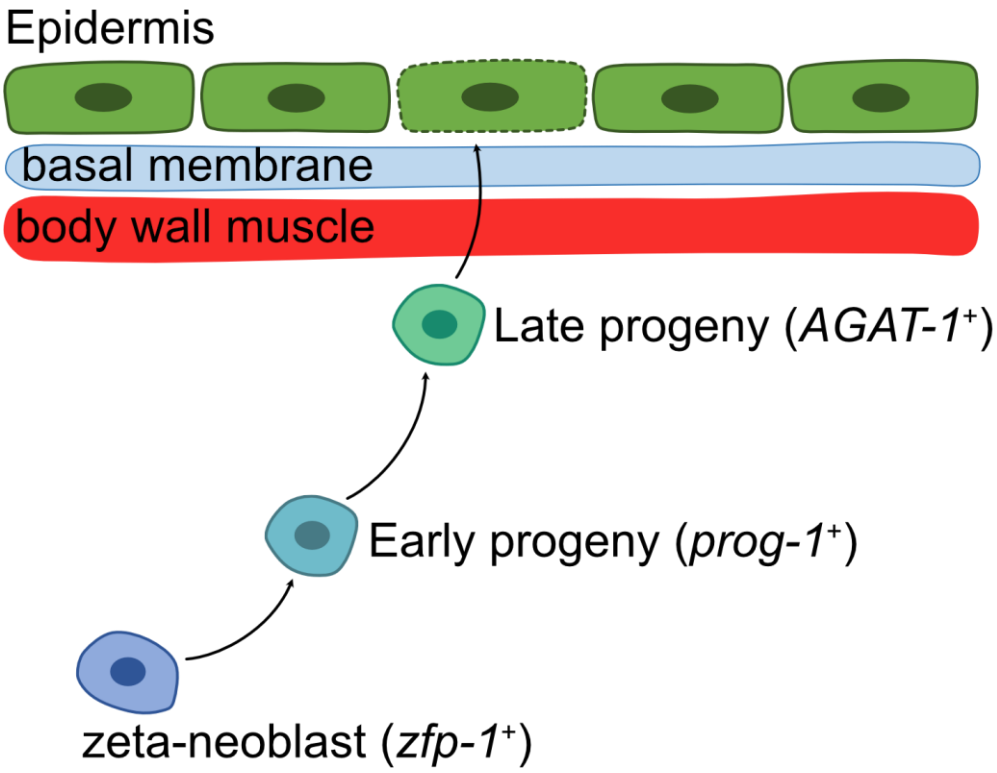

Figure 10. Lineage progression of the planarian epidermis.

Zfp-1 expressing neoblasts (zeta-neoblasts) located deep in the mesenchyme give rise to postmitotic early progenitors, which then become late progenitors. The late progenitors break through the muscle layer of the body wall and the basal membrane to incorporate into the epidermis.

Previous studies have identified several genes involved in the lineage commitment of epidermal cells. For example, the transcription factor p53 and the RNA binding protein mex3-1 are required for the differentiation of postmitotic epidermal progenitors (Pearson & Alvarado, 2010; Zhu et al., 2015). The chromatin remodeling protein (CHD4) and transcription factor (Egr5) have been reported to be involved in the maturation of late progenitors (Scimone et al., 2010; Tu et al., 2015). Furthermore, a MYB-type transcription factor and the myosin regulatory light chain have been found to regulate the rate of the epidermal lineage progression (Sun et al., 2023; Zhu & Pearson, 2018). Taken together, these studies have provided at least some insights into the molecular mechanisms involved in epidermal lineage maturation.

The second example is the differentiation of intestinal cells. Neoblasts expressing *hnf-4*, *gata4/5/6* and *nkx2.2*, which are conserved endodermal markers among metazoans, are thought to give rise to postmitotic gut progenitors that can ultimately differentiate into the three different intestinal cell types: phagocytes, goblet cells and basal cells (Fincher et al., 2018; Forsthoefel et al., 2020; Forsthoefel et al., 2011; Ishii, 1965; van Wolfswinkel et al., 2014; Willier et al., 1925). The regulation of intestinal lineage progression has also been studied previously. For example, it has been reported that the EGF signaling pathway is required for the differentiation of intestinal progenitors (Barberan et al., 2016). Furthermore, Forsthoefel and colleagues combined micro-laser dissection and RNA sequencing methods to identify the transcripts that are enriched in the different cell types of the planarian gut (Forsthoefel et al., 2020). The results show that Gli-1, the effector protein of the hedgehog signaling pathway, and RREB-2, a transcription factor, are involved in the maintenance of secretory goblet cells in the gut.

Cell death in tissue homeostasis

In contrast to cell proliferation and lineage progression in tissue homeostasis, the role of cell removal in homeostasis is still poorly understood due to limited techniques. To date, only a few techniques have been used to detect cell death. For example, terminal deoxynucleotidyl transferase dUTP nick end labeling (TUNEL) can detect double-stranded DNA breaks during apoptosis (Gavrieli et al., 1992). Pellettieri and colleagues used TUNEL to monitor cell death during regeneration and the homeostatic condition (Pellettieri et al., 2010). Their results showed an increase in apoptotic cells in long-term starved worms. Another assay to detect the level of cell death in planarians is the caspase-3 activity assay (de Sousa & Adell, 2018; Gonzalez-Estevez et al., 2012). During the activation of apoptosis,

pro-caspase-3 is cleaved and becomes the active form (Nicholson & Thornberry, 1997). This assay detects the level of active caspase-3 (the cleaved caspase-3) by measuring the fluorescence of the fluorogenic substrate, Ac-DEVD-AMC. Ac-DEVD-AMC is cleaved in the presence of active caspase-3, releasing the fluorescent AMC. Gonzalez-Estevez and colleagues performed the caspase-3 activity assay to detect the level of cell death in the planarian (Gonzalez-Estevez et al., 2012). Surprisingly, their results contradicted those of the TUNEL assay, in which they found a decrease in cell death in worms starved for a similar period of time. Besides the contradictory results, both assays have some drawbacks. For example, the penetration of the TUNEL assay into the internal tissues of the planarian is still questionable. Secondly, the caspase-3 activity assay is not able to provide spatial information on where cell death occurs. Therefore, the mechanism of regulated cell death in planarians requires further investigation.

Despite the persisting limitations of the available methods, studies have indicated molecular mechanisms that may contribute to the regulation of death in planarians. For example, the JNK pathway has been linked to apoptotic cell death. Knocking down the JNK pathway led to a decrease in the level of whole mount TUNEL staining, which in turn correlated with a failure of organ scaling during degrowth (Almuedo-Castillo et al., 2014). Another study suggested that phosphatidylinositol 3-kinase (PI3K) signaling may be required for the induction of apoptosis during regeneration (Zheng et al., 2021). Pharmacological inhibition of PI3K signaling abolished apoptosis and impaired planarian regeneration. Finally, the planarian myosin regulatory light chain homolog (MRLC) was proposed to negatively regulate cell death (Sun et al., 2023).

1.4.4 Challenges and opportunities

Although planarians are interesting models for studying tissue turnover, the study of cell turnover in planarians is still challenging due to the limited tools available. For example, unlike model organisms such as *Drosophila* and *C. elegans*, there are still no genetic tools to label specific cell types with fluorescent proteins. As a result, it is still difficult to study tissue dynamics by focusing on the dynamic movement of cells through lineage tracing. Second, live imaging in planarians has also proven challenging due to their photosensitivity (Paskin et al., 2014; Shettigar et al., 2017). Previous phototactic assays have shown that planarians are photophobic to both visible and ultraviolet light, and more aversive to short wavelength light. The worms' muscular bodies are constantly twitching during time-lapse imaging, making it difficult to track a single object over time. It has therefore not been possible so far to directly image cellular processes such as cell division or cell death during tissue turnover in vivo.

Consequently, there are still many unanswered questions about cell turnover in planarians. For example, how fast is cell turnover in planarians? So far, BrdU or EdU labeling is the only approach available to study turnover kinetics in planarians (Newmark & Alvarado, 2000; Reddien, Oviedo, et al., 2005; van Wolfswinkel et al., 2014; Zhu & Pearson, 2018). However, BrdU or EdU is toxic to the planarian protonephridia, which are responsible for osmoregulation. Animals must be cultured in 10 times higher than normal concentrated planarian water after the BrdU or EdU pulse (Bohr et al., 2021; Zhu et al., 2015; Zhu & Pearson, 2018), and it is difficult to quantify turnover at steady state. Therefore, new assays are needed to quantify the rate of cell turnover. Second, planarians undergo continuous cell turnover, so cell death should happen constantly. One of the interesting questions would be how cells are removed. For example, how does the

epidermis maintain its integrity when epidermal cells are removed? Live imaging is needed to directly observe cell removal. Third, how are dead cells removed in planarians? Many cells die when planarians shrink, but the level of cell proliferation remains at a basal state. Is it possible that the dead cells eventually become the new energy to fuel cell proliferation (Rink, 2013)? Therefore, there is a need to improve techniques in planarian research, especially in the study of tissue turnover.

1.5 Scope of the thesis

My dissertation addresses the mechanistic basis of cell turnover in planarians using the epidermis as a model system due to its external accessibility and well-understood maturation process. In particular, my research focused on cell removal during cell turnover to fill the gap in our understanding of planarian cell turnover. To address the limited tools available, I developed two imaging methods. **Chapter 2** describes the development of a pulse-chase dye labeling assay and the establishment of an imaging pipeline to quantify the turnover rate of the epidermis. In **Chapter 3**, I quantified the turnover rate using our new assay and the results show that epidermal turnover in planarians is position dependent. **Chapter 4** describes the establishment of a live imaging protocol, including an anesthetization approach and a deep learning-based denoising method, to record time-series images. In **Chapter 4**, I also observed the process of cell removal in the epidermis via live imaging and found that epidermal cells were eliminated via internalization and entered the internal tissues. In **Chapter 5** I aimed to follow internalized epidermal cell and the results show that the internalized cells were relocated to the intestine and was eventually digested inside, suggesting that the eliminated epidermal cells are reused as a new energy resource in planarians.

Chapter 2: Assay development to quantify the epidermal cell turnover rate

2.1 Introduction

As described in the first chapter, there is currently no reliable approach to directly quantify cell renewal in the planarian model species. Bromodeoxyuridine (BrdU) or ethynyl deoxyuridine (EdU), a thymidine analog that can be incorporated into newly synthesized DNA during DNA replication, is the only approach used in the field to follow the fate of differentiating neoblast progeny. Previously published results have shown that BrdU-labeled cells began to appear in the epidermis approximately 6-7 days after the BrdU pulse (Newmark & Alvarado, 2000; Reddien, Oviedo, et al., 2005; van Wolfswinkel et al., 2014; Zhu & Pearson, 2018). Although the BrdU or EdU assay is able to show the incorporation of new cells into the epidermis, it is difficult to determine the turnover rate with this assay due to its toxicity to planarians. BrdU destroys the physiological function of the protonephridia, which are responsible for osmoregulation in planarians. The current protocol requires the BrdU-pulsed worms to be cultured in 10 times higher concentrated planarian water (Bohr et al., 2021; Zhu et al., 2015; Zhu & Pearson, 2018). It is not possible to quantify the turnover rate under normal conditions after a BrdU or EdU pulse. Therefore, it is still difficult to measure the cell turnover rate in planarians. To overcome this difficulty, I developed a new assay to quantify the turnover rate in the planarian epidermis. The assay relies on covalent pulse-chase labeling of the epidermis with fluorescent dyes that are stably maintained during the chase period. Most importantly, the assay should not interfere with the physiological functions of planarians of the epidermis or other tissues. In this chapter, I will present the development of such

an assay to quantify the cell turnover rate in the planarian epidermis.

2.2 Results

2.2.1 Principle of the pulse-chase dye labeling assay

I developed a pulse-chase dye labeling assay that allowed us to distinguish the resident cells from the newly incorporated cells in the epidermis. The turnover rate can be quantified by comparing the change in the ratio of resident epidermal cells to all cells present at the time of fixation. This assay relies on live dye labeling of epidermal cells. To begin with, all epidermal cells were labeled with a dye pulse. During the chase period, the cells labeled by the dye pulse were replaced by the newly incorporated unlabeled cells. Therefore, the number of pulse-labeled cells decreased during the chase period. At the end of the chase period, all cells, including dye positive cells and dye negative cells, were labeled with a second dye pulse with different emission characteristics immediately before the worms were fixed. The turnover rate of the epidermis can be quantified by measuring the changes in the ratio of pulse labeled cells (resident cells) to second dye-positive cells (all cells including resident cells and newly generated cells during the chase) divided by the chase time **(Figure 11)**.

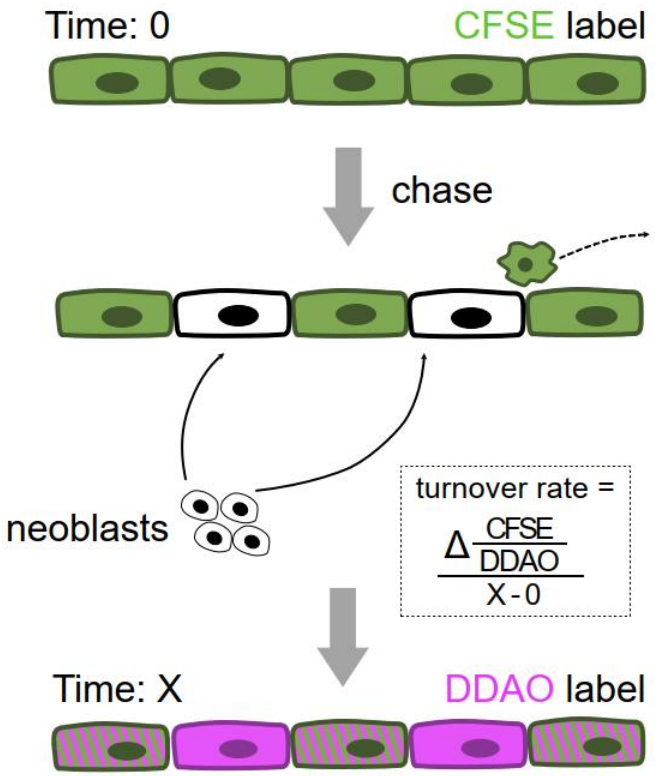

Figure 11. The pulse-chase dye labeling assay to quantify epidermal turnover rate in planarians.

At time 0, epidermal cells are labeled with a dye pulse (CFSE). During the chase period, the pulse-labeled epidermal cells are replaced by the newly incorporated cells, which are CFSE-negative. At the end of the chase, cells are labeled with the second dye (DDAO) before fixation. CFSE labels the resident cells before the CFSE pulse and DDAO labels all cells including the existing cells ($CFSE^+$) and the newly incorporated cells ($CFSE^-$). The turnover rate is the change in the ratio of CFSE to DDAO divided by the chase time.

In this thesis, carboxyfluorescein succinimidyl ester (CFSE) was used as for pulse labeling. The dye contains an N-hydroxysuccinimide ester that can covalently bind to amine groups within cells **(Figure 12)**. The epidermis was live-stained with CSFE and the dye specifically labels the epidermal tissue without penetrating into the internal tissues of the animals **(Figure 13).** As the chase time increased, more $CFSE^-$ cells and fewer $CFSE^+$ cells were observed **(Figure 14)**, indicating that the pulse dye-labeled existing cells were replaced by the newly incorporated cells ($CFSE^-$). The second dye used is 7-hydroxy-9H-(1,3-dichloro-9,9-dimethylacridin-2-one) succinimidyl ester, DDAO for short. Similar to CFSE, DDAO has an N-hydroxysuccinimide ester and binds covalently to amine groups.

The epidermis was labeled with DDAO to mark all epidermal cells including $CFSE^+$ and $CFSE^-$ cells at the end of the chase **(Figure 11 & 14)**. The turnover rate can be quantified by comparing the change in the ratio of $CFSE^+$ cells to $DDAO^+$ cells during the chase period **(Figure 11)**. In conclusion, it is possible to quantify the cell turnover rate in planarians with the pulse-chase dye labeling assay.

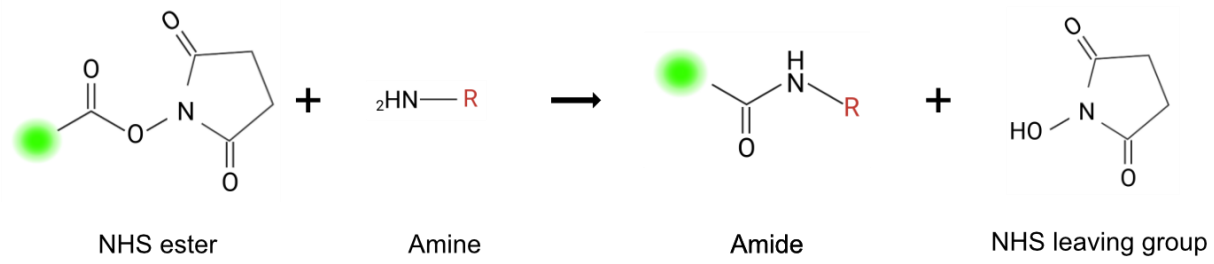

Figure 12. Reaction of N-hydroxysuccinimide (NHS) ester and amine.

N-hydroxysuccinimide (NHS) ester reacts with a primary amine in proteins. After the reaction, an amide bond is formed between a fluorophore and an amine.

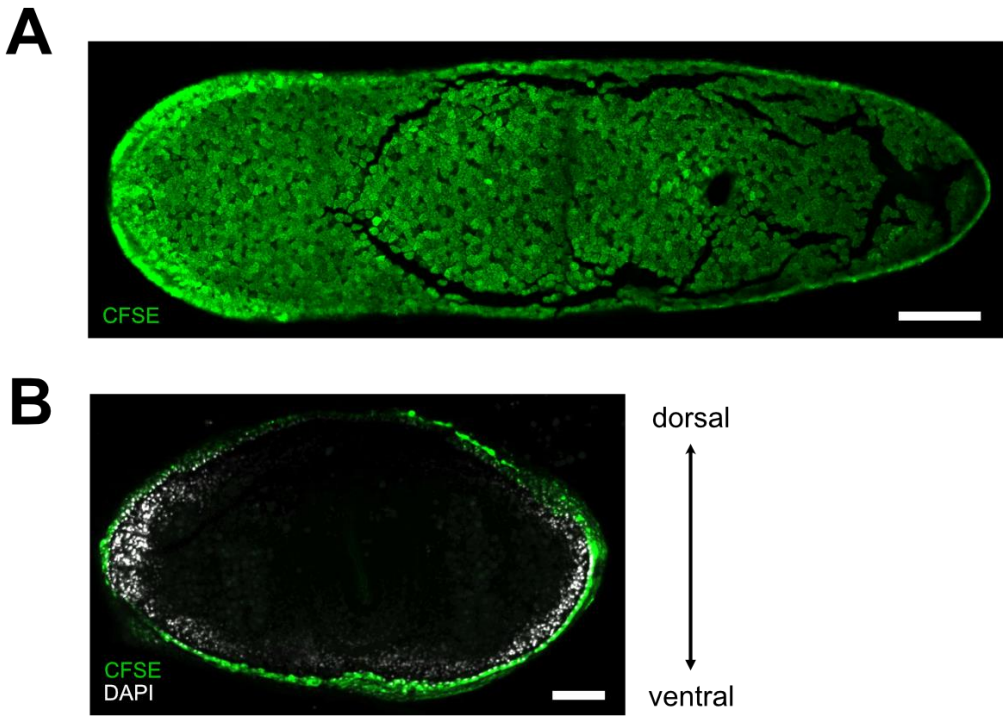

Figure 13. CFSE labeling on the planarian epidermis.

(A) A surface extracted image of CFSE labeling on ventral epidermis. The sample was fixed immediately after CFSE labeling. Scale bar: 100 µm. (B) Cross-section images of CFSE labeling on the epidermis. The sample was counterstained with DAPI and then fixed. The fixed sample was embedded in agarose and sectioned. Scale bar: 100 µm.

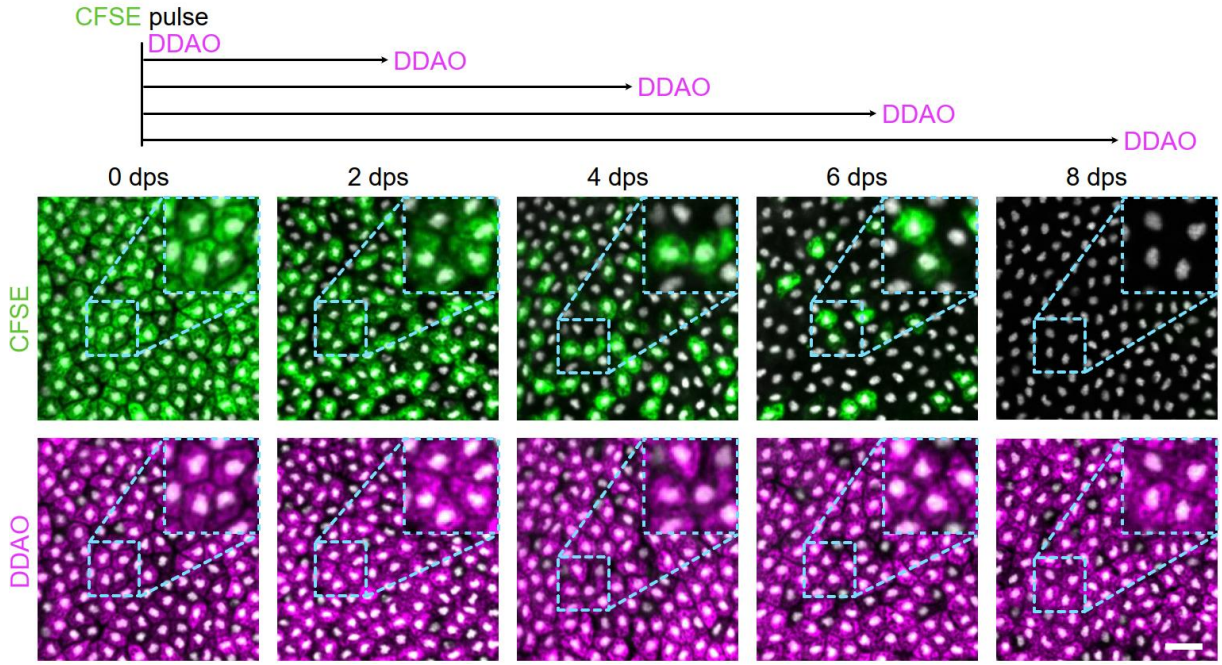

Figure 14. CFSE and DDAO staining of the ventral epidermis.

The carton illustrates that samples were fixed every two days after the CFSE pulse and stained with DDAO immediately before fixation. The top row shows CFSE labeling on the epidermis at different days after CFSE staining. The bottom row shows DDAO labeling on the epidermis. The nuclei of the epidermal cells were visualized with DAPI. These images were surface-extracted. Scale bar: 20 µm. dps: days post CFSE staining. * 0 dps: fixation immediately after CFSE staining.

2.2.2 Image analysis pipeline for quantification

Following the development of the dye labeling assay, an image analysis pipeline is required to quantify the number of $CFSE^+$ and $DDAO^+$ cells. First, images were acquired in 3D volume, which was necessary to capture all dye signals on the epidermis due to the curvature of worms. To specifically analyze the epidermis, the surface signals corresponding to the epidermis were extracted using Premosa, a surface extraction tool (Blasse et al., 2017), to extract the surface signals corresponding to the epidermis from the 3D z-stack images **(Figure 15)**. Second, due to the large number of epidermal cells in one image, it is difficult to manually quantify the $CFSE^+$ and $DDAO^+$ cells. To overcome this difficulty, I used Stardist, a deep learning-based object detection method, to automatically segment each individual epidermal cell from $CFSE^+$ or $DDAO^+$ labeling

(Schmidt et al., 2018) **(Figure 15)**. Each epidermal cell was automatically recognized by a custom-trained model. Here, I aimed to quantify the turnover rate of the ventral and dorsal epidermis, which have different morphologies, so I trained the Stardist models to automatically segment the ventral and dorsal epidermal cells respectively.

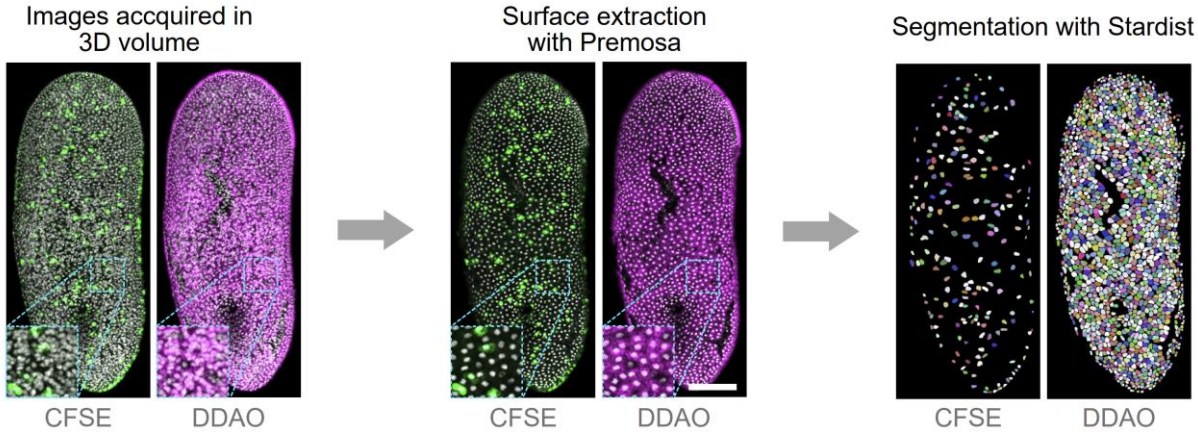

Figure 15. The image analysis pipeline for quantification of CFSE$^+$ and DDAO$^+$ cells.

The left panel shows maximum projected z-stack images viewed from the ventral side. Epidermal cells were labeled with CFSE and DDAO and nuclei were labeled with DAPI. The middle panel shows the Premosa processed images from the left panel. The right panel consists of the automatic segmentation images from the middle panel using the Stardist model. Scale bar: 100 µm.

To train the Stardist models, the raw and manually annotated image pairs were used as the inputs for model training **(Figure 16)** (Details of Stardist model training are described in Materials and Methods). In total, 1592 and 528 training pairs were used to train the Stardist models for automatic segmentation on ventral and dorsal epidermal cells respectively. The accuracy of the Stardist models was then calculated by comparing the results of the model predictions with the ground truth from the manual counts, with a total of 27668 cells counted **(Figure 17)**. Here, I trained two Stardist models for the ventral and dorsal epidermis of planarians. The results show that the accuracy of the Stardist model was greater than 90% in both CFSE and DDAO labeled epidermis in the

ventral epidermis **(Figure 18 A)**. In the dorsal epidermis, the accuracy of the Stardist model prediction exceeded 90% in the CFSE-labeled epidermal cells **(Figure 18 B)**. However, the DDAO labeled dorsal epidermal cells cannot be accurately detected with an accuracy less than 90% **(Figure 18 B)**. Alternatively, the DAPI labeled nuclei were used as a reference of total epidermal cells before fixation (accuracy > 90%). In conclusion, my imaging pipeline is able to accurately quantify $CFSE^+$, $DDAO^+$ and $DAPI^+$ epidermal cells.

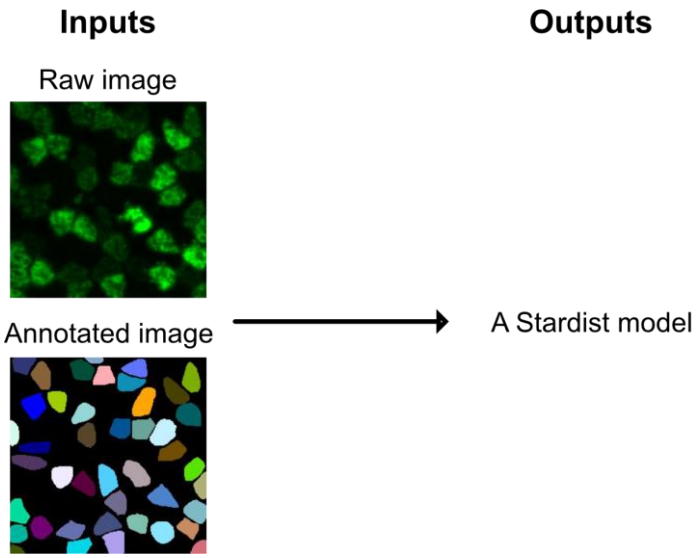

Figure 16. Stardist model training.

The raw CFSE-labeled images processed by Pemosa are paired (Upper panel) with the manually annotated images (Bottom panel) to serve as training data for the Stardist models. The images were annotated using labkit in FIJI. The detailed training parameters are documented in the Materials and Methods.

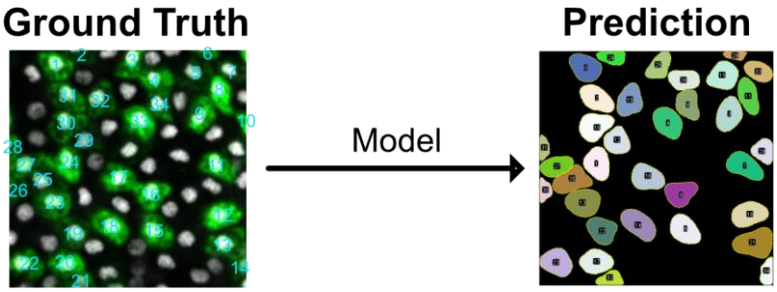

Figure 17. Strategy for quantifying the accuracy of the Stardist model

The accuracy of the models was calculated by comparing the results of the ground truth by manual counting (left panel) with the results of the Stardist model prediction (right panel). The left image was labeled with CFSE and DAPI (nuclei). Accuracy = $1 - \left|\frac{Predition - Ground\ Truth}{Ground\ Truth}\right|$.

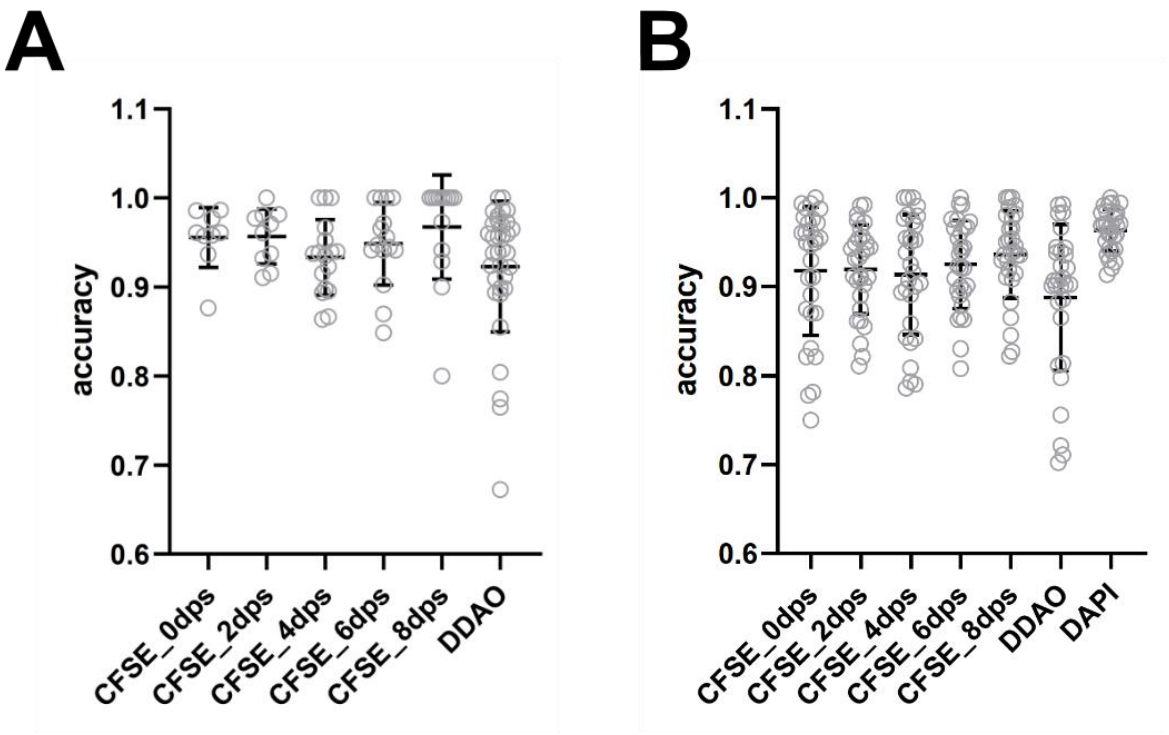

Figure 18. Accuracy of Stardist model prediction.

The accuracy of the custom-trained Stardist models was quantified on CFSE, DDAO and DAPI labeled cells on the ventral epidermis (A) and dorsal epidermis (B). An accuracy of 1 means that the results of the model prediction are identical to the ground truth. Each open circle corresponds to one accuracy quantification. For quantification in CFSE-labeled epidermal cells, images from 0, 2, 4, 6 and 8 days after CFSE staining were selected. N=99 total in A; N=210 total in B. Middle line: mean value. Error bar: standard error. dps: day post CFSE staining. (Details of the verification of the Stardist model are documented in Materials and Methods)

2.2.3 Validation of the dye-labeling assay and the image analysis pipeline

Having established the pulse-chase dye-labeling assay and image analysis pipeline, I first performed a validation experiment to rule out the possibility that the disappearance of CFSE-labeled cells was due to leakage of the CFSE dye from epidermal cells during the chase period. I performed the experiment on irradiated planarians whose neoblasts had been ablated using X-rays. For the maturation of the epidermal cell lineage, zeta-neoblasts become early and late epidermal progenitors, which in turn differentiate into mature epidermal cells (Eisenhoffer et al., 2008; Tu et al., 2015; van Wolfswinkel et al., 2014; Zhu et al., 2015; Zhu & Pearson, 2018). After neoblast depletion, the early and late progenitors can initially still incorporate the epidermis. However, at a later time point, the progenitor pools are depleted due to the disappearance of neoblasts and no new epidermal cells can enter the epidermis **(Figure 19)**. If CFSE can be maintained in epidermal cells, the ratio of $CFSE^+$ to $DDAO^+$ would eventually stop decreasing at some point because there is no new cell supply. I started the pulse-chase assay in the planarians exposed to X-rays 7 days before the CFSE pulse **(Figure 20)** and the results show that the $CFSE^+/DDAO^+$ ratios stabilized at 80% 11 days after irradiation (4 days post CFSE staining) **(Figure 20)**. These results are consistent with the previous experiment showing the disappearance of epidermal progenitor cells 10 days after irradiation (Eisenhoffer et al., 2008; Tu et al., 2015) (see Discussion). In summary, this experiment suggests that the dye can be retained in epidermal cells and that the decrease in $CFSE^+$ cells was due to the replacement of resident cells by newly arrived cells. Therefore, it is a reliable assay to quantify the epidermal turnover rate in planarians.

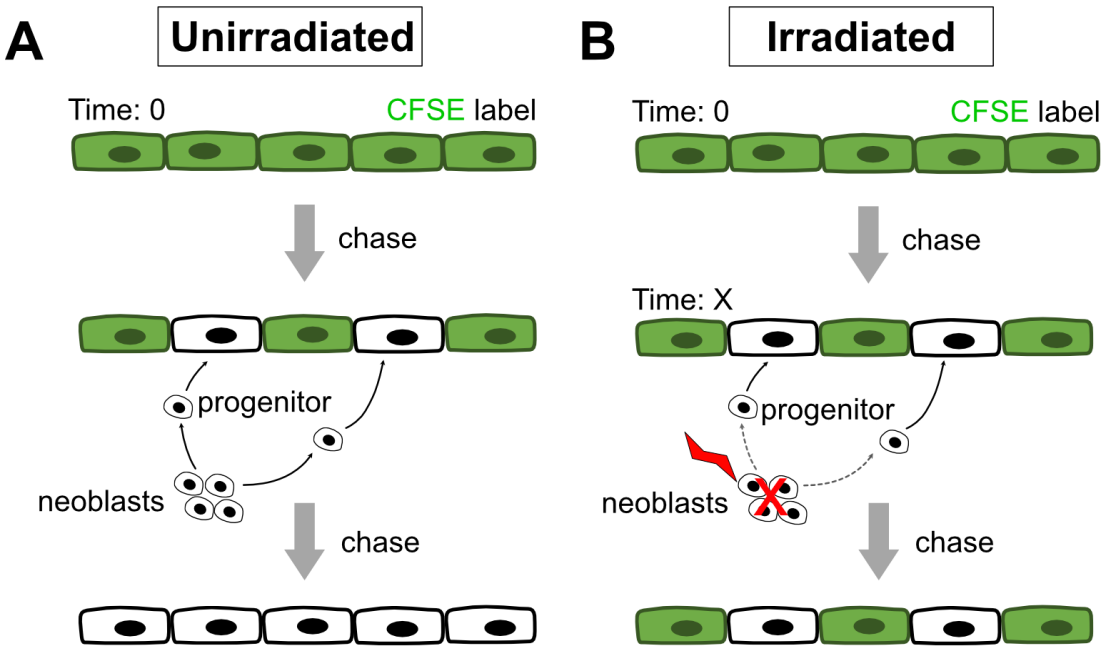

Figure 19. Illustrations of the CFSE pulse assay in irradiated worms.

(A) In unirradiated worms, CFSE-pulse cells are continuously replaced by new cells generated from neoblasts. The $CFSE^+$ cells would eventually disappear. (B) In irradiated worms, CFSE-pulse cells are replaced by new cells at the beginning of chase, but once the progenitor pool is empty, no new cells can enter the epidermis. The ratio of $CFSE^+$ to all cells should no longer decrease or decrease more slowly than in unirradiated worms.

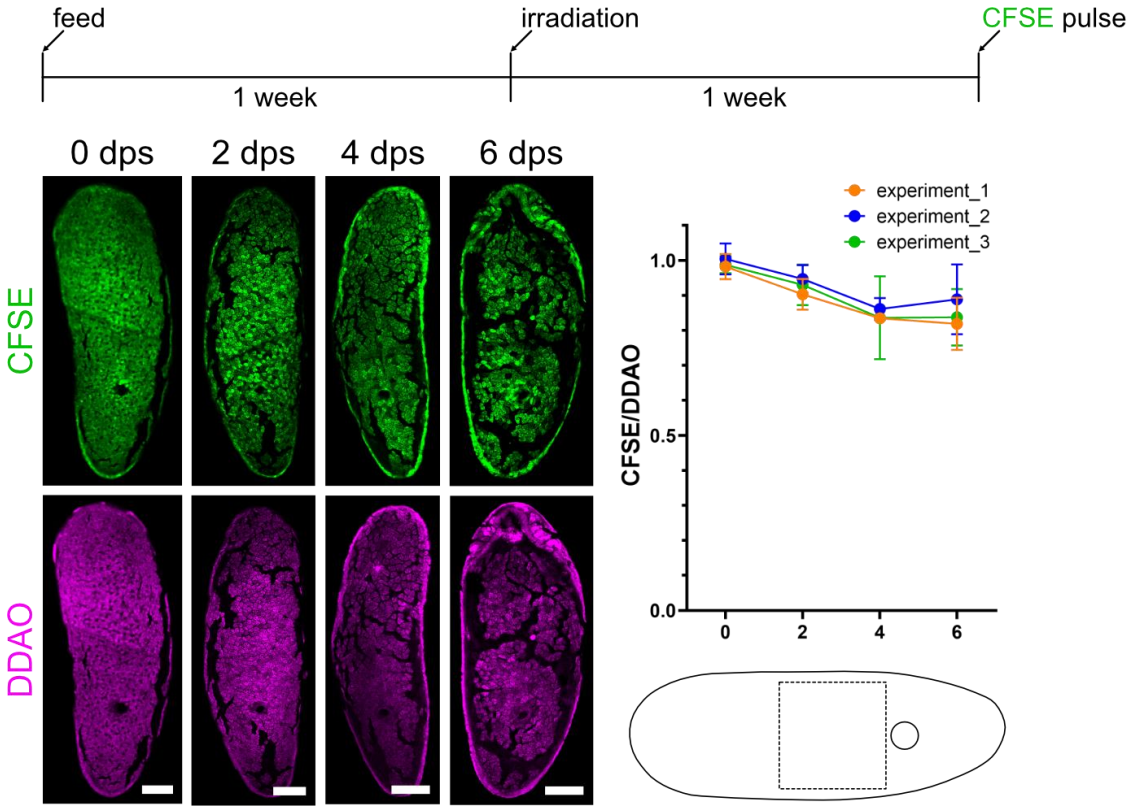

Figure 20. Quantification of CFSE$^+$/DDAO$^+$ ratios on the ventral epidermis of irradiated worms.

Worms were starved for two weeks prior to the CFSE pulse and irradiated one week prior to the CFSE pulse (top panel). Samples were labeled with DDAO and fixed every other day (0, 2, 4 and 6 days). The left panel consists of Premosa-processed images with CFSE and DAPI labeling on the ventral epidermis after different days post CFSE staining. The trunk epidermis anterior to the pharyngeal opening was selected for quantification. The data in the graph were collected from 3 independent experiments with at least 3 samples from each time point. Scale bars: 100 µm. Dot: mean value. Error bar: standard error. dps: days post CFSE staining. * 0dps: samples were fixed immediately after CFSE labeling.

2.3 Summary

In this chapter, I have developed a dye-labeling assay and an image analysis pipeline to quantify the turnover rate of the planarian epidermis. This assay is based on the covalent binding between the cell dyes and amine groups inside cells and the specific labeling of the dyes on epidermis. The pulse-chase approach distinguishes the resident epidermal cells before the CFSE pulse and the new cells ($CFSE^-$) arriving after the CFSE pulse. Using the surface extraction tool and deep learning based automatic segmentation method (Stardist), the dye-labeled epidermal cells can be accurately quantified. Furthermore, the results of the validation experiment on irradiated worms indicate that the disappearance of CFSE-labeled epidermal cells was due to the replacement of resident cells by the new cells rather than the leakage of dyes from epidermal cells during chase. In conclusion, with the development of the assay, the planarian epidermis can be used as a platform to study cell turnover rate.

Chapter 3: Quantification of epidermal cell turnover rates

3.1 Introduction

The previously developed assay allows the quantification of epidermal cell turnover. In this chapter, I aimed to quantify the cell turnover rate of the planarian epidermis and to observe the dependence of the turnover rate on the body axes. Planarians are bilaterally symmetric with distinct dorsal-ventral and anterior-posterior axes. Previous studies have shown that the anterior-posterior axis is specified by the Wnt/β-catenin pathway in planarians (Gurley et al., 2008; Petersen & Reddien, 2009; Reuter et al., 2015). The expression of *wnt* genes and β-catenin defines the tail region. Knockdown of β-catenin disrupted the anterior-posterior axis, leading to head formation in both the posterior and lateral regions. Similarly, the dorsal-ventral axis is specified by BMP signaling (Gavino & Reddien, 2011; Molina et al., 2007; Orii & Watanabe, 2007). The planarian BMP expressed in the dorsal midline is capable of specifying dorsal polarity. Depletion of BMP signaling led to the ectopic formation of ventral structures on the dorsal side. BMP signaling is also responsible for patterning the positional identity of epidermal neoblasts and progenitors (Wurtzel et al., 2017). Furthermore, the morphology of epidermal cells differs between dorsal and ventral regions (Gumbrys, 2017; McGee et al., 1997; Pedersen, 1976; Rompolas et al., 2010) **(Figure 7)**. The ventral epidermis is composed of multiciliated epithelial cells, whereas the majority of dorsal epidermal cells are non-ciliated. Using the assay established in Chapter 2, it is now possible to understand whether the turnover kinetics of the epidermis are different along the anterior-posterior and dorsal-ventral axes. I therefore carried out CFSE-DDAO pulse-chase experiments to quantify the turnover rate of epidermal cells along the planarian body axes and to compare whether the turnover rate of epidermal cells is position dependent.

3.2 Results

3.2.1 Comparison of cell turnover rates along the D-V axis

To compare the turnover rate between dorsal and ventral epidermis, I performed the established pulse-chase dye labeling assay in two-week starved planarians. I collected samples every two days for 8 days after the CFSE pulse with three independent replicates and quantified the turnover rates in both ventral and dorsal epidermis **(Figure 21 & 22)**. The results show that the ratios of resident cells to total cells ($CFSE^+/DDAO^+$) in the ventral epidermis reached 20% 8 days post CFSE staining, indicating that 80% of the CFSE-pulsed cells were replaced by newly incorporated cells **(Figure 21)**. On the other hand, in the dorsal epidermis, the ratio of $CFSE^+$ cells to $DAPI^+$ nuclei was approximately 80% 8 days post CFSE staining **(Figure 22)**. Linear regression analysis of the $CFSE^+$ cells/all cells ratios from 0 day to 8 days post CFSE staining shows that the half-lives of the ventral epidermis and dorsal epidermis are 4.5 and 20 days respectively **(Figure 23)**. In summary, the results indicate that there was a difference in turnover rates between the dorsal and ventral epidermis, with the ventral epidermis turning over much faster than the dorsal epidermis.

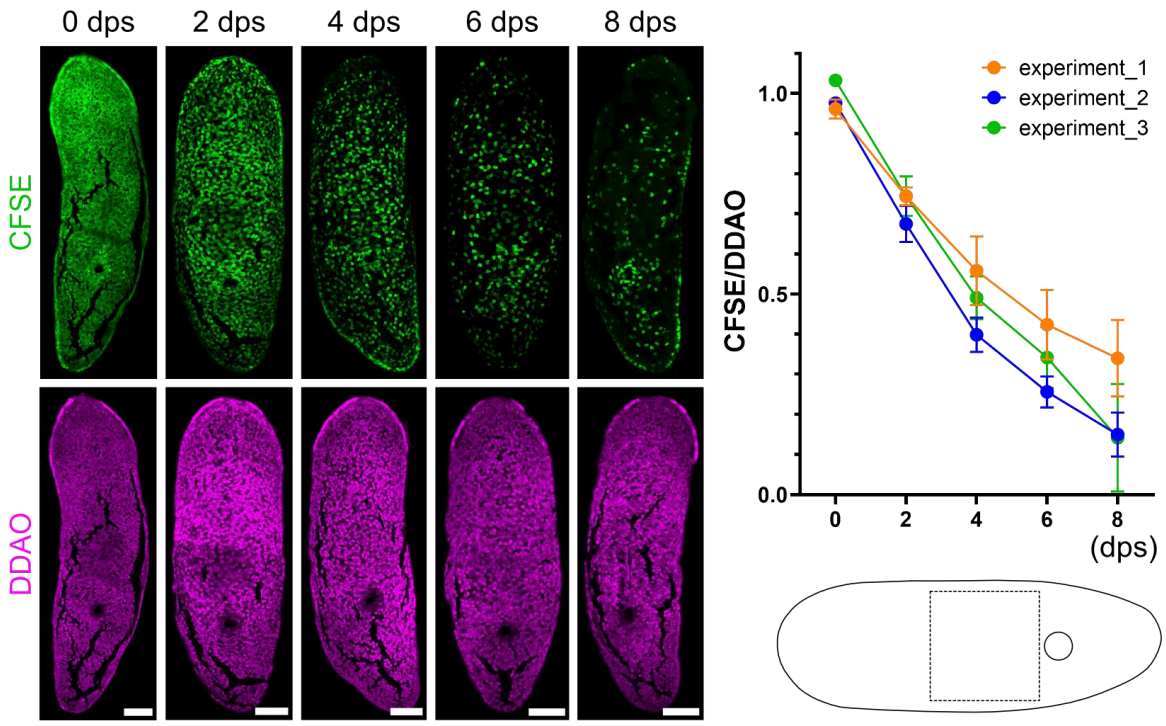

Figure 21. Quantification of cell turnover rate on the ventral epidermis.

Two weeks starved worms were used for the CFSE pulse-chase experiment. The left panel shows the images processed by Premosa with CFSE and DDAO labeling on the ventral epidermis. The samples were pulsed with CFSE and fixed at different chase days (0 days, 2 days, 4 days, 6 days and 8 days) after CFSE staining and labeled with DDAO at the end of the chase. The region (dashed square) located anterior to the pharyngeal opening (circle) was used for quantification of $CFSE^+$ and $DDAO^+$ cells. The data came from three independent experiments. At least three samples were quantified at each time point in each experiment. Dot: mean value. Error bars: standard error. Scale bars: 100 µm. dps: days post CFSE staining.

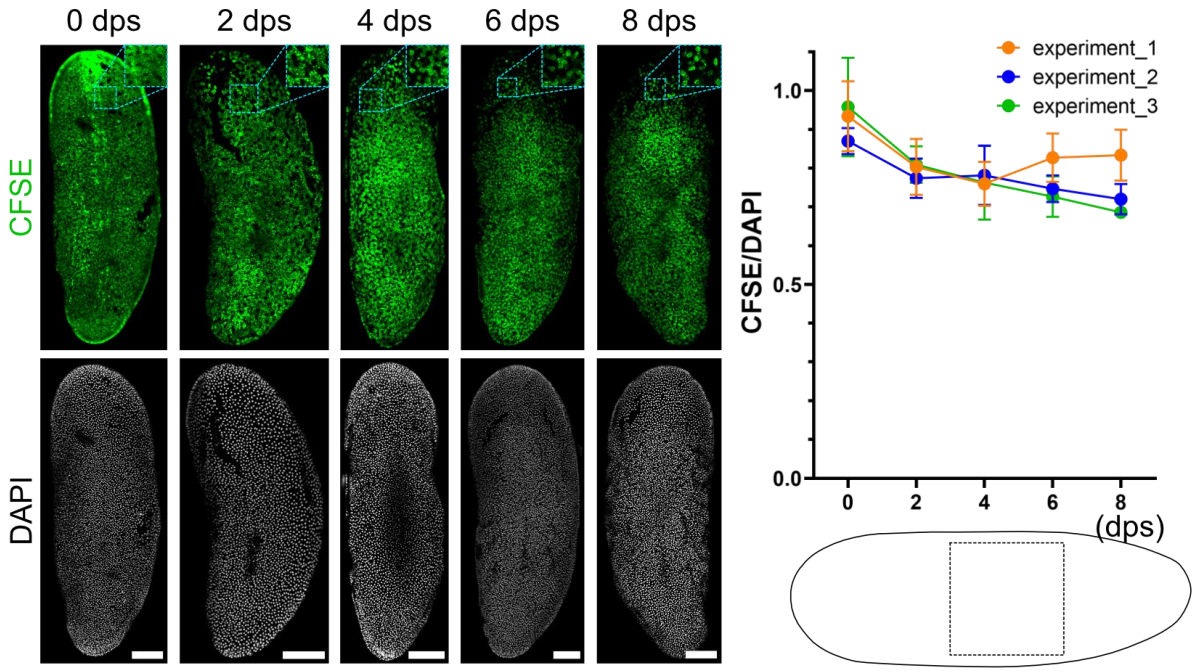

Figure 22. Quantification of cell turnover rate on the dorsal epidermis.

The left panel shows surface-extracted images with CFSE and DAPI labeling on the dorsal epidermis. Samples were fixed at different days post CFSE staining (dps). DAPI was used to label the nuclei of epidermal cells immediately prior to sample fixation. Cells located in the trunk area (dashed square) were selected for further quantification. The graph shows the ratios of $CFSE^{+}$ epidermal cells to $DAPI^{+}$ epidermal nuclei after different chase times from three independent experiments. At least three samples were taken at each time point. Dot: mean value. Error bars: standard error. Scale bars: 100 µm. dps: days post CFSE staining.

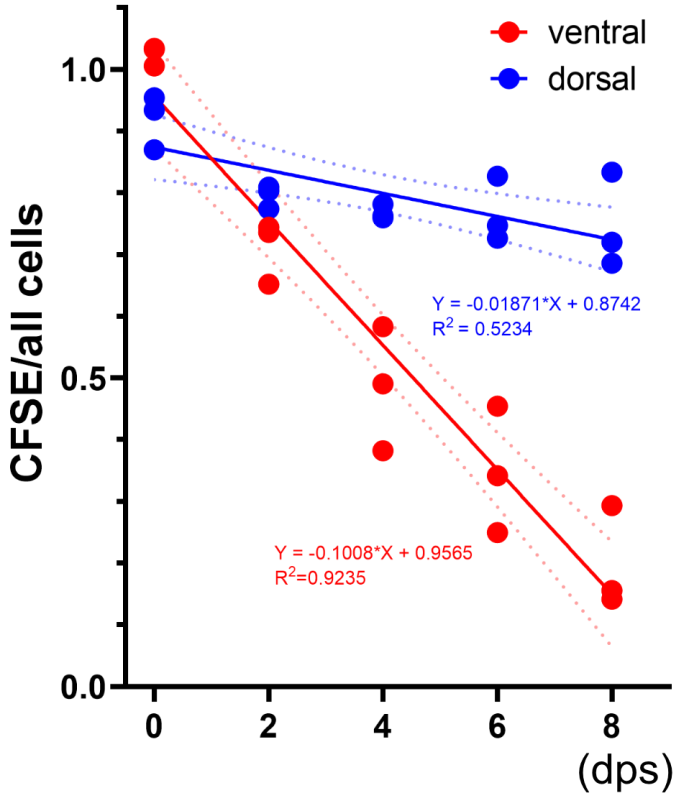

Figure 23. Linear regression analysis of the ratios of CFSE$^+$ to all cells at different chase periods.

The blue and red colors show the quantification of CFSE$^+$ cells to all cells on the dorsal and ventral epidermis respectively. A point represents the average ratio of CFSE$^+$/all cells at each time point in an experiment. The lines represent the line of best fit and the functions and R-squared values are given below the lines. Dashed lines represent 95% confidence intervals. dps: days post CFSE staining.

3.2.2 Comparison of the rates of cell turnover along the A-P axis

I continued to compare epidermal turnover rates between the head, trunk and tail regions. To do so, I cropped out regions of interest in the anterior head region, the trunk region anterior to the pharyngeal opening and the tail region **(Figure 24)** and quantified the CFSE/DDAO or CFSE/DAPI ratios in the selected areas. In the ventral epidermis, the results show that the CFSE/DDAO ratios in the head region were lower than those in the trunk or tail regions at 4 days and 6 days post CFSE staining, but the ratios of CFSE$^+$ cells to DDAO$^+$ cells were not different between these three areas at 8 days post CFSE pulse **(Figure 25 A-B)**. In the dorsal epidermis, the ratios of resident cells (CFSE$^+$) were lower in

the head region compared to the trunk and tail regions at 6 days and 8 days post CFSE staining **(Figure 25 C-D)**. The average CFSE/DAPI ratio from three independent replicates reached 30% in the anterior epidermis at 8 days post CFSE staining. On the other hand, in the trunk and posterior regions, $CFSE^{+}$ cells still accounted for 80% of all cells at 8 days post CFSE staining. In contrast to the ventral epidermis, where the ratios of existing cells at 8 days post CFSE staining does not differ between the head and the other two regions, the disparity of the CFSE/DAPI ratios increased with increasing tracking time in the dorsal epidermis. Furthermore, linear regression analysis shows that the half-life of the anterior dorsal epidermal cells is 12 days, much shorter than the half-life of trunk dorsal epidermal cells **(Figure 26)**.

In summary, these results show that head epidermal cells have a higher turnover rate on dorsal epidermis than cells located in the trunk and tail regions. However, it is not clear whether the anterior epidermal cells in the ventral epidermis have a higher turnover rate, as there is no significant difference between these three areas (head, trunk, and tail) at 8 days post CFSE staining.

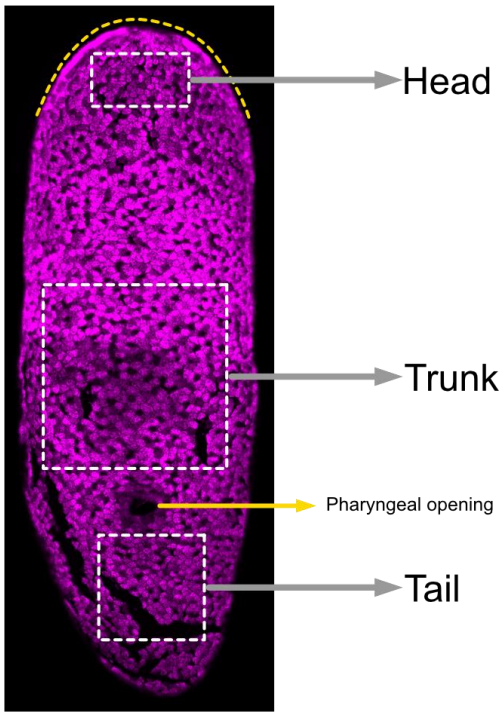

Figure 24. Illustration of how the regions selected for turnover rate quantification were created.

The head region is located at the front end of the animal. A rectangular crop was made within the semicircular outline of the head. A square crop anterior to the pharyngeal opening was used as a reference for the trunk region. The tail region is referenced to the square crop posterior to a pharyngeal opening. The sample was labeled with DDAO on epidermis and the image was surface-extracted.

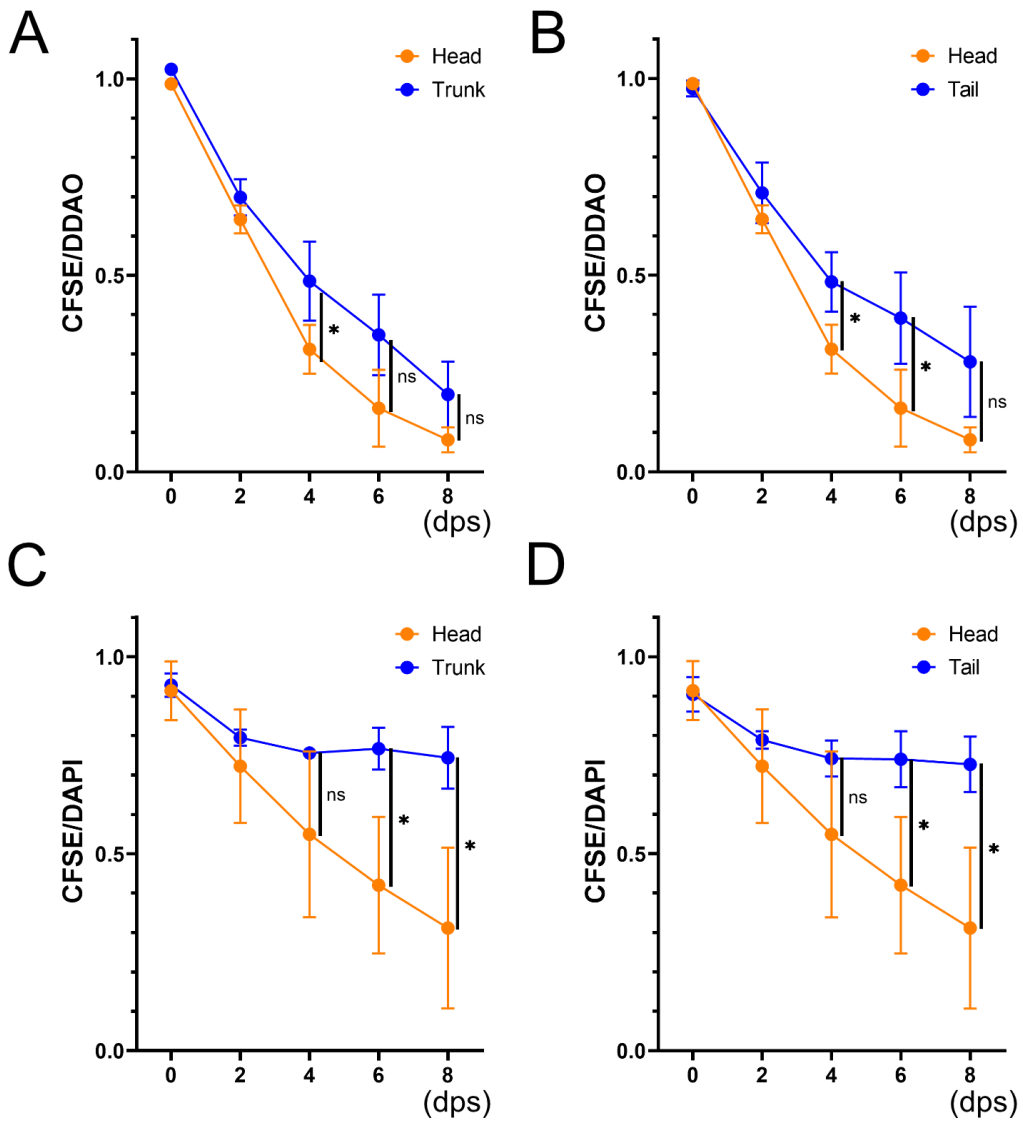

Figure 25. Comparison of epidermal cell turnover rates along the anterior-posterior axis.

CFSE/DDAO or CFSE/DAPI ratios were calculated at different days after the CFSE pulse in the head, trunk and tail regions on both the ventral (A & B) and dorsal epidermis (C & D). Results are averages of CFSE/DDAO or CFSE/DAPI from three independent experiments. Student's t-test was performed to compare CFSE/DDAO or CFSE/DAPI differences between two regions. *: $p<0.05$, ns: non-significant. Dot: mean value. Error bars: standard error. dps: day post CFSE staining.

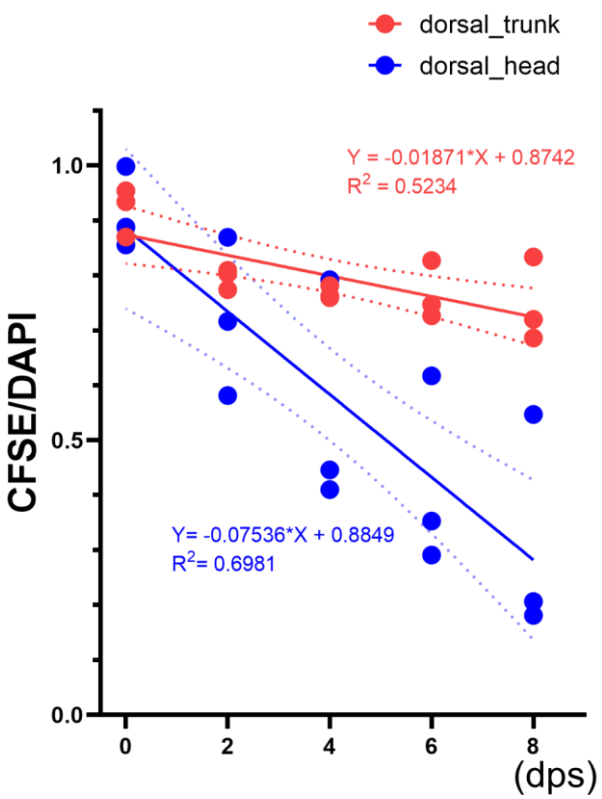

Figure 26. Linear regression analysis of CFSE/DAPI ratios over time on dorsal epidermis.

The red and blue colors represent the quantification of CFSE/DAPI ratios on the dorsal epidermis in the head and trunk areas respectively. Each point represents the average CFSE/DAPI at each time point in an experiment. The lines represent the best fit lines of CFSE/all cells over time. The functions and R-squared values are listed in the figure. The dashed lines represent the 95% confidence intervals. dps: days post CFSE staining.

3.3 Summary

In this chapter, I have used the pulse-chase dye labeling assay developed in Chapter 2 to compare the turnover rates of epidermal cells in different areas (anterior vs posterior & dorsal vs ventral). The results show that turnover rates were different between dorsal and ventral epidermis. The half-life of the ventral epidermis is 4.5 days, which is much shorter than that of the dorsal epidermis. In addition, there is no difference in cell turnover rate along the anterior-posterior axis in the ventral epidermis. However, the epidermal cells located in the anterior are renewed much faster than those located in the trunk and tail in the dorsal epidermis.

Chapter 4: Mechanics of epidermal cell removal

4.1 Introduction

The results of the previous chapter indicate that the ventral epidermis is a highly dynamic tissue and therefore a suitable model to study the mechanism of cell removal in planarians. In this chapter, I intended to understand how epidermal cells are eliminated in planarians. As described in the introduction, there are two modes of cell extrusion in epithelial tissues: apical extrusion and basal extrusion. In adult animals, most epithelial tissues eliminate unwanted cells via apical extrusion because leaving unwanted cells in internal tissues can cause several physiological problems, such as autoimmune diseases (Marshall et al., 2011; Slattum et al., 2014; Slattum & Rosenblatt, 2014). Basal extrusion is mainly observed during embryonic development, and is accompanied by clearance mechanisms after cells delaminate into internal tissues (Lolo et al., 2012; Ninov et al., 2007). To answer the question of how epidermal cells are eliminated in planarians, live imaging is required to observe the process of epidermal cell removal. However, in the case of planarians, live imaging has proven challenging due to their extreme photosensitivity (Paskin et al., 2014; Shettigar et al., 2017). Specimens twitch dramatically when exposed to laser light, making it extremely difficult to track individual objects in time-lapse recordings. In addition, there are currently no genetic tools available to label specific cell types in planarians. Previously, live imaging has been used to observe the migration of epidermal cells during regeneration (Gumbrys, 2017). Epidermal cells were labeled with cell dyes and worms were immobilized using both chemical and mechanical approaches. However, the tracking time was limited to 1 hour and the resolution was not sufficient to track every single epithelial cell. Therefore, the state-of-the-art live imaging technique was not powerful enough to track cell behavior in planarians. In this chapter, I

aimed to establish a new and improved live-imaging protocol based on the previous effort from Dr. Tobias Boothe (Boothe et al., 2017). The new protocol combines a chemical immobilization and image processing to address the photosensitivity of planarians. I used this new live imaging protocol to observe the direction in which cells are removed from the epidermis of planarians **(Figure 27)**.

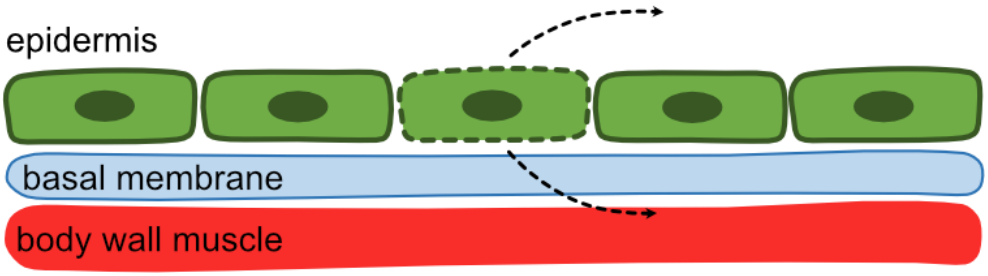

Figure 27. Hypothesis: How are cells shed from the epidermis in planarians?

First possibility: epidermal cells are removed via apical extrusion, in which the cells leave organisms. Second possibility: epidermal cells are extruded toward the basal membrane and stay in internal tissues.

4.2 Results

The live imaging protocol consists of three parts including sample preparation, imaging and post-acquisition-analysis **(Figure 28-31)**.

4.2.1 Sample preparation

Sample preparation involves live labeling of samples with cell dyes and sample immobilization. In this case, I took advantage of the selective accessibility of the cell dyes to specifically label epidermal cells. The dyes used here are RedDot™1 and CellTracker™ Deep Red Dye. RedDot™1 is a cell membrane-permeant nuclear dye and CellTracker™ Deep Red Dye contains a succinimidyl ester group that reacts with amines on proteins after entering cells. These two dyes are in the far-red spectrum, as living planarians are more aversive to shorter wavelength light (Paskin et al., 2014; Shettigar et al., 2017). Following dye labeling, the samples were anesthetized with linalool, an anesthetic that is believed to be able to block action potential in neurons and is commonly used to anesthetize animal samples for live imaging (Boothe et al., 2017; Goel et al., 2019; Leal-Cardoso et al., 2010). The planarian samples were anesthetized in 0.02% linalool for 30 minutes in planarian water with the adjustment from the previous protocol of the immobilization of planarian samples (Boothe et al., 2017). With this concentration, the samples were still alive after time-series imaging with a duration of 2 to 3 hours. Following linalool anesthetization, the samples were embedded in agarose on a glass-bottom dish **(Figure 28)**. To prevent water evaporation, the agarose was covered with an oxygen-permeable Polymethylpentene (PMP) disc and the gap between the glass bottom and the PMP disc was sealed with halocarbon oil.

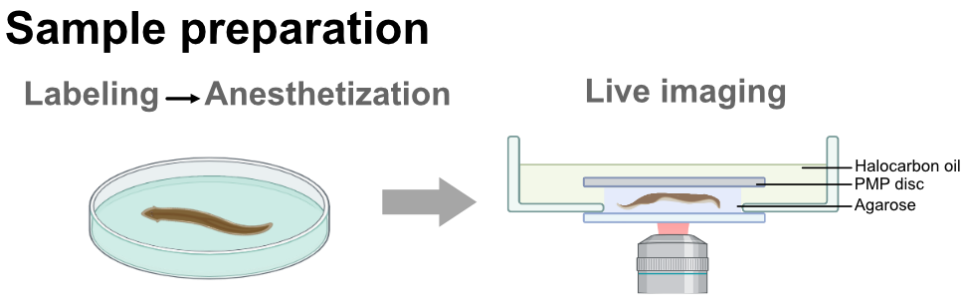

Figure 28. Sample preparation for live imaging.

A sample was first lively labeled with cell dyes and anesthetized with linalool (left panel). The sample was then embedded in low melting agarose covered with an oxygen permeable PMP disc. The sample was mounted on a glass bottom dish and the gap between the disc and the glass button was covered with Halocarbon oil. The figure was created with BioRender.com.

4.2.2 Imaging

Once the samples were mounted in the dish, the dish was placed on a stage in a thermostatic incubator with the temperature set to 15°C. After 30 minutes to 1 hour of incubation, the time series recordings were started. To minimize twitching of the samples, the time lapse images were acquired with a low exposure time (5 milliseconds) and low laser power (1%). The kymographs in **Figure 31** that plotted the pixel intensity shows that the objects could stay in nearby positions with the application of lower exposure time, indicating that lower exposure time could successfully reduce twitching and made the objects more trackable overtime. Detailed imaging conditions are described in Methods.

4.2.3 Post-analysis

Short exposure time and low laser power inevitably led to a reduced signal-to-noise ratio, making it difficult to follow a specific object over time. To overcome this problem, content-aware image restoration (CARE), a deep learning-based denoising method, was used to improve the signal-to-noise ratio of raw images (Weigert et al., 2018). Similar to Stardist, CARE involves customized model training. The z-stack image pairs, acquired

under the same conditions except for the exposure time (one with low exposure time and the other with high exposure time), were used to train the CARE models for denoising **(Figure 29)**. Detailed parameters for training the CARE models are described in Methods. With the application of CARE denoising, the dye labeling signals on the epidermal cells were easier to distinguish from the background **(Figure 30)**. Although the short exposure time and CARE made it possible to track every single epidermal cell, it is still difficult to follow the objects for a long period due to the twitching of the worm's muscular body **(Figure 31)**. To overcome this problem, a drift correction method was applied to correct the shift of objects overtime. The kymographs in **(Figure 31)** shows that it is possible to track individual objects in the epidermis over a longer period after drift correction. In summary, the new live imaging protocol including live dye labeling, CARE denoising and drift correction allowed me to observe the cellular dynamics in the planarian epidermis.

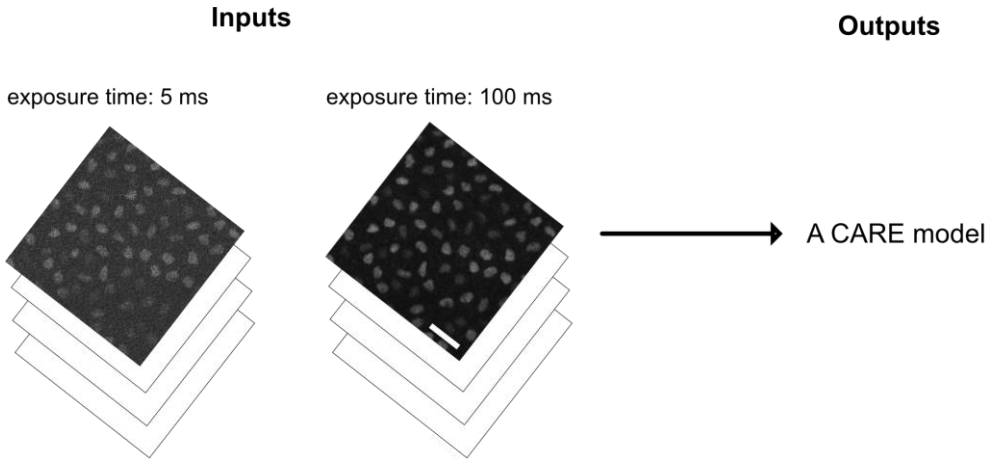

Figure 29. CARE model training.

The z-stack image pairs acquired at the same position with different exposure times (5 ms & 100 ms) were used as the input for training a CARE model. The images show the RedDot™1-labeled nuclei on the epidermis. Scale bar: 20 μm.

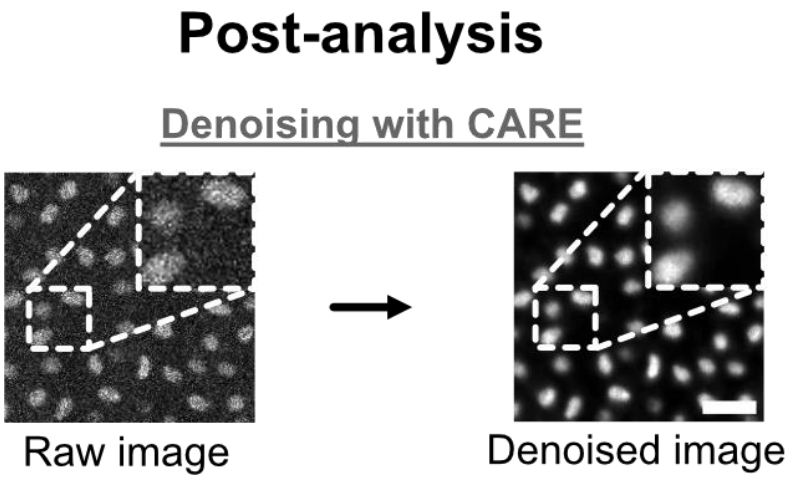

Figure 30. Post-analysis of the time-lapse images.

The low signal-to-noise resulting from the low exposure time and low laser power was enhanced by the CARE denoising tool. The single confocal section image in the left panel (raw image) contains RedDot™1-labeled nuclei. The image in the right panel (denoised image) is the CARE-processed image with the input from the left. Scale bar: 20 µm.

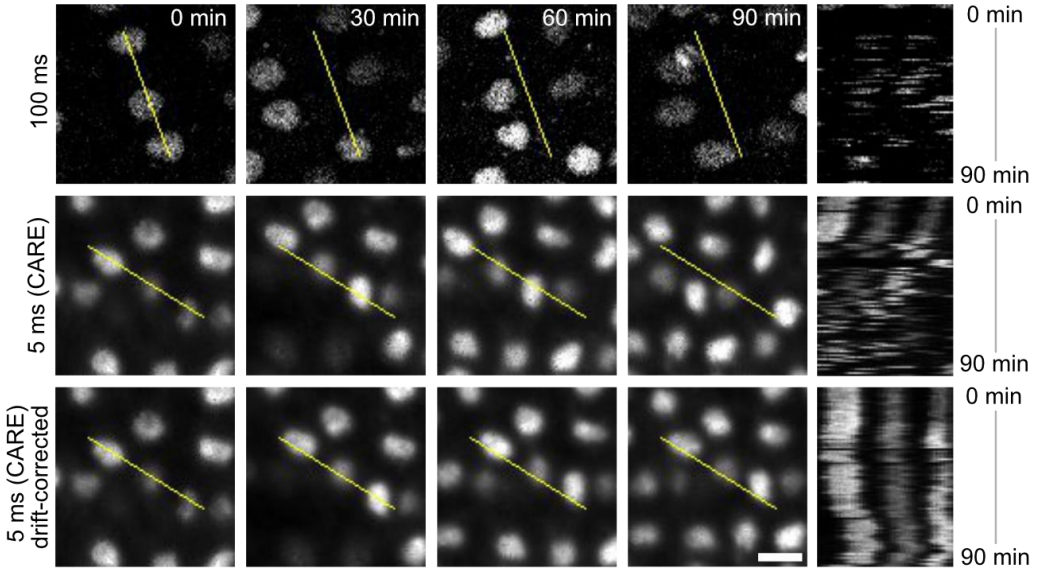

Figure 31. Epidermal nuclei can be tracked over time with low exposure time, denoising and drift correction.

This figure consists of single confocal section images of RedDot™1-labeled epidermal nuclei. The columns show the time points at which the images were documented. The rows show the images with specific imaging conditions and post-processing. The rightmost column contains the kymographs of pixel brightness over time along the yellow reference lines in the corresponding left panels. The first row consists of images acquired with an exposure time of 100 milliseconds. The second row consists of the CARE-processed images

acquired with an exposure time of 5 milliseconds. The bottom row consists of the images after drift correction with SWIFT in FIJI. Scale bar: 10 µm.

4.2.4 Epidermal cells are shed inside.

Using the established live-imaging protocol, I then investigated how epidermal cells are removed in the planarian epidermis. Are epidermal cells removed by apical extrusion, similar to intestinal epithelia or are epidermal cells removed by basal extrusion and enter the internal tissue? The time-lapse images were taken over a period of two to three hours. Interestingly, the results show that epidermal cells were removed by internalization. From 6 movies containing a total of ~4800 cells, 9 internalization events were observed in a total of 12 hours. **Figure 32 & 33** show that Reddot™1-labeled nuclei underwent internalization and moved toward the interior of the animal. The internalizing cells moved ~15 µm inward in ~2 minutes and the nucleus remained in the deeper tissue layers after internalization.

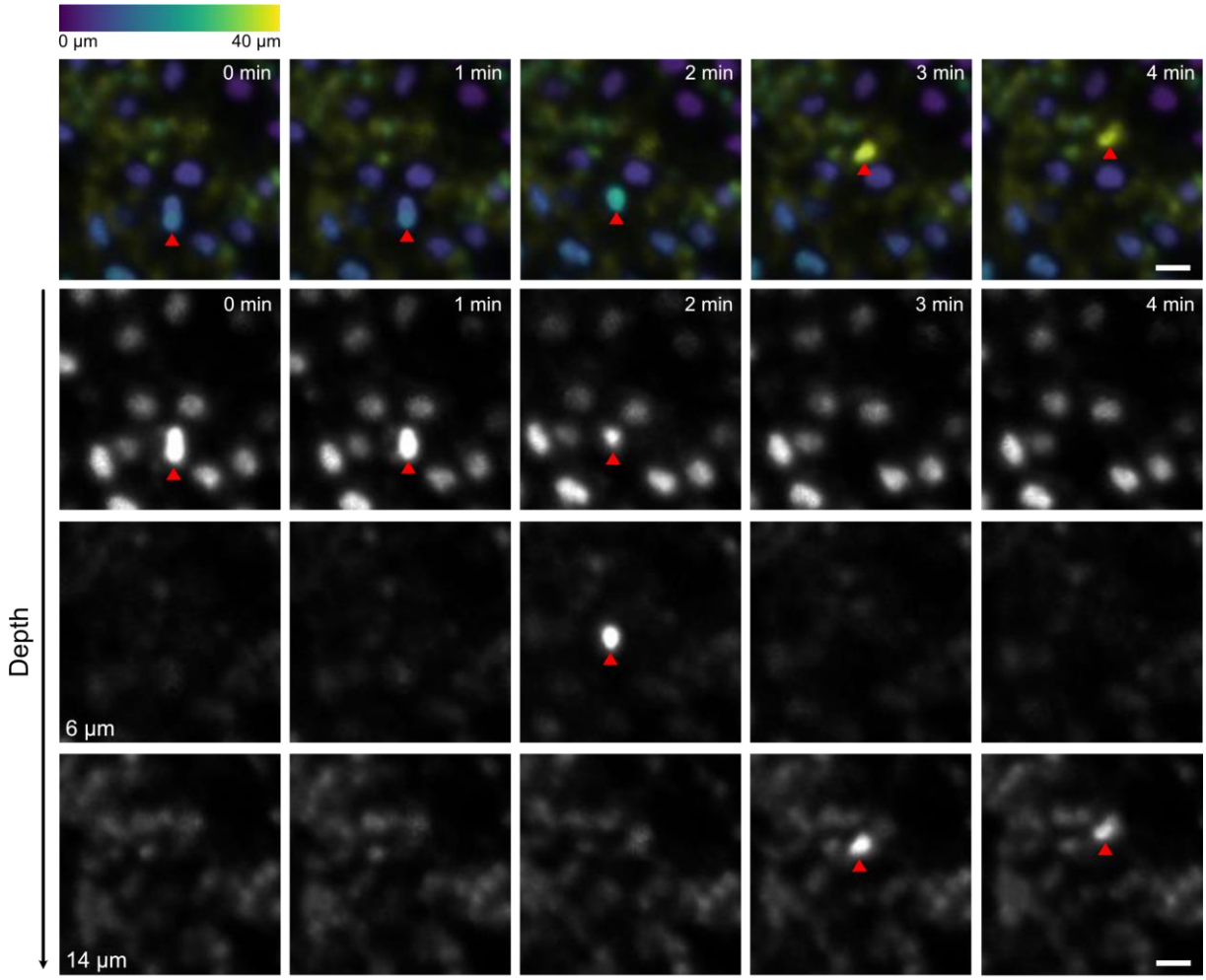

Figure 32. Epidermal cells were eliminated by internalization

The first row consists of time-lapse images that were color coded and maximum projected. The column indicates the time at which the images were acquired. The nuclei were labeled with RedDot™1. The color scale at the top indicates the depth of the objects (blue: surface layer; yellow: deepest layer). Images were processed using CARE and drift corrected using SWIFT in FIJI. Images were color coded using the integrated color LUT (mpl-viridis) in FIJI. The second through fourth rows consist of single confocal section images and the row corresponds to the depth of the images. The red arrowheads indicate the internalizing nucleus. Scale bar: 10 µm.

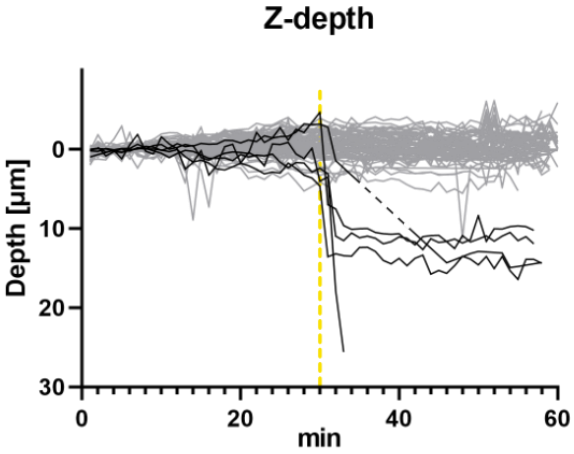

Figure 33. Quantification of the z-depth of RedDot™1-labeled epidermal nuclei.

The dark line corresponds to the internalizing cell that internalized at 30 min. The gray lines represent the other non-internalizing epidermal cells. These data were analyzed using IMARIS. The depth of each object was normalized to the average z-depth of all nuclei for the first 10 time points. Data were collected from 5 movies recorded from 4 samples. The time (30 min) when internalization happened was indicated by the yellow dashed line. The average was set to 0. (Data analyzed by Dr. Tobias Boothe).

Live imaging of Reddot™1-labeled epidermis shows the relocation of the nuclei of epidermal cells toward the internal tissues. However, this assay cannot answer the question of whether the epidermal cytoplasm also moved toward the internal tissues and whether epidermal cells underwent basal extrusion, in which the cells were squeezed toward the basal membrane by surrounding cells. To answer this question, I labeled the epidermis with CellTracker™ Deep Red Dye to visualize the cytoplasm and the outline of the epidermal cells. The data indicate that indeed the entirety of the epidermal cell moved inward, with the surrounding cells sealing the gap left by the internalizing cells **(Figure 34)**. Therefore, the results here suggest that planarian epidermal cells were eliminated by basal extrusion.

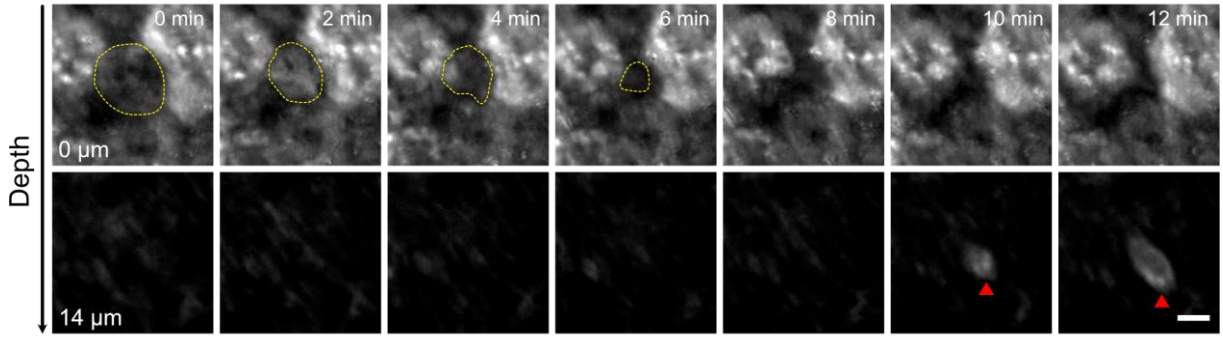

Figure 34. Time lapse recordings of CellTracker™ Deep Red labeled epidermis.

The column indicates the different time points at which the images were acquired. The row corresponds to the depth of the images. The first row consists of maximum projected images (3 stacks with a total depth of 2 µm). The second row consists of single confocal section images. The yellow dashed lines outline the basally extruded cells on the surface. The red arrowheads highlight the extruded cell in the deeper layer. Images were denoised and drft-corrected. Scale bar: 10 µm.

Previous studies have reported that epithelial cells underwent apoptosis prior to basal extrusion in different systems. For example, in *Drosophila*, epithelial cells underwent apoptosis before delamination, and apoptosis was required for the basal extrusion of epithelial cells (Levayer et al., 2016; Nakajima et al., 2011; Ohsawa et al., 2018; Teng et al., 2017; Toyama et al., 2008). Here, I was interested in whether the epidermal cells also underwent apoptosis before entering internally in planarians. Interestingly, TUNEL-positive cells, indicative of fragmented DNA, were also observed in epidermal cells, indicating that apoptosis occurs in epiderma cells **(Figure 35)**. In addition, nuclear intensity increased in the internalizing cells prior to internalization, indicating nuclear condensation, a hallmark of apoptosis, occurred in epidermal cells prior to internalization **(Figure 36)**. Both results provide the evidence that planarian epidermal cells may undergo apoptosis before basal extrusion.

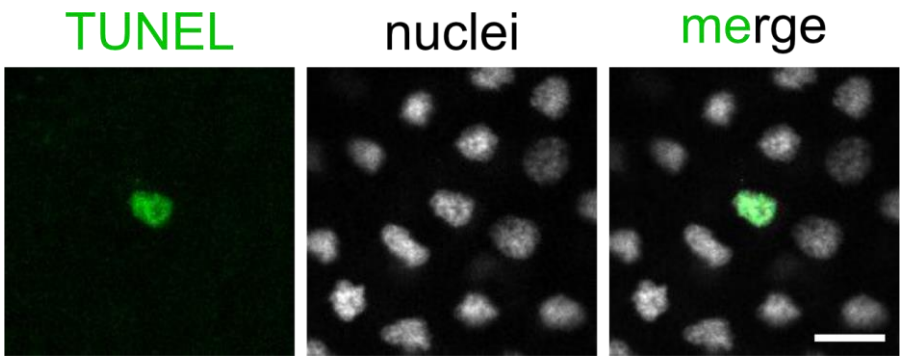

Figure 35. TUNEL staining on the planarian epidermis.

The single confocal section images show the colocalization of the TUNEL-positive signal with the epidermal nucleus. Nuclei were labeled with DAPI. Scale bar: 10 µm.

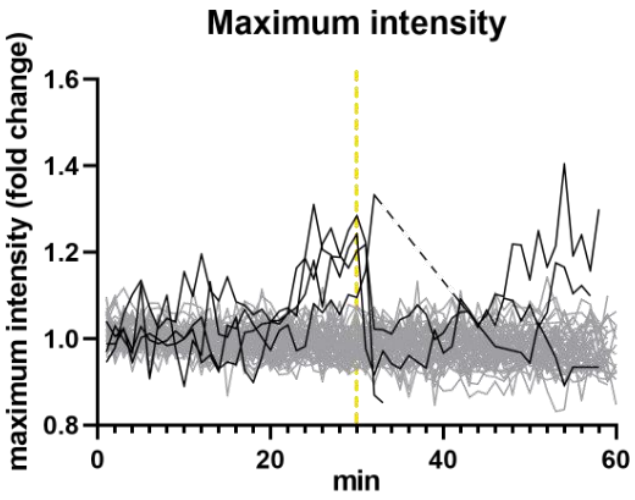

Figure 36. Quantification of epidermal nuclei intensity over time.

The fold change in intensity of individual nuclei was plotted. The dark line represents the internalizing cell and the gray lines correspond to the other non-internalizing cells. The nuclei were internalized at 30 min (yellow dashed line). The maximum intensity of each object was normalized to the average intensity of all epidermal nuclei from the first ten minutes. The average intensity was set to 1. Data were collected from 4 movies from 3 samples. (These data were analyzed by Dr. Tobias Boothe).

4.3 Summary

In this chapter, I established a live imaging protocol that includes live dye labeling of epidermal cells, anesthetic and agarose immobilization, low exposure time to reduce sample twitching and post-analysis to improve the reduced signal-to-noise ratio of the images. The live imaging protocol was used to observe the elimination of the epidermis in planarians, and the results show that epidermal cells underwent basal extrusion and entered inward in the animals. In addition, the results from TUNEL labeling and intensity quantification of nuclei provide an indication that epidermal cells may undergo apoptosis prior to internalization.

Chapter 5: The fate of internalized epidermal cells

5.1 Introduction

The results of the previous chapter showed that epidermal cells were extruded by basal extrusion and entered the inner tissues. In this chapter, I was interested in the final destination of the internalized epidermis. Beneath the epidermis is the collagen-rich basal membrane, followed by the body wall muscle (Chan et al., 2021; Cote et al., 2019; Hori, 1979). Between the body wall muscle layer and the gut is the mesenchymal tissue **(Figure 8)**. One of the interesting questions is whether the internalized epidermal cells end up in the mesenchyme or in the intestine. Second, how are internalized epidermal cells cleared once they enter internal tissues? As described in the first chapter, clearance of dead cells is important for tissue homeostasis. Failure to remove dead cells can lead to inflammation in the body (Nagata et al., 2010). It is still unclear whether macrophage-like immune cells exist in planarians to remove dead cell bodies. So far, two cell types are known to be capable of phagocytosis. One is the intestinal phagocytes, which are responsible for food digestion by phagocytosing food particles in the intestine (Forsthoefel et al., 2020; Forsthoefel et al., 2012; Ishii & Sakurai, 1991; Willier et al., 1925). The other is the *cathepsin*$^{+}$ cells which have been shown to be capable of phagocytosing bacteria in planarians (Scimone et al., 2018). However, it is still unknown whether these two cell types are responsible for the clearance of dead cell bodies. In this chapter, I would first like to understand the fate of basally extruded epidermal cells. Second, I was interested in understanding the clearance mechanism for the internalized epidermal cells.

5.2 Results

5.2.1 Internalized epidermal cells descend into the intestine

To locate the destination of the basally extruded epidermal cells, I first performed a two-color live imaging experiment on the samples with labeled epidermal nuclei and used the labeled intestine as a reference for the deepest tissue. The intestine was labeled by feeding with CellTracker™ Red CMTPX Dye, containing a bromomethyl group that can form covalent binding with thiol-containing amino acids in the red spectrum. The epidermal nuclei were then labeled with RedDot™1 in the far-red spectrum **(Figure 37)**. Interestingly, the time-lapse imaging results show that the internalized epidermal cells directly approached gut branches within 4 min after internalization **(Figure 38)**. This result suggests that basally extruded epidermal cells might enter the intestine eventually. However, due to the limited time span for the time lapse recordings, the live imaging approach was not able to show whether basally extruded epidermal cells entered the intestine.

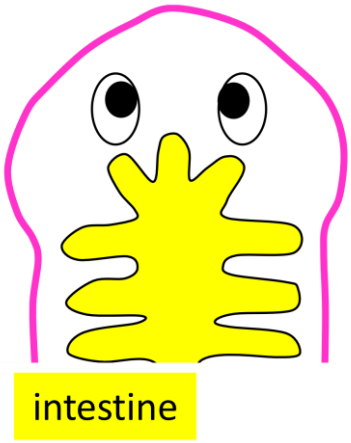

Figure 37. Dye labeling of samples for two-color live imaging.

The sample with dye-labeled epidermis (magenta) and intestine (yellow) was used for two-color imaging. The epidermal nuclei were labeled with Reddot™1. The intestine was labeled with CellTracker™ Red CMTPX Dye by feeding.

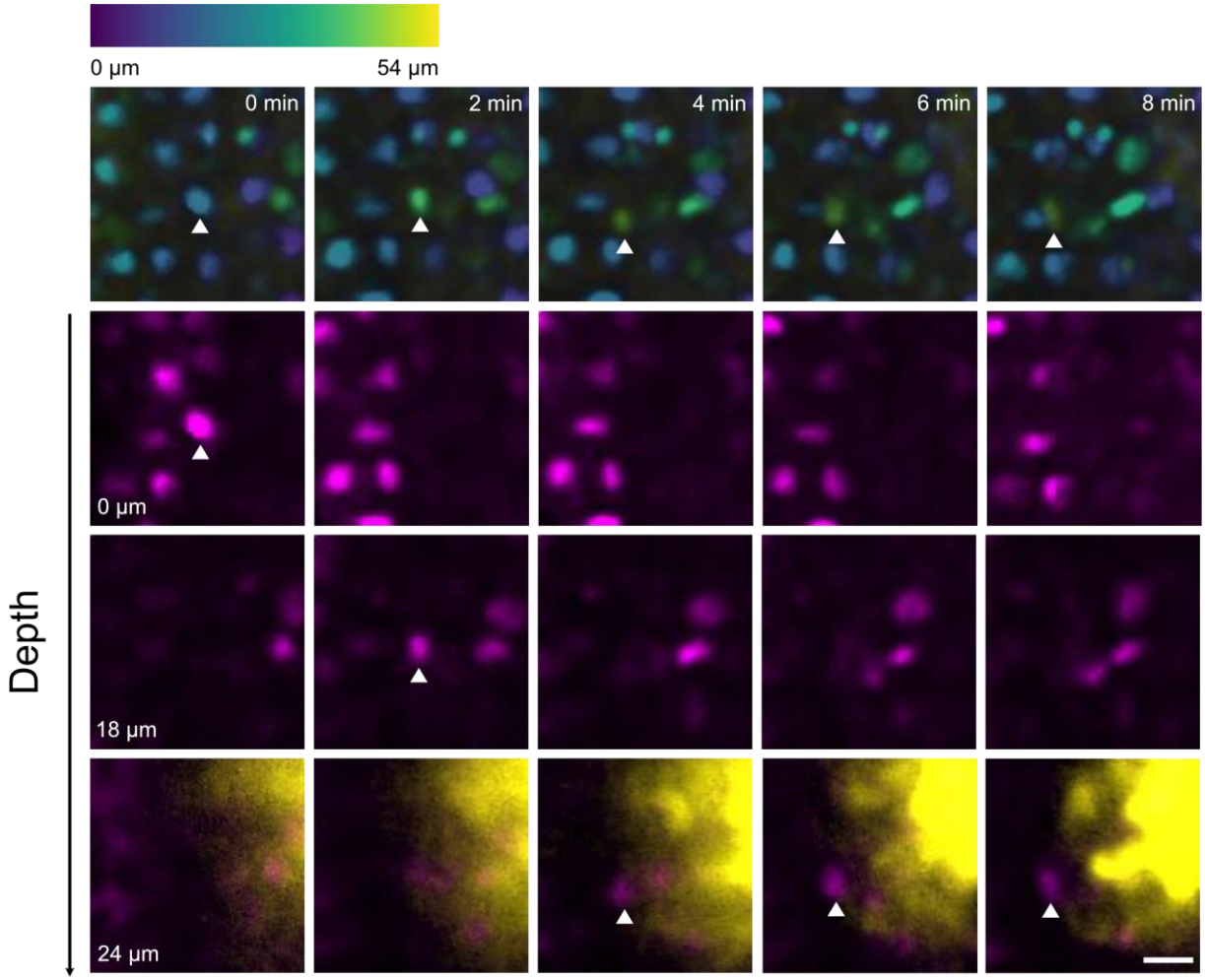

Figure 38. Basally extruded cells descend to the intestine.

The first row consists of the time-lapse images that were color-coded and maximum projected. The epidermal nuclei were labeled with RedDot™1. The columns indicate the time at which the images were acquired. The color scale at the top shows the correspondence of the color to the depth of the objects (blue: surface; yellow: deepest layer). Images were color coded using the integrated color LUT (mpl-viridis) in FIJI. White arrowheads highlight the internalizing cell. The second to fourth rows consist of single confocal section images of RedDot™1-labeled epidermal nuclei. Yellow color in the fourth row refers to the deep gut branch. White arrowheads indicate the internalizing nucleus. Images were denoised with CARE and drift corrected using Fast4Dreg in FIJI. Magenta: nuclei. Yellow: an intestinal branch. Scale: 10 µm.

As an alternative approach, I labeled the epidermis with CFSE and then observed whether CFSE-labeled surface epidermal cells appeared in the intestine 4 days after the CFSE pulse **(Figure 39)**. The results show that $CFSE^{+}$ objects were present in the intestine 4 days after the CFSE pulse, indicating that the internalized epidermal cells eventually

entered the intestine. Furthermore, no CFSE$^+$ objects were observed in the intestine at 0 day post CFSE pulse, when the epidermis was labeled with CFSE just before fixation **(Figure 40)**. This observation suggests that the CFSE$^+$ signals in the intestine were not due to penetration of CFSE dye into the intestine during the CFSE pulse. Furthermore, CFSE$^+$ objects were not observed in the mesenchymal tissue, and this observation further confirms the live imaging results that the epidermal cell entered into the intestine without staying in the mesenchyme **(Figure 41)**. In summary, the results here provide the evidence that internalized epidermal cells entered the intestine after basal extrusion **(Figure 42)**.

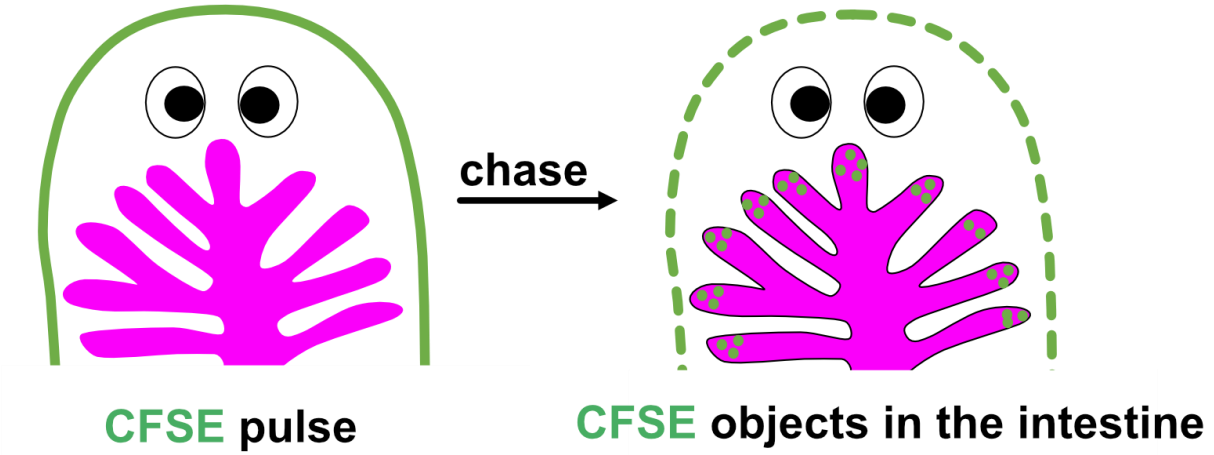

Figure 39. Hypothesis: Epidermal cells enter the intestine after basal extrusion.

To test the hypothesis that epidermal cells enter the intestine, the epidermis was pulsed with CFSE (green) (left panel) and the samples were fixed after chase to observe if CFSE$^+$ objects (green dots) appeared in the intestine (magenta).

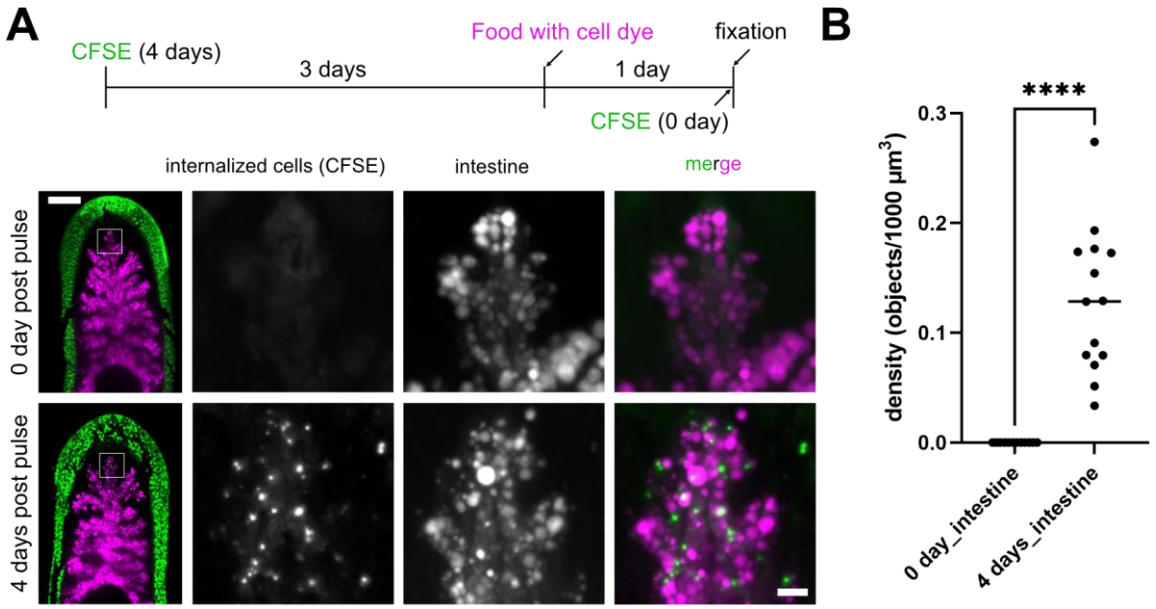

Figure 40. Basally extruded epidermal cells appeared in the intestine.

(A) The upper cartoon shows the experimental design. Worms were labeled with CFSE 4 days or immediately (0 day) prior to fixation. To visualize the intestine, worms were fed liver containing CellTracker™ Deep Red Dye (magenta) one day prior to fixation. The far left panel consists of overview images and the right panels show the images from the CFSE and CellTracker™ Deep Red Dye (intestine) channels with magnified view from the white squares in the left panel. The images were maximum projected. The scale bar (left panel): 100 µm; scale bar (right panel): 10 µm. (B) The density of $CFSE^+$ objects in the intestine was quantified by dividing the number of $CFSE^+$ objects by the volume of the intestine in the selected areas. The gray-scale images of CFSE and CellTracker™ Deep Red Dye labeled objects were converted into binary by thresholding in FIJI, and the number and volume of objects were quantified using Cellprofiler. (Details of image analysis are documented in Materials and Methods). 12 worms and 14 worms were analyzed in 0 day and 4 days respectively. Mann-Whitney-U-Test was used to compare density differences between conditions. ****: $p<0.0001$.

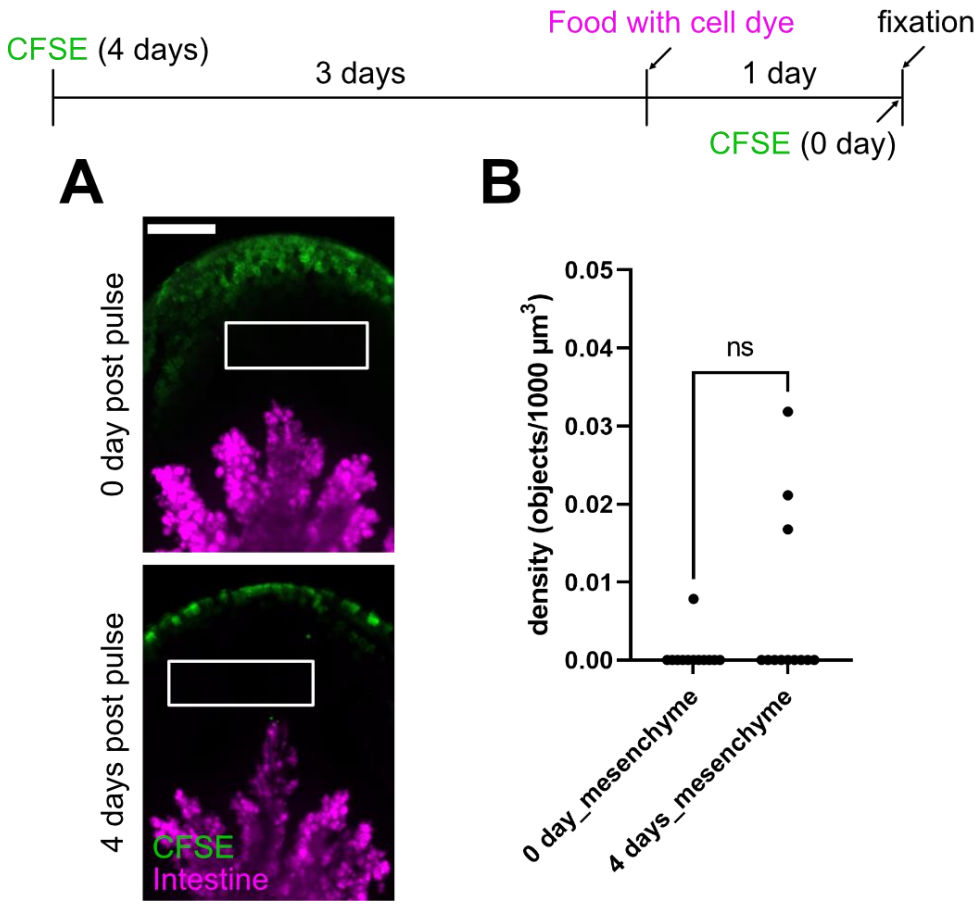

Figure 41. No internalized epidermal cells appeared in mesenchymal tissues.

(A) The top and bottom panels show the maximum projected images of the 0 day and 4 days post CFSE samples respectively. The white rectangles outline the mesenchymal tissue between the epidermis and the intestine. The intestines were labeled with CellTracker™ Deep Red Dye (magenta) by feeding one day prior to fixation (top cartoon). Scale bar: 50 µm. (B) Quantification of $CFSE^+$ density in the mesenchyme. Density was quantified by dividing the number of $CFSE^+$ objects by the total volume of the selected mesenchyme. The $CFSE^+$ objects from the gray scale images were converted to binary for analysis by thresholding inf FIJI. The number of $CFSE^+$ objects was then quantified using Cellprofiler. 12 worms were analyzed in both 0 day and 4days. The Mann-Whitney-U-Test was used to test whether there is a significant difference between two experimental conditions. ns: non-significant.

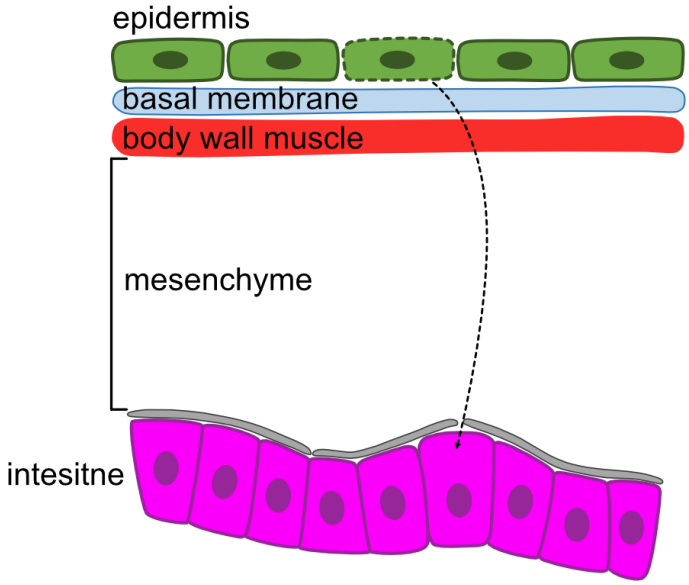

Figure 42. Schematic conclusion of the final destination of basally extruded epidermal cells.

The basally extruded epidermal cell breaks through the basal membrane, the layer of body wall muscle and mesenchymal tissue, and then enters the intestine.

5.2.2 Internalized epidermal cells colocalize with intestinal phagocytes.

The planarian intestine is composed of three distinct cell types: absorptive phagocytes, secretory goblet cells, and basal cells that outline the intestinal branches (Fincher et al., 2018; Forsthoefel et al., 2020; Forsthoefel et al., 2012; Forsthoefel et al., 2011; Ishii, 1965; Willier et al., 1925). Intestinal phagocytes digest nutrients via phagocytosis, followed by intracellular digestion and nutrient storage (Garciacorrales & Gamo, 1988; Willier et al., 1925). Previous results show that internalized epidermal cells ended up in the intestine. The next question would be whether the epidermal cells are phagocytosed by intestinal phagocytes. To test this hypothesis, I simultaneously visualized $CFSE^+$ objects in the intestine and the expression of the phagocyte maker gene *Smed_dd_75* (Fincher et al., 2018). The results show that $CFSE^+$ signals colocalized with *Smed_dd_75* expression in the 4 days post CFSE pulse samples, but not in the 0 day post CFSE pulse samples, indicating that epidermal cells are ultimately colocalized intestinal phagocytes **(Figure 43)**. In conclusion, the colocalization of $CFSE^+$ objects and intestinal

phagocytes indicates that internalized epidermal cells entered the intestine and were engulfed by intestinal phagocytes.

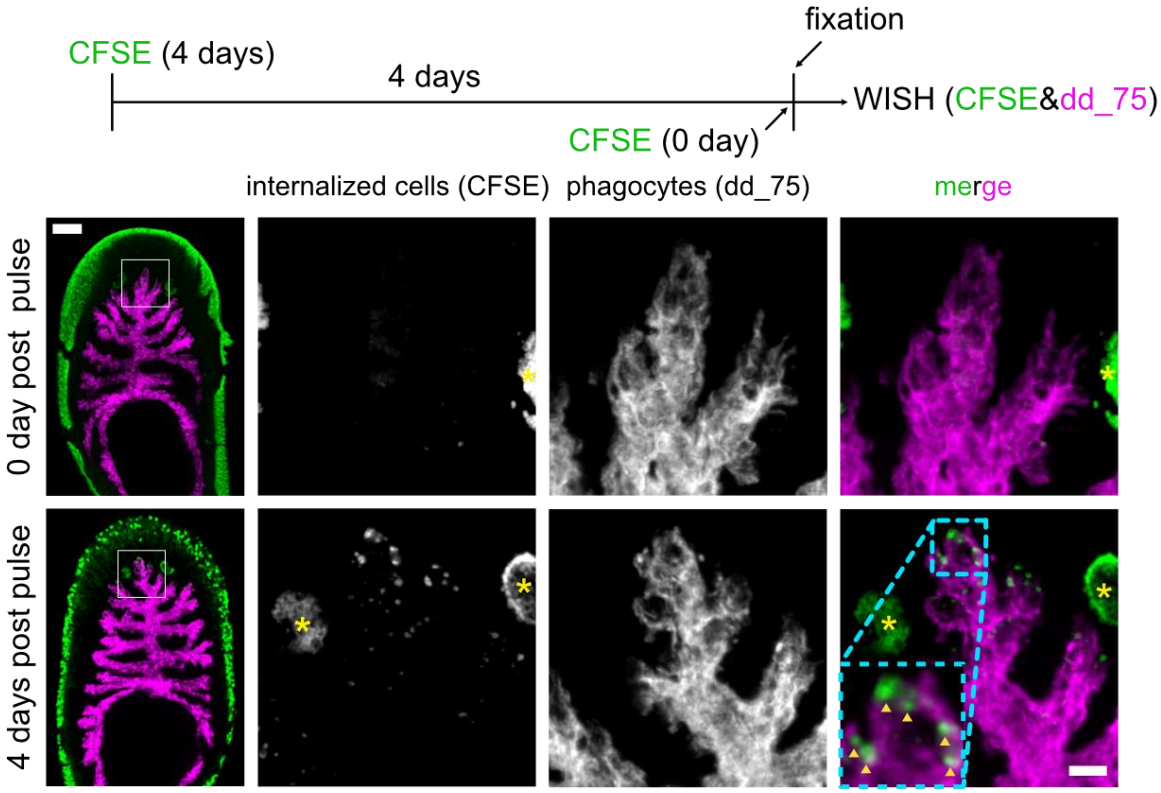

Figure 43. Colocalization of the internalized epidermal cells with intestinal phagocytes.

Maximum projected images of *in situ* hybridization of *Smed_dd_75* at 0 and 4 days after CFSE pulse samples are shown in the top and bottom rows, respectively. The top cartoon shows the experimental design. Samples were labeled with CFSE immediately (0 day) or 4 days before fixation. After fixation, $CFSE^{+}$ objects were visualized by anti-fluorescein antibody (green) and the intestinal phagocytes was visualized by *in situ* hybridization of *Smed_dd_75* (magenta) (the detailed experimental procedure is described in Materials and Methods). The left panel consists of overview images and the three right panels consist of the images with magnified view for the white squares in the corresponding left panels. The light blue dashed lines show the colocalization of $CFSE^{+}$ signals and phagocytes (yellow arrowheads). Yellow stars indicate non-specific staining in the photoreceptors. Scale bar (left panel): 100 µm. Scale bar (right panel): 20 µm.

To further confirm this conclusion, I intended to deplete the intestinal phagocytes by knocking down *hnf4*, which encodes an intestinal fate-specific transcription factor (Raz et al., 2021; van Wolfswinkel et al., 2014). The expression of *hnf4* genes was silenced by

feeding double-stranded RNA. If intestinal phagocytes are responsible for clearing the basally extruded epidermal cells, the cells would accumulate in the mesenchyme when the intestinal phagocytes are ablated. The results show the accumulation of CFSE$^+$ structures in the *hnf4* RNAi worms 2 days post CFSE staining and no CFSE$^+$ objects were observed in the control (*gfp* RNAi) worms **(Figure 44)**, further supporting the idea that intestinal phagocytes are involved in the clearance of internalized epidermal cells. However, this experiment was difficult to replicate due to the early development of the lethal phenotype before the observation of CFSE$^+$ object accumulation in the mesenchyme. I therefore continued with an alternative approach to confirm the role of intestinal phagocytes in tissue clearance.

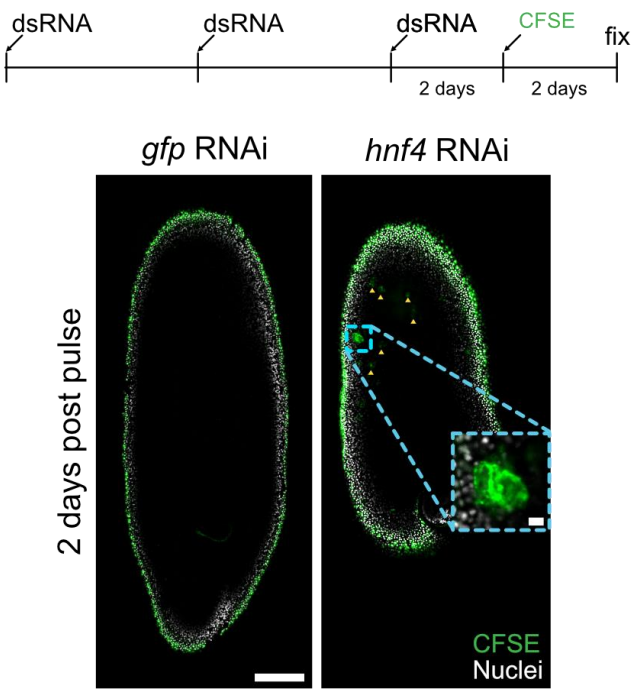

Figure 44. Accumulation of basally extruded epidermal cells in *Smed_hnf4* RNAi worms.

hnf4 was knocked down by feeding double-stranded RNA (dsRNA). 3 mm worms were fed with 2 mg/mL dsRNA in liver paste three times in one week and worms were fixed 2 days after CFSE staining (top cartoon). The single section of confocal images of *gfp* control RNAi (left panel) and *hnf4* RNAi (right panel) worms are shown. The yellow arrowheads indicate the accumulation of CFSE$^+$ objects in the mesenchyme. Nuclei were labeled with DAPI. Scale bar in left panel: 100 µm. Scale bar in magnified image: 10 µm.

5.2.3 Internalized epidermal cells are digested by intestinal phagocytes.

Since intestinal phagocytes digest food via phagocytosis and intracellular digestion, I was interested in whether intestinal phagocytes also digest internalized cells, which is similar to the degradation process when phagocytic cells remove dead cells. After phagocytes engulf particles, the phagosome forms and fuses with the lysosome, an acidic organelle containing digestive enzymes, to lyse the engulfed particles (Kinchen & Ravichandran, 2008). To test the hypothesis that epidermal cells are digested in intestinal phagocytes, I attempted to block intracellular digestion with the lysosome inhibitor, chloroquine, which raises the pH of lysosomes (Halcrow et al., 2021; Homewood et al., 1972; Mauthe et al., 2018; Schlesinger et al., 1988). If internalized epidermal cells ($CFSE^+$) are digested in phagocytes, $CFSE^+$ objects would accumulate in the intestine when intracellular digestion is blocked **(Figure 45)**. First, I tested whether chloroquine would lead to severe effects on the physiological functions of planarians. I observed the survival rate and conducted *in situ* hybridization to visualize the intestinal structures in the planarians cultured in chloroquine. The results show that planarians could survive for more than two weeks without causing significant changes on their intestinal structures after being cultured in 5 μM chloroquine **(Figure 46)**. Then, I performed the CFSE pulse experiment in the chloroquine-treated planarians and compared the volume of $CFSE^+$ objects in the intestine. Interestingly, the results show that the volume of $CFSE^+$ objects was larger in the chloroquine-treated samples compared to the control samples cultured in plain planarian water **(Figure 47 & 48 A)**. Furthermore, the density of $CFSE^+$ objects in the intestine was also higher in the intestine after chloroquine treatment **(Figure 48 B)**. These results indicate that internalized epidermal cells were digested by intestinal phagocytes after engulfment. Furthermore, the density of $CFSE^+$ objects was also higher in the mesenchyme under chloroquine treatment **(Figure 49)**, indicating that some

internalized epidermal cells cannot be cleared by intestinal phagocytes, probably due to the overloading of the engulfment capacity by the accumulation of the epidermal corpse inside the phagocytes. In conclusion, these results strongly support the idea that epidermal cells are digested by intestinal phagocytes after entering the intestine.

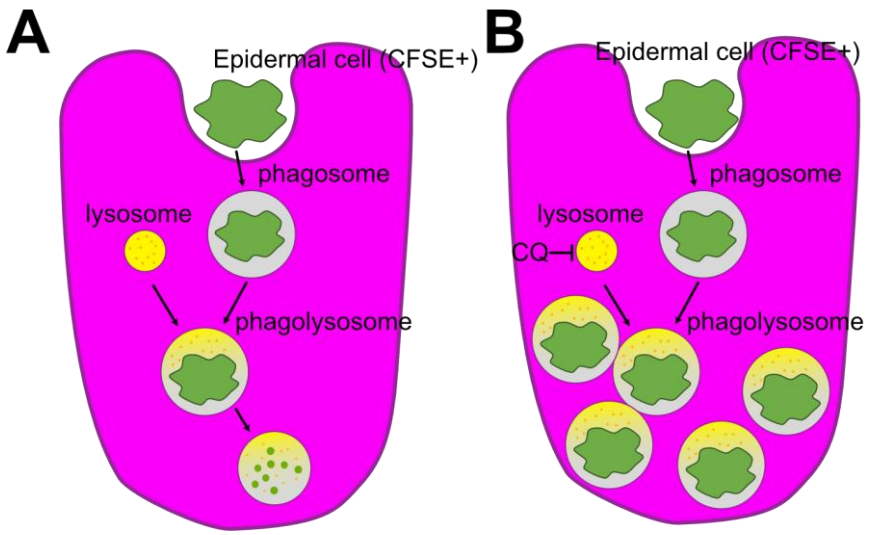

Figure 45. Hypothesis: Internalized epidermal cells are digested in the intestinal phagocytes.

(A) Internalized epidermal cells ($CFSE^+$) are phagocytosed by the intestinal phagocytes. Phagosomes are formed in the cytoplasm and fuse with lysosome to degrade the engulfed epidermal cell. (B) Treatment with chloroquine (CQ) inhibits the functions of lysosomes and causes the failure of degradation of internalized epidermal cells, which in turn leads to the accumulation of $CFSE^+$ objects in intestinal phagocytes.

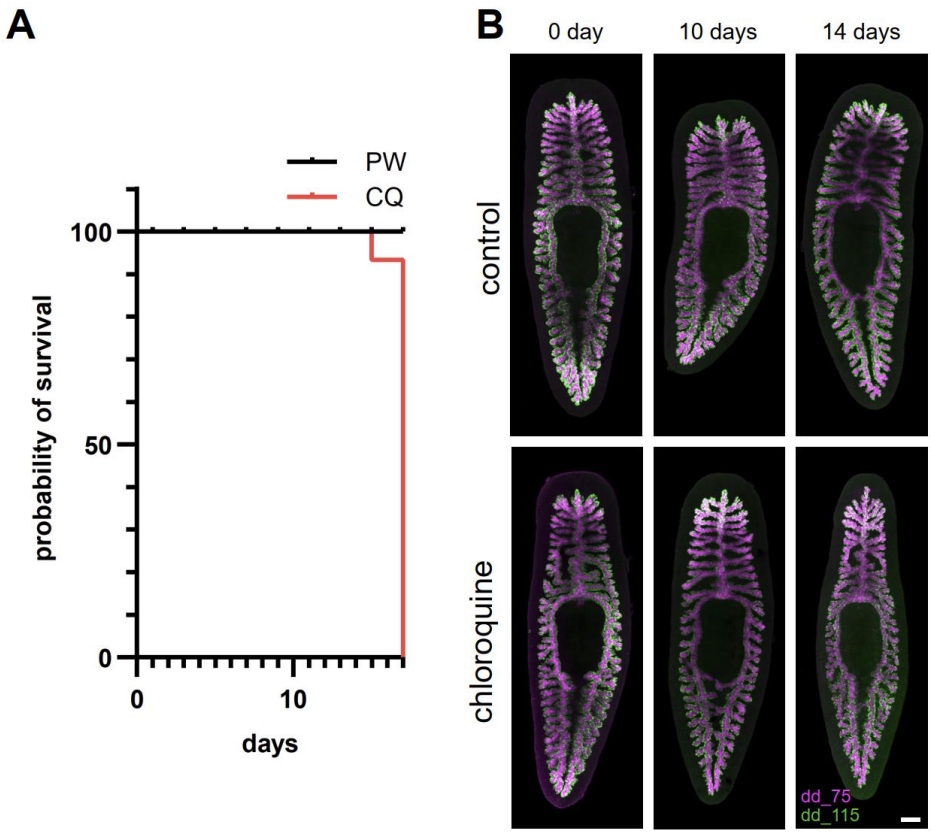

Figure 46. The survival rate and intestinal structure of planarians cultured in chloroquine.

(A) The survival rates of planarians cultured in planarian water (control) or in 5 µM chloroquine. The 5-6 mm worms were used and starved for one week before the survival rate counting. These data were collected from three independent replicates with N=5 worms in each replicate. (B) *in situ* hybridization of phagocytes (dd_75) and basal cell (dd_115) marker genes on the worms cultured in planarian water (control) or 5 µM chloroquine. The sample were fixed at different days (0 day, 10 days & 14 days) post planarian water or 5 µM chloroquine incubation and proceeded for *in situ* hybridization. 5-6 mm worms were used for this experiment. The images were maximum-projected. Scale bar: 200 µm.

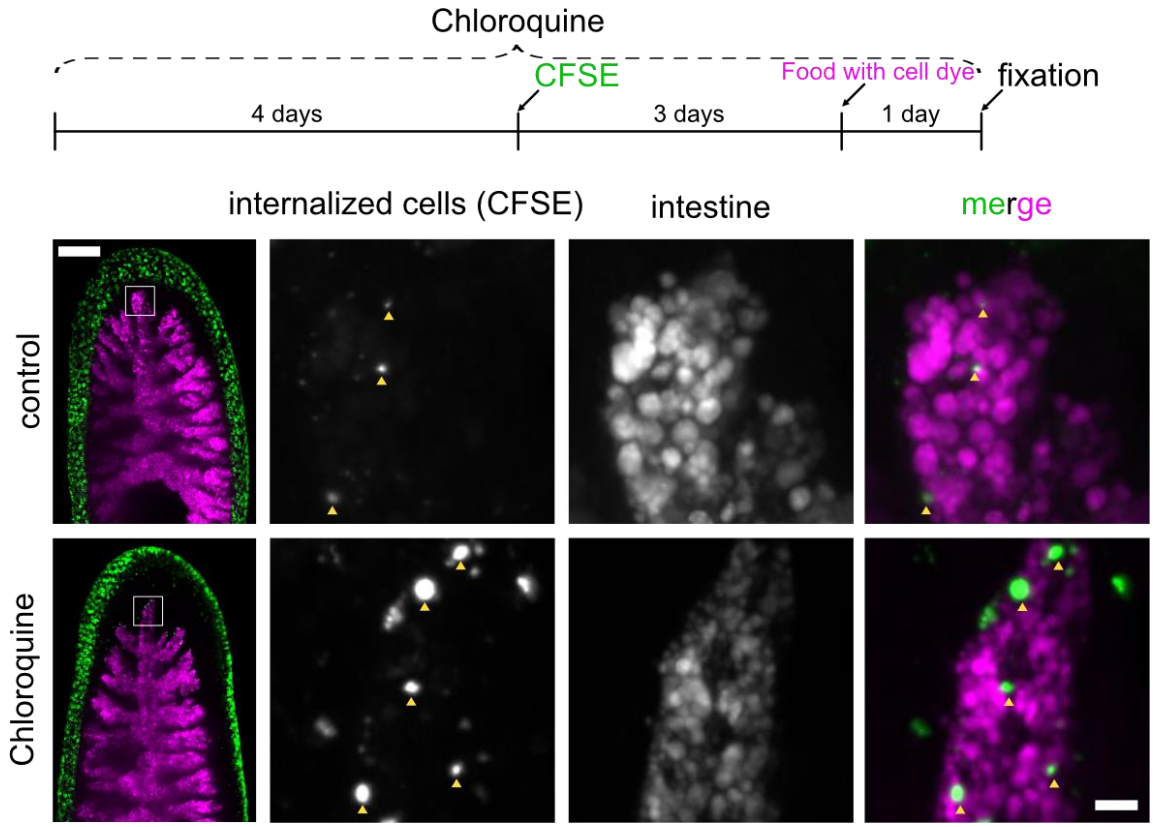

Figure 47. Chloroquine treatment caused the accumulation of internalized epidermal cells in the intestines.

The upper cartoon shows the experimental design. Worms were first soaked in planarian water containing chloroquine for 4 days first and epidermal cells were labeled with CFSE on the fifth day. Samples were fixed 4 days after the CFSE pulse. One day before fixation, worms were fed liver containing CellTracker™ Deep Red Dye to visualize intestinal structures. For the control (top row), worms were cultured in plain planarian water. Images were maximum projected. The left panel consists of the overview images and the images in the right panels are the magnified views of the white squares in the left panel. The yellow arrowheads indicate the $CFSE^{+}$ objects in the intestines. Scale bar (left panel): 100 µm; scale bar (right panel): 10 µm.

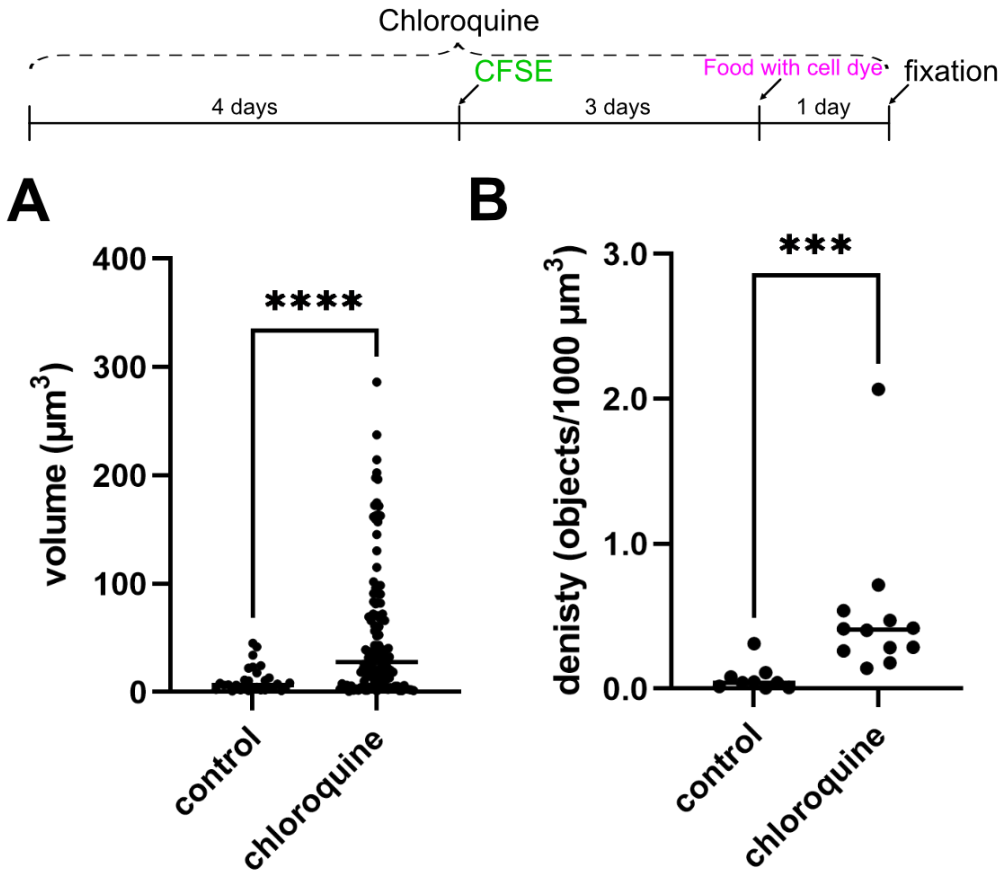

Figure 48. Quantification of volume and density of CFSE⁺ objects between control and chloroquine treatment.

The volume of CFSE⁺ objects (A) and the density of CFSE⁺ objects in the intestine (B) were quantified between the control group (cultured in plain planarian water) and the chloroquine group 4 days after the CFSE pulse. The top cartoon shows the experimental design. (A) Each dot represents a single CFSE⁺ object. 9 worms in control and 12 worms in chloroquine were used for analysis. (B) Each dot represents the CFSE⁺ density calculated from one worm. Density was quantified by dividing the number of CFSE⁺ objects by the volume of intestine in the selected regions. 9 worms in control and 12 worms in chloroquine were analyzed. For quantification of the number and density of CFSE⁺ objects, the gray scale images of CFSE labeling in the intestines were converted to binary images by thresholding in FIJI. The binary images were used for quantification by Cellprofiler. The Mann-Whitney-U-Test was used to test for significant differences between the control and chloroquine-treated groups. ****: $p<0.0001$; ***: $p<0.001$.

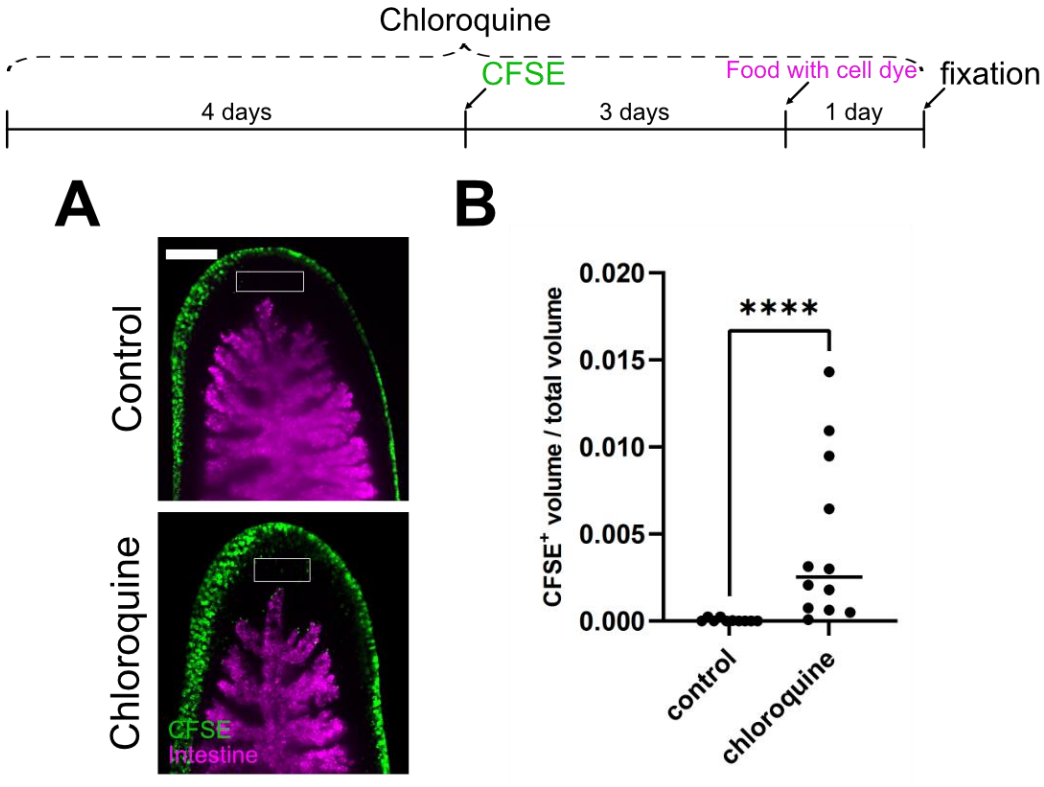

Figure 49. Accumulation of internalized epidermal cells in the mesenchyme after chloroquine treatment

The upper cartoon shows the experimental design. Samples were treated with chloroquine for 4 days before the CFSE pulse and fixed 4 days after the CFSE pulse. The intestines were labeled with CellTracker™ Deep Red Dye one day prior to fixation. (A) Maximum projected images of control (in plain planarian water) (top) and chloroquine-treated worms (bottom) that were fixed 4 days post CFSE staining. Scale bar: 100 µm. (B) The ratio of $CFSE^+$ volume to total volume in the selected regions corresponding to mesenchyme (white brackets in (A) was quantified. Each point represents one quantification from one worm. 10 worms in control and 12 worms in chloroquine were used for analyses. Binary images converted from gray-scale images of CFSE labeling were analyzed using Cellprofiler. Mann-Whitney-U-Test was used to compare whether the two results were significantly different. ****: $p<0.0001$.

5.3 Summary

In this chapter, I uncovered the fate of the internalized epidermal cells. First, using two-color time-lapse recordings, I found the relocation of epidermal cells from epidermis to the intestinal branch. Second, I used the CFSE pulse assay to locate the final destination of the basally extruded epidermal cells, and the results show that the CFSE-labeled epidermal cells ended up in the intestine of planarians. Third, the colocalization of $CFSE^+$ signals (internalized epidermal cells) and expression of a gut phagocyte gene (*Smed_dd_75*) in the intestine indicates that the epidermal cells were engulfed by intestinal phagocytes. Finally, the accumulation of $CFSE^+$ signals in the intestine after the lysosomal inhibitor treatment provides the evidence that internalized epidermal cells were digested inside the intestinal phagocytes. In conclusion, the results of this chapter demonstrate that the basally extruded epidermal cells reached the intestine and were digested by intestinal phagocytes, suggesting that the planarian gut phagocytes are responsible for clearing basally extruded epidermal cells, which may allow their reuse as energy resource **(Figure 50)**.

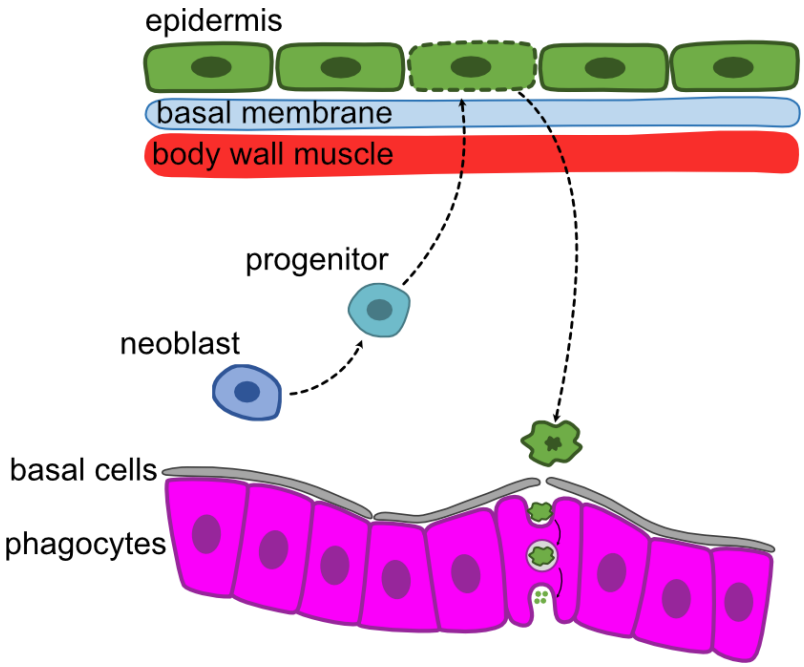

Figure 50. Model of the removal of epidermal cells in planarians.

Planarian epidermal cells are removed by basal extrusion. Basally extruded epidermal cells pass through the basal membrane, the muscle layer of the body wall and the mesenchyme to reach the intestine. Finally, the cells are digested intracellularly by intestinal phagocytes.

Chapter 6: Discussion

6.1 Assay development to quantify the epidermal cell turnover rate and its limitations

In Chapter 2, I developed an assay that allowed me to quantify the epidermal turnover rate of planarians. This assay involves covalent dye labeling and deep learning-based automatic segmentation. The results of the validation experiment with irradiated planarians, whose neoblasts were ablated, rule out the possibility that the disappearance of pulse-labeled signals over time resulted from the dye leakage from the pulse-labeled epidermal cells. Instead, the disappearance of the pulse-labeled signals resulted from the replacement of resident cells (pulse-labeled) by the newly incorporated cells (dye-negative). With the development of the assay, the planarian epidermis can be used as a platform to study cell turnover. Furthermore, the results indicate that the epidermal progenitor pool was depleted at 11 days post-irradiation since the ratio of resident cells (CFSE) to all cells (DDAO) plateaued at 11 days post-irradiation **(Figure 20 & 51)**. These results are also consistent with previously published results. Tu and colleagues found that late epidermal progenitor cells (agat-1^{+}) disappeared 10 days post-irradiation respectively (Eisenhoffer et al., 2008; Tu et al., 2015), suggesting that all epidermal progenitor cells had differentiated into mature epidermal cells within 10 days post-irradiation and that no new epidermal cells were able to be incorporated into the epidermis. In summary, their conclusion is identical to the results from the pulse-chase dye labeling assay and this reinforces the validity of my assay to measure cell turnover rate in the planarian epidermis.

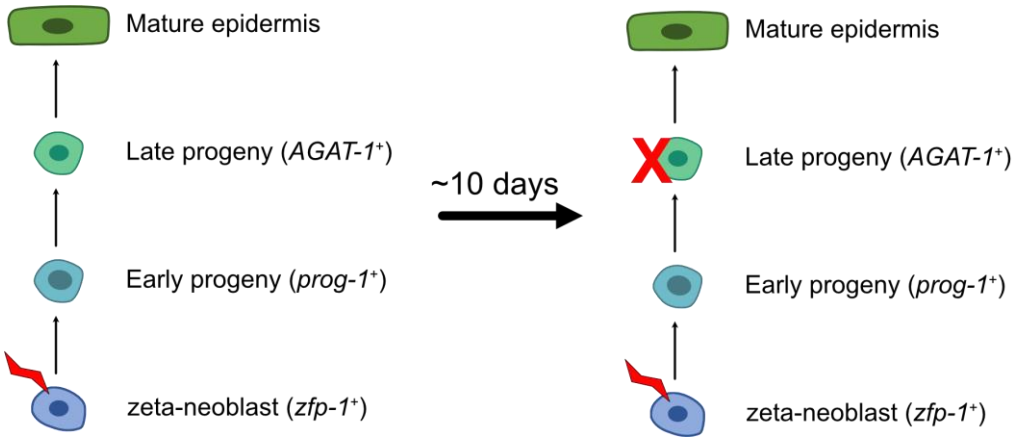

Figure 51. Disappearance of late epidermal progenitors after irradiation

Late epidermal progenitors disappear approximately 10 days after the depletion of zeta-neoblasts (specialized neoblasts for the epidermal lineage) by irradiation.

However, the assay still has several technical limitations. First, the dorsal Stardist model cannot reliably segment DDAO$^+$ cells (all cells present at the time of fixation) on the dorsal epidermis with an accuracy of less than 90%. This is likely due to the morphology of the dorsal epidermis. Dorsal epidermal cells are more densely populated and the surface of the dorsal epidermis is less smooth compared to the ventral epidermis (Gumbrys, 2017; Pedersen, 1976), resulting in a less clear outline of DDAO-labeled dorsal epidermal cells. Second, the chasing time is also limited. The signal intensity of the live cell dyes (CFSE and DDAO) decreased as the chase time increased, and the live dye signals were indistinguishable from the background 10 days after the pulse in the ventral epidermis. Therefore, further works are required for the segmentation of dorsal epidermis and increasing the chasing time of this assay.

6.2 The dependence of cell turnover rate on the body axes

I used the pulse-chase dye labeling assay developed in Chapter 2 to compare the turnover rates of epidermal cells in different areas (anterior vs posterior & dorsal vs

ventral). The results show that the ventral and dorsal epidermis have different turnover rates, with a higher turnover rate in the ventral epidermis **(Figure 21 & 22)**. This conclusion is consistent with the observation of worm morphology after irradiation. Irradiated planarians bend around their ventral side region **(Figure 52)**. This curvature could be explained by the shorter half-life of the ventral epidermis. The ventral epidermal cells disappear faster than the dorsal epidermal cells after irradiation due to the shorter half-life, which lead to the loss of support on the ventral surface and the curvature of the dorsal structures toward the ventral region. In the following paragraphs, I listed some factors that may contribute to the difference in the turnover rate between dorsal and ventral epidermis.

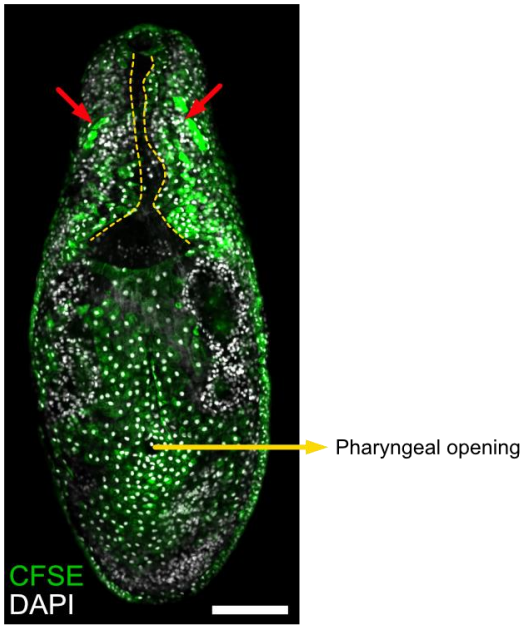

Figure 52. Ventral curve of an irradiated worm.

The sample was irradiated 13 days prior to fixation with CFSE labeling on epidermis. The image was surface extracted using Premosa. Worms are irradiated 13 days before fixation. Yellow dashed lines indicate the boundaries between ventral and dorsal epidermis. The red arrows indicate the bending of the dorsal structures towards the ventral sides. Scale bar: 100 µm.

6.2.1 Morphological difference

The difference in cell renewal rate between ventral and dorsal epidermis may result from the morphological differences in the epidermis. The ventral epidermis is multiciliated and the dorsal epidermis is less ciliated or non-ciliated (McGee et al., 1997; Pedersen, 1976; Rompolas et al., 2010). The results show that the ciliated ventral epidermis was replaced much faster than the dorsal epidermal cells, most of which are non-ciliated. Previous electron microscopy data showed that the cilia in the planarian epidermis are morphologically similar to the multiciliated epithelia in the mammalian trachea, with typical 9+2 microtubular axonemes driven by dyneins (Rompolas et al., 2013). Ciliated epithelia require a higher metabolic rate to maintain the energy-consuming beat of the cilia (King, 2016), and the higher metabolic rate may lead to the shorter lifespan of ciliated epithelia. For example, reactive oxygen species generated by metabolism can induce apoptosis (Redza-Dutordoir & Averill-Bates, 2016). To test whether the difference in epidermal lifespan is due to the difference in morphology, it would be interesting to observe the lifespan of the ventral epidermis with reduced number of cilia. One of the candidate genes to knock down is *Smed_ift88,* which encodes intraflagellar transport proteins, and previous studies have shown *Smed_ift88* worms had reduced cilia number on epidermal cells (Rink et al., 2009; Rompolas et al., 2010).

6.2.2 Mechanical stress

Besides the morphological difference, another difference between dorsal and ventral epidermis is the mechanical force. Planarians glide with ventral ciliated epithelial cells, which generates more wastage on the ventral epidermis (Rompolas et al., 2010; Vu et al., 2019). It was previously hypothesized that dying cells can send “division signals” and “differentiation signals” to stem cells and progenitors to induce the generation of

new differentiated cells (Death control model) (Pellettieri & Alvarado, 2007) **(Figure 53A)**. In the case here, more wastage on the ventral epidermis induces cell death and triggers the generation and maturation of new epidermal cells, leading to faster cell renewal than on the dorsal epidermis. This hypothesis can also explain the faster turnover rate in the anterior dorsal epidermis compared to the trunk and tail dorsal epidermal cells. The anterior epidermal cells are subject to greater mechanical pressure as they counteract water currents as the worms move.

6.2.3 Difference in gene expression signatures

Another possibility leading to the difference in cell replacement rate between the dorsal and ventral epidermis is the difference in gene expression signatures. A previous study has shown that gene expression signatures were different in the zeta-neoblasts and progenitors between the dorsal and ventral epidermal lineages, which are specified by BMP signaling (Wurtzel et al., 2017). It is possible that the difference in gene expression signatures determines the difference of the cell division rate of stem cells and the progenitor maturation rate, which in turn leads to the difference in cell replacement rate between dorsal and ventral epidermis. This hypothesis applies to the “stem cell or progenitor control model” (Pellettieri & Alvarado, 2007) **(Figure 53b)**, which suggests that stem cell division and progenitor maturation are the primary triggers for cell turnover, in which stem cells and progenitors send messages to mature cells and trigger the death of mature cells.

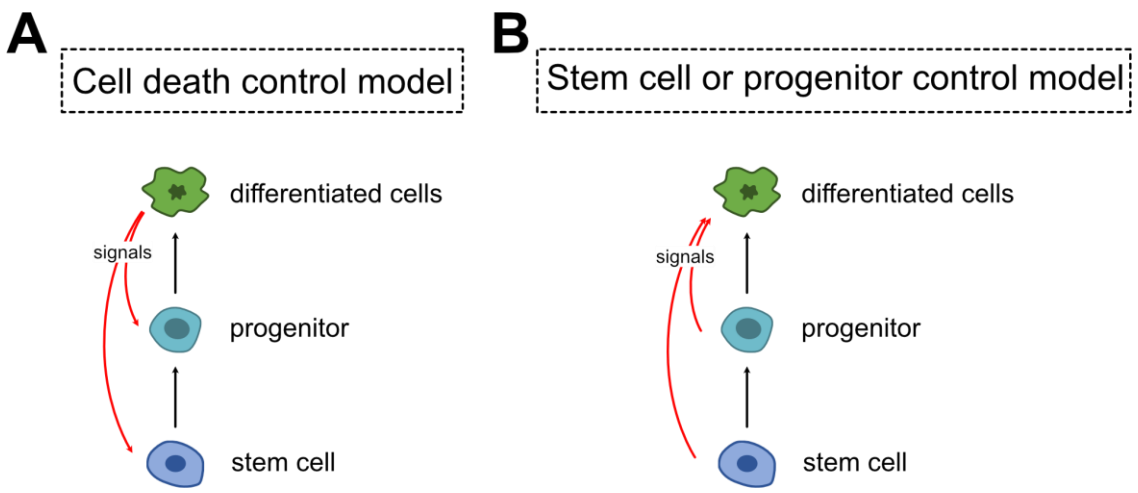

Figure 53. Models for the regulation of cell turnover in planarians

(A) In the cell death control model, the death of differentiated cells induces the proliferation of stem cells and the maturation of progenitor cells to accomplish cell replacement. (B) Cell turnover is triggered by progenitors and stem cells, which send signals to mature cells and induce the death of differentiated cells.

6.3 Method development for time-lapse imaging and its limitations

In Chapter 4, I developed a live imaging protocol that included live cell dye labeling, sample immobilization and post-analysis. This protocol allowed us to observe the cellular dynamics of planarian epidermal cells. Although it is now possible to observe cell dynamics via the live imaging approach, the live imaging protocol still has some limitations. First, the imaging time is limited to 2-3 hours. Animals can be immobilized with linalool anesthesia for the first 2 hours. However, as the imaging time increased, the animals started to twitch, probably due to the decreasing anesthetic effect on the specimens or the formation of harmful substances such as ROS after prolonged laser exposure (Icha et al., 2017). Second, the observation of cellular dynamics via live imaging was still limited to the surface layer, which corresponds to the epidermis, due to the lack of genetic engineering tools in planarians and the problem of light penetration into deeper tissues. Finally, linalool and agarose embedding could cause irreversible side

effects to the samples. The anesthetized and embedded samples cannot be recovered after time series imaging and this probably results from the side effect of anesthesia or physical damage from agarose embedding.

In addition, the frequency of internalization events observed by live imaging is 0.75 cells per hour per 800 cells, which is six times lower than the turnover kinetics (4.5 cells per hour per 800 cells) quantified by CFSE pulse-chase assay in ventral epidermis. This may result from the side effects of anesthesia and agarose embedding. Another possibility is that basal extrusion is not the primary way for the epidermis to remove unwanted cells. Instead, the main way to eliminate unwanted epidermal cells is through apical extrusion, but this is less likely because epidermal cells were not observed to be extruded apically in live imaging. In conclusion, the negative effect of anesthesia or agarose embedding could lead to the decreased turnover rate in the live imaging samples. Therefore, many works remain to be done to improve the short recording duration, the light penetrance issue and the negative effect of anesthesia and agarose embedding.

6.4 Epidermal cells undergo basal extrusion in planarians.

6.4.1 Basal extrusion occurs unusually in adult epithelia

The results for the time lapse recordings reveal that planarian epidermal cells underwent basal extrusion rather than apical extrusion, which is the primary mechanism for eliminating adult epithelial cells in other model systems. For example, vertebrate intestinal epithelia are apically extruded in the apical region (Heath, 1996; Potten, 1992, 1997). In contrast, basal extrusion is mainly observed during embryonic development and metamorphosis. For example, imaginal discs, notum and larval epidermal cells undergo basal extrusion during the *Drosophil*a metamorphosis (Ninov et al., 2007; Pastor-Pareja

et al., 2004; Toyama et al., 2008). When basal extrusion occurs in adult stages, it is mainly in a pathological context. For example, epithelia with mutations in tumor suppressor genes and oncogenic Kras transformation underwent basal extrusion and were able to migrate to other tissues after being extruded (Marshall et al., 2011; Slattum et al., 2014; Slattum & Rosenblatt, 2014). Surprisingly, in my thesis, I found that basal extrusion occurred in the epidermis of adult planarians, which is an unusual way to eliminate epithelial cells in adult animals. The planarian epidermal cells did not migrate to other tissues after basal extrusion, as was the case in other systems. Instead, they eventually approached the intestine and were digested. From the perspective of energy conservation, basal extrusion of epidermal cells in planarians can save the energy from the faster turned over tissues, which may be important for their survival during food deprivation (see discussion in the following sections).

6.4.2 Is apoptosis the trigger for the basal extrusion of planarian epidermal cells?

The observation of TUNEL^{+} cells on the epidermis and nuclear condensation of epidermal cells prior to internalization suggests that epidermal cells underwent apoptosis before basal extrusion, similar to the epithelial basal extrusion in *Drosophila*. Apoptosis has been shown to play an important role in *Drosophila* basal extrusion and blocking apoptosis would cause delay of the epithelia delamination. (Levayer et al., 2016; Nakajima et al., 2011; Ohsawa et al., 2018; Teng et al., 2017; Toyama et al., 2008). These observations of TUNEL+ cells on the epidermis and nuclear condensation give an indication that apoptosis may also play an important role in basal extrusion of the planarian epidermis. However, further experiments are needed to prove this hypothesis. For example, it would be interesting to observe the number of internalized epidermal cells in the intestine after blocking apoptosis in planarians. If apoptosis is also involved in basal extrusion in planarians, few internalized epidermal cells should be observed inside

the animals after blocking apoptosis.

6.5 The planarian gut is the terminal destination of epidermal cells undergoing replacement.

In Chapter 5, I identified the destination and fate of basally extruded epidermal cells. After being extruded toward the basal membrane, epidermal cells broke through the basal membrane and the body wall muscle and moved toward the gut branches. Then, the intestinal phagocytes act as scavengers to move the epidermal cells, possibly by phagocytosis. Finally, the dead epidermal cells were digested by the intestinal phagocytes. These results strongly suggest that intestinal phagocytes are not only responsible for digesting food, but also for removing dead cells, and that dead epidermal cells may be recycled as new energy resources. However, there are still many unanswered questions about the fate and clearance of internalized epidermal cells due to the limitations of the techniques.

6.5.1 How do basally extruded epidermal cells arrive at the intestine?

During the journey to the intestine, epidermal cells must cross several barriers from the epidermis to the intestine and how epidermal cells arrive at the intestine is unknown. The first possibility is that epidermal cells actively migrate to the intestine **(Figure 54 A)**. The second possibility for the relocation of epidermal cells to the intestine is that epidermal cells are passively transported to the intestine by other cells such as migratory phagocytic cells **(Figure 54 B)**. The second possibility seems less likely since the result from the two-color live imaging shows that the epidermal nucleus approached the intestine in relatively short time (4 minutes) **(Figure 38)**. However, more works are required to further verify whether epidermal cells active approach the intestine.

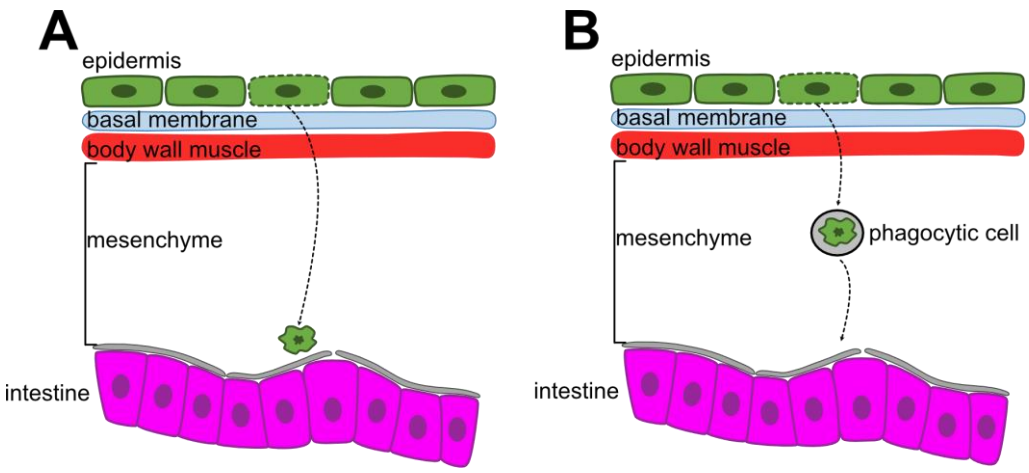

Figure 54. Hypotheses for the arrival of epidermal cells to the intestine

(A) Internalized epidermal cells arrive in the intestine and pass through the mesenchyme by active migration. (B) A relay mechanism is involved in the relocation of internalized epidermal cells. The cells are transported to the intestine by phagocytic-like cells.

6.5.2 How do epidermal cells enter the intestine?

The results in Chapter 5 show that internalized epidermal cells entered the intestine and were digested in the intestinal phagocytes. So far, it is still not clear how basally extruded epidermal cells enter the intestine and how phagocytes engulf the epidermal cells. The live imaging results show that epidermal cells directly approached the intestine within a few minutes **(Figure 38)**. However, it is not yet known whether the cells actively enter the intestine or whether the intestinal phagocytes engulf the cells in the mesenchymal tissue. Similar to the epidermis, intestinal tissue is surrounded by a basal membrane and a muscle layer (Bowen et al., 1974; Garciacorrales & Gamo, 1988). In the first scenario, epidermal cells pass through the muscle layer and basal membrane surrounding the intestine and are engulfed by the phagocytes **(Figure 55 A)**. In the second scenario, phagocytes pass through the barriers and phagocytose epidermal cells in the mesenchyme **(Figure 55 B)**. Live-imaging is the most direct approach to observe how internalized epidermal cells enter the intestine. However, it is still difficult to observe

phagocytosis by live imaging due to the light penetrance issue in deeper tissues and the limited duration of imaging. An alternative experiment would be to use electron microscopy to check whether intestinal phagocytes engulf epidermal cells in the mesenchyme. Therefore, it is still unclear how basally extruded epidermal cells enter the intestine. Furthermore, to the best of my knowledge, previous studies have shown that intestinal phagocytes can only phagocytose from the luminal side (Bowen et al., 1974; Garciacorrales & Gamo, 1988; Ishii & Sakurai, 1991; Willier et al., 1925), but my results show that the intestinal phagocytes passed through the mesenchyme and approached the basal sides of phagocytes, indicating that intestinal phagocytes are also able to engulf the epidermal cells from the basal sides.

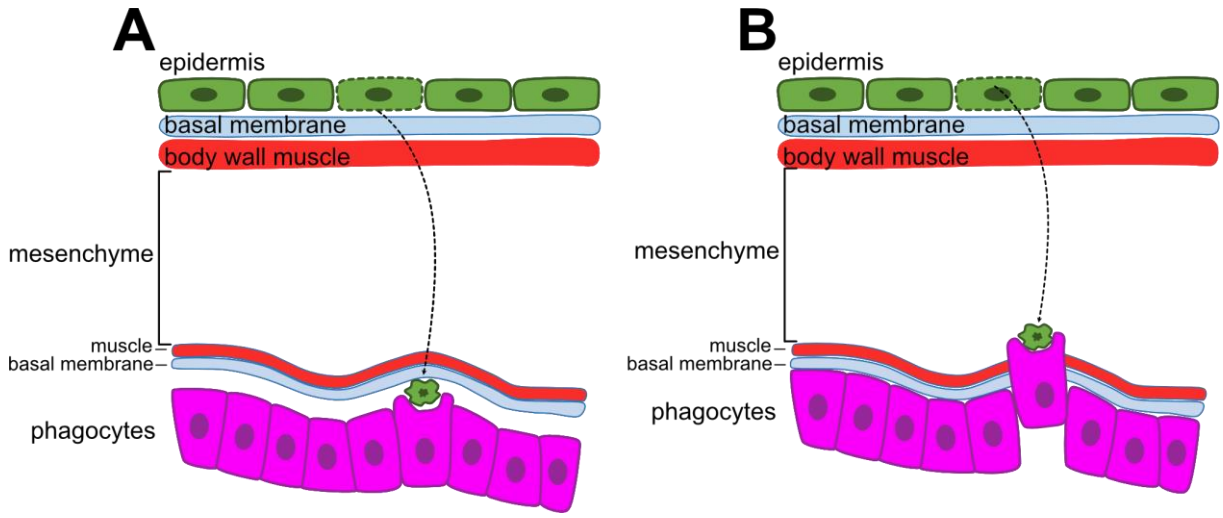

Figure 55. Hypotheses for the entry of internalized epidermal cells into the intestine.

(A) Internalized epidermal cells pass through the muscle layer and the basal membrane enclosing the intestine and are phagocytosed by the intestinal phagocytes. (B) The second possibility is that the phagocytes break through the basal membrane and the muscle layer and engulf the epidermal cells in the mesenchyme.

6.6 Self-digestion in planarians

My results suggest that intestinal phagocytes play an important role in tissue clearance. This result is consistent with the previous gene ontology analysis showing that some transcripts enriched in phagocytes are related to innate immunity (Forsthoefel et al., 2020), suggesting that gut phagocytes in planarians may also resemble the function of immune cells. In addition, large worms have more intestinal branches than small worms, which is not only necessary for the nutritional delivery but also necessary for clearing dead epidermal cells more efficiently in large worms (Forsthoefel et al., 2011). From an energetic point of view, tissue clearance by intestinal phagocytes would be one way to recycle energy from dead cells. In my thesis, I identified that eliminated epidermal cells are digested by the intestinal phagocytes during the cell turnover. Perhaps, not only epidermal cells but also other cell types may be cleared and digested by the intestinal phagocytes. Planarians can survive long-term starvation with a decrease in body size and a net loss of total cell number (Baguna & Romero, 1981; Thommen et al., 2019). However, neoblast proliferation remained at a basal level during long-term starvation (Gonzalez-Estevez et al., 2012). Therefore, it is possible that cell loss during starvation may be used as energy resources to fuel new cell generation, especially in short-lived tissues such as the epidermis. In addition, I found that the planarians cultured in chloroquine have the faster degrowth rate during starvation than the planarians cultured in planarian water **(Figure 56)**, further supporting the idea that planarians might be able to digest their own tissue during starvation. Interestingly, a recent paper published by the Bret Pearson's lab shows that the intestinal phagocytes are able to phagocytose the dead pigmented cells induced by light exposure followed by excretion through the gut lumen (Lindsay-Mosher et al., 2024). Their finding gives another example of the clearance of dead cells by the intestinal phagocytes. However, it is unlikely that dead pigment cells are reused as energy

in gut phagocytes since reactive oxygen species will be generated in pigment cells after light exposure (He et al., 2017; Stubenhaus et al., 2016). In the future, it would be interesting to investigate whether other planarian cell types are also cleared and digested by intestinal phagocytes. In conclusion, tissue clearance in planarians may involve not only the removal of unwanted cells, but also an important process of recycling the energy from dead cells **(Figure 57)**.

The phenomenon of self-digestion has been proposed in hydra. The endodermal epithelia are the digestive cells responsible for food digestion through phagocytosis and intracellular digestion (Buzgariu et al., 2015; Davis, 1975). These digestive cells are also involved in tissue clearance by engulfing apoptotic cells (Buzgariu et al., 2015; Reiter et al., 2012). Therefore, the hydra gastrodermis is likely responsible for tissue clearance and undergoes self-digestion to provide energy during nutrient deprivation, similar to the functions of planarian gut phagocytes. Interestingly, hydra shares many similarities with planarians in several aspects. First, hydra also undergoes tissue renewal and stem cells proliferate continuously (Bosch, 2008). Second, a recent study has shown that they harbor adult pluripotent stem cells, called interstitial cells, which are capable of giving rise to all cell types in hydra (Varley et al., 2023). Third, hydra does not have a fixed body size. Body size increases or decreases depending on food availability (Buzgariu et al., 2008). It is therefore possible that self-digestion is a common energy conservation scenario in animals that undergo tissue turnover throughout their lives.

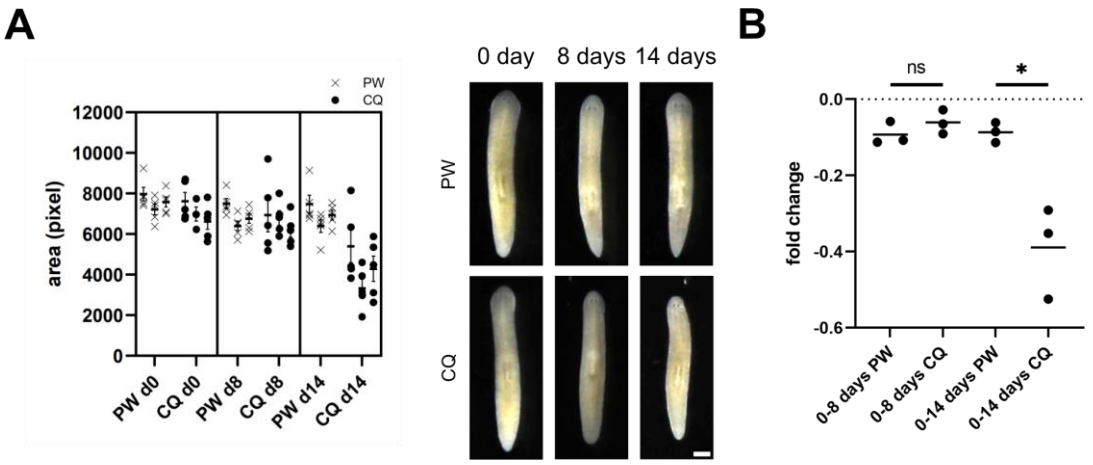

Figure 56. Chloroquine treatment led to a faster degrowth rate in planarians.

(A) The area measurement of the planarians cultured in planarian water (PW) or 5 µM chloroquine (CQ). The worm sizes were documented different days (0 day, 8 days & 14 days) after being cultured in PW or CQ. The result was collected by measuring three independent replicates with 5 worms in each replicate. Dot: the area measured from one worm. Center: mean; error: SEM. Scale bar: 0.5 mm. (B) The fold change of areas between 0 day and 8 days or between 0 day to 14 days. Dot: the average from single batch. Center: mean. T-test was performed to investigate the fold change difference. ns: non-significant. *: $p<0.05$.

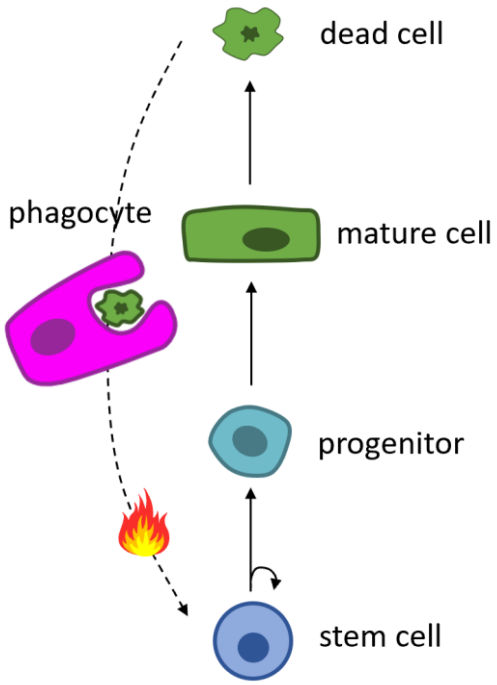

Figure 57. Proposed model of "self-digestion" in planarians

Dead cells might be digested by gut phagocytes and reused as energy to refuel the proliferation of neoblasts during tissue homeostasis in planarians.

Chapter 7: Significance and outlook

In this thesis, I first established a pulse-chase dye-labeling assay and an image analysis procedure using surface extraction and deep learning-based object detection method to quantify the turnover rate of the planarian epidermis. I used this tool to compare the turnover rate of the epidermis in different regions. My data show that, first, the half-life of the ventral epidermis is 4.5 days which is much faster than that of the dorsal epidermis. Second, in the dorsal epidermis, there was a difference in turnover rate along the anterior-posterior axis with a faster turnover rate in the anterior epidermis. The development of the pulse-chase dye labeling assay allowed us to address many questions remain unanswered about cell turnover in the planarian epidermis. For example, it is not yet clear whether cell turnover rates are size dependent. The previous study shows that growth/degrowth rates are size dependent (Thommen et al., 2019). Small worms grow and degrow faster than large worms. Therefore, it would be interesting to observe whether small worms also have higher turnover kinetics. In conclusion, my assay developments make the planarian epidermis a platform to functionally and quantitatively study cell turnover kinetics and mechanisms.

In the second part of my thesis, I aimed to understand the process of epidermal cell removal. The live imaging results show that planarian epidermal cells underwent basal extrusion and relocated inward. Basal extrusion is commonly observed during embryogenesis, as it is necessary to generate conformational changes in epithelial layers and cell dedifferentiation (Gracia et al., 2019; Hartenstein et al., 1994; Kissa & Herbomel, 2010; Monier et al., 2015; Slattum & Rosenblatt, 2014; Zulueta-Coarasa & Rosenblatt, 2022). However, it is rarely observed in adult animals as it can lead to pathological problems. The observation of basal cell extrusion during tissue homeostasis in planarians

is unusual and raises many questions about cell turnover in planarians. For example, why do planarians use this strategy to eliminate epidermal cells, and what are the mechanisms that regulate basal extrusion in the planarian epidermis? Are these mechanisms similar to those involved in basal extrusion during animal development?

In the last part of the thesis, I tried to identify the final destination and fate of the basally extruded epidermal cells. The results of two-color live imaging show that the internalized cells passed through the basal membrane and body wall muscles and reached the intestine within a few minutes after being extruded from the epidermis. The cells eventually appeared in the intestine and were digested by intestinal phagocytes. These results show that intestinal phagocytes are able to clear dead cells in the body. Most importantly, these results suggest that the planarian undergoes “self-digestion” to recycle the dead cells as energy resources. Planarians constantly renew their cells, and recycling the dead cells is more economical from an energy point of view. This self-digestion phenomenon has also been described in hydra, which also continuously renew their tissues (Buzgariu et al., 2015; Reiter et al., 2012). Therefore, this may be a common strategy for animals with continuous cell renewal. In the future, it will be interesting to investigate whether self-digestion occurs not only in the epidermis, but also in other tissues of planarians.

In this thesis, I established the live imaging protocol that includes live cell labeling, anesthesia, and post-imaging analysis with my colleague Dr. Tobias Boothe. This protocol overcame the photosensitivity of planarians by using short exposure times and low laser power during image acquisition together with CARE, a deep learning based denoising tool, to improve the low signal-to-noise ratio. Although my study is not the first to use live-

imaging in planarians, it is the first study to use the live-imaging approach to record cell dynamics in planarians, and live-imaging will be an important technique in the planarian field in the future, as it can help answer many unresolved questions regarding tissue dynamics in planarians.

Chapter 8: Materials and Methods

8.1 Animal husbandry

The animals used in my thesis are the asexual strain of *Schmidtea mediterranea* (CIW4). Planarians were maintained in planarian water (1.6 mM NaCl, 1.0 mM $CaCl_2$, 1.0 mM $MgSO_4$, 0.1 mM $MgCl_2$, 0.1 mM KCl and 1.2 mM $NaHCO_3$ in Milli-Q water) with 5 µg/mL Ciprofloxacin and incubated at 20˚C. To obtain worms of small size (~2-3 mm), large worms were cut into several pieces and the pieces were cultured for 2 weeks until fully regenerated. Fully regenerated animals were then regularly fed (every two weeks) with macerated cow liver. Based on the requirements of the experiments, either 1-week-starved or 2-week-starved worms were used.

8.2 X-ray irradiation

To deplete the neoblasts, the animals were exposed to X-ray radiation. First, planarians were transferred to 10 cm petri dishes and the dishes were placed in the irradiator (CellRad Precision Irradiator). The irradiation dose was 6,000 rad. After irradiation, the worms were cultured in planarian water containing 5 µg/mL Ciprofloxacin, and the water was changed every day.

8.3 Cloning and RNA Probe synthesis for *in situ* hybridization

The target genes (*Smed_dd_75, Smed_dd_115* and *Smed_hnf4*) were first amplified from asexual *Schmidtea Mediterranea* cDNA using gene-specific primers **(Table 1)**. The PCR products were then inserted into the pPRT4P vector using the NEBuilder® HiFi DNA Assembly Master Mix (NEB, Cat. E2621L). The RNA probe for *in situ* hybridization was synthesized by *in vitro* transcription using the linear DNA amplified from the gene-

inserted construct. After overnight incubation at 37°C, RNA was precipitated by salt solution. 20 µL of *in vitro* transcription mixture was mixed with 7.5 mM ammonium acetate and 50 µL ice-cold 100% EtOH and centrifuged at 4°C. After air drying for a few minutes at room temperature, deionized Formamide (AppliChem, Cat. A2156) was added to dissolve the RNA pellets.

Table 1. Primer pairs for gene cloning

Gene name	**PlanMine ID**	**forward primers**	**reverse primers**
Smed_dd_75	dd_Smed_v6_75_0_1	Plasmid obtained from the Rink lab	
Smed_dd_115	dd_Smed_v6_115_0_1	Plasmid obtained from the Rink lab	
Smed_hnf4	dd_Smed_v6_1694_0_1	CATTACCATCCCGCACTATGGGATGACC CAGAATTCGCTT	CCAATTCTACCCGCACAGTCATTGTGCT GTTGGTTCGCTT

*The underlined nucleotides are the overhang sequences to the cloning sites of the pPRT4P vector for Gibson assembly.

8.4 RNA interference

Double-stranded RNA was synthesized by *in vitro* transcription. The reaction mixture was incubated overnight at 37°C for RNA synthesis. After overnight incubation, single-stranded RNA was annealed by incubating the reaction at 75°C for 3 minutes at 1000 rpm, and the mixture was gradually cooled to room temperature by turning off the incubator. RNA was pelleted by mixing the *in vitro* transcription reaction with NaCl/PEG-8000 precipitation solution (2.5 M NaCl, 20% Polyethyene glycol 8000, 10 mM Tris-HCl, pH 8.0) and centrifuging at 4°C. The double-stranded RNA was delivered into the animals via

feeding. The RNA was mixed with liver at a final concentration of 2 mg/ml. To knock down *hnf4*, worms were fed with double-stranded RNA three times within 1 week.

8.5 Whole-mount *in situ* hybridization

Sample fixation

The whole-mount *in situ* hybridization procedure was modified from the previously published protocol (King & Newmark, 2013). Initially, animal samples were euthanized with 5% N-acetylcysteine (NAC) in PBS for 5 min on a rotator. Samples were then fixed in 4% Paraformaldehyde (EMS, Cat. 15710) in 50% PBS with 0.15% Triton-X. After fixation, the samples were immersed in the reduction solution (1% NP-40, 0.5% SDS, 50 mM DTT in 1XPBS in H_2O) at 37°C for 10 minutes. The samples were then dehydrated and stored in 100% MeOH at -20°C.

RNA probe hybridization

For RNA probe hybridization, samples were first rehydrated in PBS and then incubated in bleaching solution (1.2% H_2O_2, 5% formamide, 0.5XSSC) on a light table at room temperature for 1 hour to remove pigment. After bleaching, the samples were treated with Protease K (NEB, Cat. PB107S) by immersion in PBSTx0.3 (0.3 % Triton-X in PBS) and 2 µg/mL Protease K for 10 minutes. Following the Protease K treatment, samples were post-fixed in 4% PFA for 10 minutes at room temperature. After post-fixation, the samples were incubated in Pre-Hybe solution at 58°C for 2 hours. The samples were then transferred to Hybe solution together with the RNA probes (dd_75 or dd_115) and incubated overnight at 58°C. After overnight incubation, the RNA probes in Hybe were removed followed by a series wash in Wash Hybe, 50% Wash Hybe in 1X SSC, 2XSSSC, and

0.2X SSC.

*composition of the Pre-Hybe, Hybe and Wash Hybe solution are listed below

Pre-Hybe solution: 50% formamide, 5X SSC, 1X Denhardts, 100 µg/µL Heparin, 1% Tween-20, 1 mg/mL torula yeast RNA, 50 mM DTT in water

Hybe solution: 50% Formamide, 5X SSC, 1X Denhardts, 100 µg/µL Heparin, 1% Tween-20, 0.25 mg/mL torula yeast RNA, 50 mM DTT, 0.05 g/mL dextran sulfate in water

Wash Hybe: 50% formamide, 0.5% Tween-20, 5XSSC, 1 X Denhardts in water

Antibody incubation

After the series of washes, the animals were immersed in blocking solution (5% sterile horse serum, 0.5% Roche Western Blocking Reagent in TNTx) for 2 hours on a rotator. After blocking, the antibody was added and the samples were incubated overnight at 4°C. After the antibody incubation, the samples were washed in TNTx (0.1 M Tris pH 7.5, 0.15 M NaCl, 0.3% Triton X-100 in H_2O) for 3 hours and the color reaction was performed.

Color reaction

The color reaction was performed by immersing the samples in TSA buffer (2M NaCl, 0.1M Boric acid in H_2O, pH8.5) containing 0.006 % hydrogen peroxide, 20 µg/mL 4-Iodophenylboronic acid and Rhodamine tyramide for 45 minutes in a box to avoid light. To quench the peroxidase activity of the first antibody, samples were treated with 100 mM sodium azide for at least 1 hour, followed by TNTx washes. The second color reaction was performed as the first color reaction. Finally, the samples were cleared in Scale S4 (10% Glycerol, 40% Sorbitol, 15% DMSO, 2.5% DABCO, 4 M Urea, 0.1% TritonX-100 in

water) and mounted on slides for imaging.

8.6 Whole mount TUNEL staining

DNA double-stranded breaks were detected using the ApopTag Fluorescein Direct *In Situ* Apoptosis Detection Kit (Merck, Cat. S7160). 2-3 mm worms were used for TUNEL labeling. Worms were first fixed using the same fixation procedure as for *in situ* hybridization (8.5). After rehydration from MeOH to PBS, the samples were depigmented with ammonia bleach. The worms were incubated in the bleaching solution (3% H_2O_2, 0.075% NH_4OH and 0.3% Triton-X in PBS) for 4-5 hours on a light table at room temperature. After bleaching, the samples were rinsed twice with 0.3% Triton-X in PBS (PBSTx0.3) and incubated in 2 µg/mL Protease K in PBSTx0.3 for 10 minutes at room temperature. The samples were then post-fixed in 4% formaldehyde (4% formaldehyde, 0.15% Triton-X, 0.5XPBS in H_2O) followed by two washes in PBSTx0.3 and one wash in PBS. After post-fixation, samples were soaked in equilibration buffer for 10 minutes at room temperature. The fragmented DNA was tagged with the fluorescein-labeled nucleotides by incubating the samples in the solution containing reaction buffer and TdT enzyme (reaction buffer: TdT enzyme = 7:3) for 4 hours at 37°C. After the reaction, the samples were washed four times with PBSTx0.3 for 15-30 minutes each, followed by post-fixation in 4% PFA for 15 minutes at room temperature. After several washes in PBSTx0.3, the samples were mounted by immersion in Scale S4.

8.7 Sample preparation of the pulse-chase dye labeling assay

The live cell dyes CFSE (Life Technologies, Cat. 6585084) and DDAO (Invitrogen, Cat. C34553) were used to label epidermal cells in planarians. First, worms were immersed in planarian water containing 10 µM CFSE and 1 µM DDAO at 20°C for 1.5 hours. Worms

were then euthanized with 5% NAC in PBS for 3 minutes on a rotator followed by the fixation by incubating the samples in 100% MeOH at -20°C for 2 hours. After fixation, samples were rehydrated by a series of rehydration in 75% MeOH, 50% MeOH, 25% MeOH and PBS, followed by DAPI or Hoechst staining at room temperature for 30 minutes. The samples were then soaked in 80% glycerol in PBS and mounted between two different sized of coverslips (24*60 mm, No. 1.5H and 22*22 mm, 1.5H; Schott). For cross sections, animals were embedded in 4% SeaPlaque™ agarose (Lonza, Cat. 50100), and bisected with a knife.

8.8 Image acquisition

An Olympus IX83 microscope integrated with a Yokogawa CSUW1-T2S Spinning Disk system and a Hamamatsu Orca Flash4.0 V3 camera was used to image the fixed specimens mounted on slides. Imaging was performed using a 20X air objective with a numerical aperture (NA) of 0.8. or 10X air objective with a NA of 0.4.

An Olympus IX83 microscope equipped with a Yokogawa CSUW1-T2S Spinning Disk system and an Andor iXon Ultra 888 EMCCD camera was used for time series recording. Either 60X with an NA of 1.3 or 30X with an NA of 1.05 was used to collect the images. To minimize the twitching, samples were incubated in a thermostatically controlled chamber at 15°C during the time series recording. 1% laser power and 5 milliseconds exposure time were used for imaging. The duration of time lapse imaging was approximately 2-3 hours images were acquired every minute.

8.9 Sample preparation for time-lapse recordings

To obtain the time lapse images of the epidermis, the planarian epidermis was labeled with the live cell dyes: Reddot™1 Far-Red Nuclear Stain (Biotium, Cat. 40060) and

CellTracker™ Deep Red Dye (Invitrogen, Cat. C34565). For nuclear labeling, worms were incubated overnight at 20°C in planarian water containing 2X Reddot™1 and 10% DMSO. For cytoplasmic labeling, worms were immersed in 1 µM CellTracker™ Deep Red Dye in planarian water at 20°C for 1.5 hours. After the live cell dye labeling, worms were anesthetized by incubation in 0.02% linalool in planarian water at room temperature for half an hour, followed by mucus removal by incubation in neutralized 0.5% NAC in Milli-Q water (pH = ~7) for 10 seconds. Samples were then mounted on a µ-Dish 35mm (ididi, Cat. 81158) in 1% SeaPlaque™ agarose in planarian water with 0.02% linalool. The agarose was covered with an oxygen-permeable PMP disc and Halocarbon oil 700 (Sigma-Aldrich, Cat. H8898) was used to seal the gap between the PMP disc and the bottom of the dish to prevent water evaporation from the agarose. For two-color imaging, worms were fed liver paste containing live cell dye (20% liver paste, 0.3% SeaPlaque™ Agarose, 0.02 mM CellTracker™ Red CMTPX Dye) to visualize the intestinal structures.

8.10 Image processing

8.10.1 Surface extraction with Premosa

The CFSE- and DDAO-labeled samples were imaged using a confocal microscope due to the curvature of the worms. The surface signals corresponding to the epidermis were extracted from the z-stack images using Premosa (Blasse et al., 2017). The DDAO signals, which label the entire epidermis, were used as a reference for the surface extraction.

8.10.2 Visualization of time-lapse images

To visualize the time lapse images, the signal-to-noise ratio of the images was enhanced by the custom-trained CARE models. Second, the drift of the images at different time points was corrected by linear stack alignment with SWIFT or Fast4Dreg in FIJ

(Schindelin et al., 2012). Finally, to distinguish the signal from different stacks representing depth in the maximum projected images, the color LUT (mpl-viridis) in FIJI was used to label signals from different stacks with different colors.

8.11 Stardist model generation

8.11.1 Stardist model training

Stardist models were trained to automatically segment CFSE-labeled and DDAO-labeled epidermal cells. For model training, the raw images pairing with manually annotated images were used as the training materials. The raw images were taken from the CFSE-labeled samples processed by Premosa and the annotated images were taken from the manual annotation of each individual $CFSE^+$ epidermal cells using labkit in FIJI. The images of unirradiated and irradiated worms were used to train a ventral epidermis model. 1% pixels of the images from unirradiated worms were normalized to saturation and 256*256 $pixel^2$ were cropped. Images from the irradiated samples were cropped and 0.3% of the pixels were normalized to saturation. To train a model to segment the dorsal epidermis, 1% of the pixels from the CFSE-labeled images were saturated and cropped after normalization. Each pair of raw image-annotated image was rotated 90, 180, 270 degrees followed by mirroring every image. Therefore, the training data were expanded to 8 times in quantity. In total, the ventral and dorsal epidermal cell models were trained with 199*8 and 66*8 training pairs, respectively. Below are the parameters used to train the Stardist model **(Table 2)**.

Table 2. Parameters used to train the Stardist models

Training Parameters	Number of rays (n_rays)	64
	Number of patch size (train_patch_size)	128, 128
	Number of epochs (train_epochs)	200
	Steps per epoch	200
	Batch size (train_batch_size)	32
	Learning_rate (train_learning_rate)	0.0003

8.11.2 Verification of the Stardist models

To validate the performance of the Stardist model prediction, 256x256 pixel^2 random crops were made from the epidermal cells labeled with DDAO, CFSE, and DAPI. Before making the crops, 1% or 3% of the total pixels of the images were saturated in CFSE or DDAO-labeled images. The parameters used to validate the Stardist model are listed in **Table 3**. To eliminate objects oversegmented by the Stardist model, 200 pixel^2 was used as the minimum size limit for predicted objects in the ventral epidermis. The number of objects obtained from the model predictions was compared to the number of cells obtained from manual counting. The formula used to quantify the accuracy of the Stardist model prediction is given here: $1 - \left|\frac{Prediction - Ground\ Truth}{Ground\ truth}\right|$.

Table 3. Parameters used to quantify the number of CFSE$^+$, DDAO$^+$ and DAPI$^+$ objects using the Stardist models.

	Ventral epidermis		Dorsal epidermis		
	CFSE	DDAO	CFSE	DDAO	DAPI
Models	Custom-trained ventral epidermis model	Custom-trained ventral epidermis model	Custom-trained dorsal epidermis model	Custom-trained dorsal epidermis model	Built-in fluorescent nuclei
% pixels to saturation	1	3	1	3	0
Neural Network Prediction					
Percentile Low	0	0	0	0	0
Percentile High	100	100	100	100	100
NMS Postprocessing					
Scored threshold	0.6	0.6	0.4	0.4	0.6
Overlap threshold	0.3	0.3	0.3	0.3	0.3

8.12 CARE model generation

To overcome the low signal-to-noise ratio due to the low laser power and short exposure time, Content-Aware Image Restoration (CARE) was used to improve the signal-to-noise ratio (Weigert et al., 2018). The CARE models were trained with the inputs from

the z-stack image pairs acquired at the same positions with short exposure time (5 milliseconds) and long exposure time (100 milliseconds). Each training set contained two to five short and long exposure image pairs. The parameters used to train the CARE model are as follows **(Table 4)**.

Table 4. Parameters used to train CARE models for denoising.

		Reddot™-1 labeling	CellTracker™ Deep Red Dye labeling
Microscope parameters for generating raw training data	XYZ camera ROI (pixels, unbinned)	1024*1024*16	1024*1024*16
	Z stepping	30 µm	15 µm
	Number of Stacks	16	16
	Objective	30X	60X
Processed Training data	Patch dimensions OXY (pixels) (patch_size)	64*64*16	64*64*16
	Number of randomly sampled patches per raw image stack (n_patches_per_image)	200	200
Training Parameters	Number of epochs (train_epochs)	10	10
	Steps per epoch	100	100
	Batch size	128	100
	Fraction used for validation	0.1	0.1

8.13 Image analysis

8.13.1 Quantification of CFSE$^+$ cells, DDAO$^+$ cells and DAPI$^+$ nuclei

The CFSE-, DDAO-, and DAPI-labeled epidermal cells were automatically segmented and quantified with the custom-trained Stardist models. The same parameters used to verify the Stardist models were used to quantify CFSE$^+$ and DDAO$^+$ and DAPI$^+$ cells for the turnover rate.

8.13.2 Quantification of the volume and density of CFSE$^+$ objects in the intestines or mesenchyme

The volume of CFSE$^+$ objects and intestines (CellTracker™ Deep Red Dye$^+$) and the number of CFSE$^+$ objects were quantified by converting grayscale images to binary images using the thresholding function in FIJI. The volume and number were then quantified using the CellProfiler pipelines. The CFSE$^+$ objects with a volume of less than 10 voxels were eliminated. The density of CFSE$^+$ objects in mesenchyme or intestine was calculated by dividing the number of CFSE$^+$ objects by the volume of mesenchyme or intestine.

8.13.3 Quantification of z-depth and pixel intensity of epidermal nuclei

Z-stack images acquired at 60 consecutive time points with one minute intervals were used for analysis. Individual nuclei were tracked using IMARIS software. First, 3D object detection was performed by intensity and size thresholding. The nuclei were then tracked across different time points using the object tracking function in IMARIS. Finally, the position and intensity of each nucleus was analyzed every minute.

8.13.4 Quantification of the area of planarians

The planarian samples were imaged with a Canon EOS 6D MarkII digital camera. The images were then segmented with the previously trained pixel classifier in ilastik (from Dr. Tobias Boothe) and the areas were quantified by the Cellprofiler pipeline.

8.14 Chloroquine treatment

3 mm worms were selected and cultured in planarian water containing 5 µM chloroquine and 5 µg/mL ciprofloxacin (Sigma-Aldrich, Cat. C6628). For the control group, worms of the same size were cultured in planarian water containing 5 µg/mL ciprofloxacin. After 4 days of chloroquine treatment, a CFSE pulse was applied and worms were euthanized by immersing in 5% NAC in PBS and fixed in 100% MeOH 4 days post CFSE pulse. The intestinal structures were visualized by feeding liver and live cell dye mixture. The mixture contains 20% liver paste, 0.3% SeaPlaque™ agarose and 0.02 mM CellTracker™ Deep Red Dye in water.

8.15 Statistics

The Mann-Whitney-U-test or Student's t-test was conducted to compare the significant differences between the sample under different treatment in this thesis.

8.16 Software used

Images acquired from the microscopes were processed using Fiji (Schindelin et al., 2012) and analyzed using CellProfiler (Carpenter et al., 2006) or ilastik (Berg et al., 2019). Figures and cartoons were generated using Affinity Designer or Microsoft PowerPoint. The statistics and graph plots were performed with GraphPad Prism 9.

Acknowledgments

Foremost, I thank my supervisor Dr. Jochen Rink for his support and enthusiasm in my thesis project and for giving me an amazing Ph.D. journey.

Second, I would like to thank my mentor Dr. Tobias Boothe for introducing me to the world of imaging. Without his help in every aspect, I don't think I could finish my thesis.

My special thanks go to Prof. Herbert Jäckle and Prof. Ernst Wimmer for their fruitful discussions and constructive feedback at every TAC meeting.

Further, I would like to thank Prof. Daniel Jackson, Dr. Peter Lénárt and Dr. Gerd Vorbrüggen for serving on my examination board.

I would also like to thank Clemens Mauksch for his contribution to this project during his master rotation in our lab.

I would like to express my gratitude to the past and present members of the Rink lab for their support.

Finally, I thank my family for their support throughout my Ph.D. journey.

Chapter 9: References

Adler, C. E., Seidel, C. W., McKinney, S. A., & Sanchez Alvarado, A. (2014). Selective amputation of the pharynx identifies a FoxA-dependent regeneration program in planaria. *Elife*, *3*, e02238. https://doi.org/10.7554/eLife.02238

Agata, K., Soejima, Y., Kato, K., Kobayashi, C., Umesono, Y., & Watanabe, K. (1998). Structure of the planarian central nervous system (CNS) revealed by neuronal cell markers. *Zoological Science*, *15*(3), 433-440. https://doi.org/10.2108/zsj.15.433

Agata, K., & Watanabe, K. (1999). Molecular and cellular aspects of planarian regeneration. *Seminars in Cell & Developmental Biology*, *10*(4), 377-383. https://doi.org/10.1006/scdb.1999.0324

Almuedo-Castillo, M., Crespo, X., Seebeck, F., Bartscherer, K., Salò, E., & Adell, T. (2014). JNK Controls the Onset of Mitosis in Planarian Stem Cells and Triggers Apoptotic Cell Death Required for Regeneration and Remodeling. *Plos Genetics*, *10*(6). https://doi.org/10.1371/journal.pgen.1004400

Andrade, D., & Rosenblatt, J. (2011). Apoptotic regulation of epithelial cellular extrusion. *Apoptosis*, *16*(5), 491-501. https://doi.org/10.1007/s10495-011-0587-z

Arandjelovic, S., & Ravichandran, K. S. (2015). Phagocytosis of apoptotic cells in homeostasis. *Nature Immunology*, *16*(9), 907-917. https://doi.org/10.1038/ni.3253

Arwert, E. N., Hoste, E., & Watt, F. M. (2012). Epithelial stem cells, wound healing and cancer. *Nat Rev Cancer*, *12*(3), 170-180. https://doi.org/10.1038/nrc3217

Baehrecke, E. H. (2003). Autophagic programmed cell death in. *Cell Death and Differentiation*, *10*(9), 940-945. https://doi.org/10.1038/sj.cdd.4401280

Baguna, J. (2012). The planarian neoblast: the rambling history of its origin and some current black boxes. *International Journal of Developmental Biology*, *56*(1-3), 19-37. https://doi.org/10.1387/ijdb.113463jb

Baguñà, J. (2012). The planarian neoblast: the rambling history of its origin and some current black boxes. *International Journal of Developmental Biology*, *56*(1-3), 19-37. https://doi.org/10.1387/ijdb.113463jb

Baguna, J., & Romero, R. (1981). Quantitative-Analysis of Cell-Types during Growth, Degrowth and Regeneration in the Planarians Dugesia-Mediterranea and Dugesia-Tigrina. *Hydrobiologia*, *84*(Oct), 181-194. https://doi.org/10.1007/Bf00026179

Baguna, J., Romero, R., Salo, E., Collet, J., Auladell, C., Ribas, M., Riutort, M., Garciafernandez, J., Burgaya, F., & Bueno, D. (1990). Growth, Degrowth and Regeneration as Developmental Phenomena in Adult Fresh-Water Planarians. *Experimental Embryology in Aquatic Plants and Animals*, *195*, 129-162.

Baguna, J., Salo, E., & Auladell, C. (1989). Regeneration and pattern formation in planarians:

III. Evidence that neoblasts are totipotent stem cells and the source of blastema cells. *Development*, *107*(1), 77-86. https://doi.org/10.1242/dev.107.1.77

Banjac, I., Maimets, M., & Jensen, K. B. (2023). Maintenance of high-turnover tissues during and beyond homeostasis. *Cell Stem Cell*, *30*(4), 348-361. https://doi.org/10.1016/j.stem.2023.03.008

Barberan, S., Fraguas, S., & Cebria, F. (2016). The EGFR signaling pathway controls gut progenitor differentiation during planarian regeneration and homeostasis. *Development*, *143*(12), 2089-2102. https://doi.org/10.1242/dev.131995

Bardeen, C. R., & Baetjer, F. H. (1904). The inhibitive action of the Roentgen rays on regeneration in planarians. *Journal of Experimental Zoology*, *1*(1), 191-195. https://doi.org/DOI 10.1002/jez.1400010107

Barker, N. (2014). Adult intestinal stem cells: critical drivers of epithelial homeostasis and regeneration. *Nature Reviews Molecular Cell Biology*, *15*(1), 19-33. https://doi.org/10.1038/nrm3721

Berg, S., Kutra, D., Kroeger, T., Straehle, C. N., Kausler, B. X., Haubold, C., Schiegg, M., Ales, J., Beier, T., Rudy, M., Eren, K., Cervantes, J. I., Xu, B., Beuttenmueller, F., Wolny, A., Zhang, C., Koethe, U., Hamprecht, F. A., & Kreshuk, A. (2019). ilastik: interactive machine learning for (bio)image analysis. *Nature Methods*, *16*(12), 1226-1232. https://doi.org/10.1038/s41592-019-0582-9

Berry, D. L., & Baehrecke, E. H. (2007). Growth arrest and autophagy are required for salivary gland cell degradation in. *Cell*, *131*(6), 1137-1148. https://doi.org/10.1016/j.cell.2007.10.048

Beumer, J., & Clevers, H. (2021). Cell fate specification and differentiation in the adult mammalian intestine. *Nat Rev Mol Cell Biol*, *22*(1), 39-53. https://doi.org/10.1038/s41580-020-0278-0

Bianconi, E., Piovesan, A., Facchin, F., Beraudi, A., Casadei, R., Frabetti, F., Vitale, L., Pelleri, M. C., Tassani, S., Piva, F., Perez-Amodio, S., Strippoli, P., & Canaider, S. (2013). An estimation of the number of cells in the human body. *Annals of Human Biology*, *40*(6), 463-471. https://doi.org/10.3109/03014460.2013.807878

Bischoff, M. (2012). Lamellipodia-based migrations of larval epithelial cells are required for normal closure of the adult epidermis of Drosophila. *Developmental Biology*, *363*(1), 179-190. https://doi.org/10.1016/j.ydbio.2011.12.033

Blasse, C., Saalfeld, S., Etournay, R., Sagner, A., Eaton, S., & Myers, E. W. (2017). PreMosa: extracting 2D surfaces from 3D microscopy mosaics. *Bioinformatics*, *33*(16), 2563-2569. https://doi.org/10.1093/bioinformatics/btx195

Bohr, T. E., Shiroor, D. A., & Adler, C. E. (2021). Planarian stem cells sense the identity of the missing pharynx to launch its targeted regeneration. *Elife*, *10*. https://doi.org/10.7554/eLife.68830

Bonnet, D. (2002). Haematopoietic stem cells. *J Pathol*, *197*(4), 430-440. https://doi.org/10.1002/path.1153

Boothe, T., Hilbert, L., Heide, M., Berninger, L., Huttner, W. B., Zaburdaev, V., Vastenhouw, N. L., Myers, E. W., Drechsel, D. N., & Rink, J. C. (2017). A tunable refractive index matching medium for live imaging cells, tissues and model organisms. *Elife*, *6*. https://doi.org/10.7554/eLife.27240

Borges, M. D., & Sesti-Costa, R. (2022). Macrophages: key players in erythrocyte turnover. *Hematol Transfus Cell Ther*, *44*(4), 574-581. https://doi.org/10.1016/j.htct.2022.07.002

Bosch, T. C. G. (2008). Stem Cells in Immortal Hydra. In. Springer, Dordrecht. https://doi.org/10.1007/978-1-4020-8274-0_3

Bowen, I. D., Ryder, T. A., & Thompson, J. A. (1974). The fine structure of the planarian Polycelis tenuis Iijima. II. The intestine and gastrodermal phagocytosis. *Protoplasma*, *79*(1), 1-17. https://doi.org/10.1007/BF02055779

Buzgariu, W., Al Haddad, S., Tomczyk, S., Wenger, Y., & Galliot, B. (2015). Multi-functionality and plasticity characterize epithelial cells in Hydra. *Tissue Barriers*, *3*(4), e1068908. https://doi.org/10.1080/21688370.2015.1068908

Buzgariu, W., Chera, S., & Galliot, B. (2008). Methods to Investigate Autophagy during Starvation and Regeneration in Hydra. *Autophagy: Lower Eukaryotes and Non-Mammalian Systems, Pt A*, *451*, 409-437. https://doi.org/10.1016/S0076-6879(08)03226-6

Carmell, M. A., Girard, A., van de Kant, H. J. G., Bourc'his, D., Bestor, T. H., de Rooij, D. G., & Hannon, G. J. (2007). MIWI2 is essential for spermatogenesis and repression of transposons in the mouse male germline. *Developmental Cell*, *12*(4), 503-514. https://doi.org/10.1016/j.devcel.2007.03.001

Carpenter, A. E., Jones, T. R., Lamprecht, M. R., Clarke, C., Kang, I. H., Friman, O., Guertin, D. A., Chang, J. H., Lindquist, R. A., Moffat, J., Golland, P., & Sabatini, D. M. (2006). CellProfiler: image analysis software for identifying and quantifying cell phenotypes. *Genome Biology*, *7*(10). https://doi.org/10.1186/gb-2006-7-10-r100

Chan, A., Ma, S., Pearson, B. J., & Chan, D. (2021). Collagen IV differentially regulates planarian stem cell potency and lineage progression. *Proc Natl Acad Sci U S A*, *118*(16). https://doi.org/10.1073/pnas.2021251118

Chinnaiyan, A. M. (1999). The apoptosome: heart and soul of the cell death machine. *Neoplasia*, *1*(1), 5-15. https://doi.org/10.1038/sj.neo.7900003

Cote, L. E., Simental, E., & Reddien, P. W. (2019). Muscle functions as a connective tissue and source of extracellular matrix in planarians. *Nature Communications*, *10*. https://doi.org/10.1038/s41467-019-09539-6

Cox, D. N., Chao, A., Baker, J., Chang, L., Qiao, D., & Lin, H. (1998). A novel class of

evolutionarily conserved genes defined by piwi are essential for stem cell self-renewal. *Genes Dev*, *12*(23), 3715-3727. https://doi.org/10.1101/gad.12.23.3715

Crosnier, C., Stamataki, D., & Lewis, J. (2006). Organizing cell renewal in the intestine: stem cells, signals and combinatorial control. *Nat Rev Genet*, *7*(5), 349-359. https://doi.org/10.1038/nrg1840

Dai, X., & Segre, J. A. (2004). Transcriptional control of epidermal specification and differentiation. *Curr Opin Genet Dev*, *14*(5), 485-491. https://doi.org/10.1016/j.gde.2004.07.002

Davis, L. E. (1975). Histological and ultrastructural studies of the basal disk of Hydra. III. The gastrodermis and the mesoglea. *Cell Tissue Res*, *162*(1), 107-118. https://doi.org/10.1007/BF00223266

de Sousa, N., & Adell, T. (2018). Detection of Cell Death in Planarians. *Bio-Protocol*, *8*(19). https://doi.org/10.21769/BioProtoc.3039

Dewson, G., & Kluck, R. M. (2009). Mechanisms by which Bak and Bax permeabilise mitochondria during apoptosis. *Journal of Cell Science*, *122*(16), 2801-2808. https://doi.org/10.1242/jcs.038166

Dini, L., Pagliara, P., & Carla, E. C. (2002). Phagocytosis of apoptotic cells by liver: A morphological study. *Microscopy Research and Technique*, *57*(6), 530-540. https://doi.org/10.1002/jemt.10107

Eisenhoffer, G. T., Kang, H., & Alvarado, A. S. (2008). Molecular analysis of stem cells and their descendants during cell turnover and regeneration in the planarian Schmidtea mediterranea. *Cell Stem Cell*, *3*(3), 327-339. https://doi.org/10.1016/j.stem.2008.07.002

Eisenhoffer, G. T., Loftus, P. D., Yoshigi, M., Otsuna, H., Chien, C. B., Morcos, P. A., & Rosenblatt, J. (2012). Crowding induces live cell extrusion to maintain homeostatic cell numbers in epithelia. *Nature*, *484*(7395), 546-549. https://doi.org/10.1038/nature10999

Eisenhoffer, G. T., & Rosenblatt, J. (2013). Bringing balance by force: live cell extrusion controls epithelial cell numbers. *Trends in Cell Biology*, *23*(4), 185-192. https://doi.org/10.1016/j.tcb.2012.11.006

Elliott, S. A., & Sanchez Alvarado, A. (2013). The history and enduring contributions of planarians to the study of animal regeneration. *Wiley Interdiscip Rev Dev Biol*, *2*(3), 301-326. https://doi.org/10.1002/wdev.82

Elmore, S. (2007). Apoptosis: A review of programmed cell death. *Toxicologic Pathology*, *35*(4), 495-516. https://doi.org/10.1080/01926230701320337

Fadok, V. A., Voelker, D. R., Campbell, P. A., Cohen, J. J., Bratton, D. L., & Henson, P. M. (1992). Exposure of Phosphatidylserine on the Surface of Apoptotic Lymphocytes Triggers Specific Recognition and Removal by Macrophages. *Journal of Immunology*, *148*(7),

2207-2216.

Fincher, C. T., Wurtzel, O., de Hoog, T., Kravarik, K. M., & Reddien, P. W. (2018). Cell type transcriptome atlas for the planarian Schmidtea mediterranea. *Science*, *360*(6391). https://doi.org/10.1126/science.aaq1736

Forsthoefel, D. J., Cejda, N. I., Khan, U. W., & Newmark, P. A. (2020). Cell-type diversity and regionalized gene expression in the planarian intestine. *Elife*, *9*. https://doi.org/10.7554/eLife.52613

Forsthoefel, D. J., James, N. P., Escobar, D. J., Stary, J. M., Vieira, A. P., Waters, F. A., & Newmark, P. A. (2012). An RNAi screen reveals intestinal regulators of branching morphogenesis, differentiation, and stem cell proliferation in planarians. *Dev Cell*, *23*(4), 691-704. https://doi.org/10.1016/j.devcel.2012.09.008

Forsthoefel, D. J., Park, A. E., & Newmark, P. A. (2011). Stem cell-based growth, regeneration, and remodeling of the planarian intestine. *Developmental Biology*, *356*(2), 445-459. https://doi.org/10.1016/j.ydbio.2011.05.669

Galluzzi, L., Vitale, I., Aaronson, S. A., Abrams, J. M., Adam, D., Agostinis, P., Alnemri, E. S., Altucci, L., Amelio, I., Andrews, D. W., Annicchiarico-Petruzzelli, M., Antonov, A. V., Arama, E., Baehrecke, E. H., Barlev, N. A., Bazan, N. G., Bernassola, F., Bertrand, M. J. M., Bianchi, K., . . . Kroemer, G. (2018). Molecular mechanisms of cell death: recommendations of the Nomenclature Committee on Cell Death 2018. *Cell Death and Differentiation*, *25*(3), 486-541. https://doi.org/10.1038/s41418-017-0012-4

Garciacorrales, P., & Gamo, J. (1988). The Ultrastructure of the Gastrodermal Gland-Cells in the Fresh-Water Planarian Dugesia-Gonocephala s.l. during food digestion (Plathelmonthes). *Acta Zoologica*, *67*(1), 43-51. https://doi.org/10.1111/j.1463-6395.1986.tb00848.x

Gavino, M. A., & Reddien, P. W. (2011). A Bmp/Admp regulatory circuit controls maintenance and regeneration of dorsal-ventral polarity in planarians. *Curr Biol*, *21*(4), 294-299. https://doi.org/10.1016/j.cub.2011.01.017

Gavrieli, Y., Sherman, Y., & Ben-Sasson, S. A. (1992). Identification of programmed cell death in situ via specific labeling of nuclear DNA fragmentation. *J Cell Biol*, *119*(3), 493-501. https://doi.org/10.1083/jcb.119.3.493

Goel, T., Wang, R., Martin, S., Lanphear, E., & Collins, E. M. S. (2019). Linalool acts as a fast and reversible anesthetic in. *PLoS One*, *14*(10). https://doi.org/10.1371/journal.pone.0224221

Gonzalez-Estevez, C., Felix, D. A., Rodriguez-Esteban, G., & Aboobaker, A. A. (2012). Decreased neoblast progeny and increased cell death during starvation-induced planarian degrowth. *International Journal of Developmental Biology*, *56*(1-3), 83-91. https://doi.org/10.1387/ijdb.113452cg

Goodell, M. A., & Rando, T. A. (2015). Stem cells and healthy aging. *Science*, *350*(6265), 1199-

1204. https://doi.org/10.1126/science.aab3388

Gracia, M., Theis, S., Proag, A., Gay, G., Benassayag, C., & Suzanne, M. (2019). Mechanical impact of epithelial-mesenchymal transition on epithelial morphogenesis in Drosophila. *Nature Communications*, *10*(1), 2951. https://doi.org/10.1038/s41467-019-10720-0

Green, D. R., & Llambi, F. (2015). Cell Death Signaling. *Cold Spring Harbor Perspectives in Biology*, *7*(12). https://doi.org/10.1101/cshperspect.a006080

Gu, Y. P., Forostyan, T., Sabbadini, R., & Rosenblatt, J. (2011). Epithelial cell extrusion requires the sphingosine-1-phosphate receptor 2 pathway. *Journal of Cell Biology*, *193*(4), 667-676. https://doi.org/10.1083/jcb.201010075

Gudipaty, S. A., & Rosenblatt, J. (2017). Epithelial cell extrusion: Pathways and pathologies. *Semin Cell Dev Biol*, *67*, 132-140. https://doi.org/10.1016/j.semcdb.2016.05.010

Gumbrys, A. (2017). *Epidermis and Re-epithelialization in Schmidtea mediterranea* PhD thesis The Open University.

Gurley, K. A., Rink, J. C., & Alvarado, A. S. (2008). β-catenin defines head versus tail identity during planarian regeneration and Homeostasis. *Science*, *319*(5861), 323-327. https://doi.org/10.1126/science.1150029

Halcrow, P. W., Geiger, J. D., & Chen, X. (2021). Overcoming Chemoresistance: Altering pH of Cellular Compartments by Chloroquine and Hydroxychloroquine. *Front Cell Dev Biol*, *9*, 627639. https://doi.org/10.3389/fcell.2021.627639

Hall, P. A., Coates, P. J., Ansari, B., & Hopwood, D. (1994). Regulation of cell number in the mammalian gastrointestinal tract: the importance of apoptosis. *Journal of Cell Science*, *107 (Pt 12)*, 3569-3577. https://doi.org/10.1242/jcs.107.12.3569

Hanahan, D., & Weinberg, R. A. (2011). Hallmarks of Cancer: The Next Generation. *Cell*, *144*(5), 646-674. https://doi.org/10.1016/j.cell.2011.02.013

Hanayama, R., Tanaka, M., Miyasaka, K., Aozasa, K., Koike, M., Uchiyama, Y., & Nagata, S. (2004). Autoimmune disease and impaired uptake of apoptotic cells in MFG-E8-deficient mice. *Science*, *304*(5674), 1147-1150. https://doi.org/10.1126/science.1094359

Hartenstein, V., Younossi-Hartenstein, A., & Lekven, A. (1994). Delamination and division in the Drosophila neurectoderm: spatiotemporal pattern, cytoskeletal dynamics, and common control by neurogenic and segment polarity genes. *Developmental Biology*, *165*(2), 480-499. https://doi.org/10.1006/dbio.1994.1269

He, X., Lindsay-Mosher, N., Li, Y., Molinaro, A. M., Pellettieri, J., & Pearson, B. J. (2017). FOX and ETS family transcription factors regulate the pigment cell lineage in planarians. *Development*, *144*(24), 4540-4551. https://doi.org/10.1242/dev.156349

Heath, J. P. (1996). Epithelial cell migration in the intestine. *Cell Biol Int*, *20*(2), 139-146. https://doi.org/10.1006/cbir.1996.0018

Hochreiter-Hufford, A., & Ravichandran, K. S. (2013). Clearing the Dead: Apoptotic Cell Sensing, Recognition, Engulfment, and Digestion. *Cold Spring Harbor Perspectives in Biology*, *5*(1). https://doi.org/10.1101/cshperspect.a008748

Hoijman, E., Hakkinen, H. M., Tolosa-Ramon, Q., Jimenez-Delgado, S., Wyatt, C., Miret-Cuesta, M., Irimia, M., Callan-Jones, A., Wieser, S., & Ruprecht, V. (2021). Cooperative epithelial phagocytosis enables error correction in the early embryo. *Nature*, *590*(7847). https://doi.org/10.1038/s41586-021-03200-3

Homewood, C. A., Warhurst, D. C., Peters, W., & Baggaley, V. C. (1972). Lysosomes, pH and the anti-malarial action of chloroquine. *Nature*, *235*(5332), 50-52. https://doi.org/10.1038/235050a0

Hori, I. (1979). Structure and regeneration of the planarian basal lamina: an ultrastructural study. *Tissue Cell*, *11*(4), 611-621. https://doi.org/10.1016/0040-8166(79)90018-1

Horvitz, H. R. (1999). Genetic control of programmed cell death in the nematode Caenorhabditis elegans. *Cancer Res*, *59*(7 Suppl), 1701s-1706s. https://www.ncbi.nlm.nih.gov/pubmed/10197583

Icha, J., Weber, M., Waters, J. C., & Norden, C. (2017). Phototoxicity in live fluorescence microscopy, and how to avoid it. *Bioessays*, *39*(8). https://doi.org/10.1002/bies.201700003

Ishii, S. (1965). Electron microscopic observations on the Planarian tissues II. The intestine. *Fukushima J Med Sci*, *12*(1), 67-87. https://www.ncbi.nlm.nih.gov/pubmed/5863488

Ishii, S., & Sakurai, T. (1991). Food Ingestion by Planarian Intestinal Phagocytic-Cells - a Study by Scanning Electron-Microscopy. *Hydrobiologia*, *227*, 179-185. https://doi.org/10.1007/Bf00027600

Ivankovic, M., Haneckova, R., Thommen, A., Grohme, M. A., Vila-Farre, M., Werner, S., & Rink, J. C. (2019). Model systems for regeneration: planarians. *Development*, *146*(17). https://doi.org/10.1242/dev.167684

Jasper, H. (2020). Intestinal Stem Cell Aging: Origins and Interventions. *Annu Rev Physiol*, *82*, 203-226. https://doi.org/10.1146/annurev-physiol-021119-034359

Jung, S., Jeong, H., & Yu, S. W. (2020). Autophagy as a decisive process for cell death. *Experimental and Molecular Medicine*, *52*(6), 921-930. https://doi.org/10.1038/s12276-020-0455-4

Junttila, M. R., & Evan, G. I. (2009). p53-a Jack of all trades but master of none. *Nature Reviews Cancer*, *9*(11), 821-829. https://doi.org/10.1038/nrc2728

Kerr, J. F., Wyllie, A. H., & Currie, A. R. (1972). Apoptosis: a basic biological phenomenon with wide-ranging implications in tissue kinetics. *Br J Cancer*, *26*(4), 239-257. https://doi.org/10.1038/bjc.1972.33

Kiehart, D. P., Galbraith, C. G., Edwards, K. A., Rickoll, W. L., & Montague, R. A. (2000). Multiple forces contribute to cell sheet morphogenesis for dorsal closure in

Drosophila. *J Cell Biol*, *149*(2), 471-490. https://doi.org/10.1083/jcb.149.2.471

Kinchen, J. M., & Ravichandran, K. S. (2008). Phagosome maturation: going through the acid test. *Nature Reviews Molecular Cell Biology*, *9*(10), 781-795. https://doi.org/10.1038/nrm2515

King, R. S., & Newmark, P. A. (2013). In situ hybridization protocol for enhanced detection of gene expression in the planarian Schmidtea mediterranea. *Bmc Developmental Biology*, *13*. https://doi.org/10.1186/1471-213x-13-8

King, S. M. (2016). Axonemal Dynein Arms. *Cold Spring Harb Perspect Biol*, *8*(11). https://doi.org/10.1101/cshperspect.a028100

Kischkel, F. C., Hellbardt, S., Behrmann, I., Germer, M., Pawlita, M., Krammer, P. H., & Peter, M. E. (1995). Cytotoxicity-Dependent Apo-1 (Fas/Cd95)-Associated Proteins Form a Death-Inducing Signaling Complex (Disc) with the Receptor. *Embo Journal*, *14*(22), 5579-5588. https://doi.org/10.1002/j.1460-2075.1995.tb00245.x

Kissa, K., & Herbomel, P. (2010). Blood stem cells emerge from aortic endothelium by a novel type of cell transition. *Nature*, *464*(7285), 112-115. https://doi.org/10.1038/nature08761

Labi, V., & Erlacher, M. (2015). How cell death shapes cancer. *Cell Death & Disease*, *6*. https://doi.org/10.1038/cddis.2015.20

Leal-Cardoso, J. H., da Silva-Alves, K. S., Ferreira-da-Silva, F. W., dos Santos-Nascimento, T., Joca, H. C., de Macedo, F. H., de Albuquerque-Neto, P. M., Magalhaes, P. J., Lahlou, S., Cruz, J. S., & Barbosa, R. (2010). Linalool blocks excitability in peripheral nerves and voltage-dependent Na+ current in dissociated dorsal root ganglia neurons. *Eur J Pharmacol*, *645*(1-3), 86-93. https://doi.org/10.1016/j.ejphar.2010.07.014

Lechler, T., & Fuchs, E. (2005). Asymmetric cell divisions promote stratification and differentiation of mammalian skin. *Nature*, *437*(7056), 275-280. https://doi.org/10.1038/nature03922

Levayer, R., Dupont, C., & Moreno, E. (2016). Tissue Crowding Induces Caspase-Dependent Competition for Space. *Current Biology*, *26*(5), 670-677. https://doi.org/10.1016/j.cub.2015.12.072

Lindsay-Mosher, N., Lusk, S., & Pearson, B. J. (2024). Planarians require *ced-12/elmo-1* to clear dead cells by excretion through the gut. *Cell Reports*, *43*(1). https://doi.org/10.1016/j.celrep.2023.113621

Liu, B. B., Qu, J., Zhang, W. Q., Belmonte, J. C. I., & Liu, G. H. (2022). A stem cell aging framework, from mechanisms to interventions. *Cell Reports*, *41*(3). https://doi.org/10.1016/j.celrep.2022.111451

Locksley, R. M., Killeen, N., & Lenardo, M. J. (2001). The TNF and TNF receptor superfamilies: Integrating mammalian biology. *Cell*, *104*(4), 487-501. https://doi.org/10.1016/S0092-8674(01)00237-9

Lolo, F. N., Casas-Tintó, S., & Moreno, E. (2012). Cell Competition Time Line: Winners Kill Losers, which Are Extruded and Engulfed by Hemocytes. *Cell Reports*, *2*(3), 526-539. https://doi.org/10.1016/j.celrep.2012.08.012

Marinari, E., Mehonic, A., Curran, S., Gale, J., Duke, T., & Baum, B. (2012). Live-cell delamination counterbalances epithelial growth to limit tissue overcrowding. *Nature*, *484*(7395), 542-U177. https://doi.org/10.1038/nature10984

Marshall, T. W., Lloyd, I. E., Delalande, J. M., Nathke, I., & Rosenblatt, J. (2011). The tumor suppressor adenomatous polyposis coli controls the direction in which a cell extrudes from an epithelium. *Molecular Biology of the Cell*, *22*(21), 3962-3970. https://doi.org/10.1091/mbc.E11-05-0469

Marshman, E., Booth, C., & Potten, C. S. (2002). The intestinal epithelial stem cell. *Bioessays*, *24*(1), 91-98. https://doi.org/10.1002/bies.10028

Mauthe, M., Orhon, I., Rocchi, C., Zhou, X., Luhr, M., Hijlkema, K. J., Coppes, R. P., Engedal, N., Mari, M., & Reggiori, F. (2018). Chloroquine inhibits autophagic flux by decreasing autophagosome-lysosome fusion. *Autophagy*, *14*(8), 1435-1455. https://doi.org/10.1080/15548627.2018.1474314

McGee, C., Fairweather, I., & Blackshaw, R. P. (1997). Ultrastructural features of the epidermis of the planarian Artioposthia triangulata (Dendy). *Hydrobiologia*, *347*, 15-24. https://doi.org/Doi 10.1023/A:1002934504296

Molina, M. D., Salo, E., & Cebria, F. (2007). The BMP pathway is essential for re-specification and maintenance of the dorsoventral axis in regenerating and intact planarians. *Developmental Biology*, *311*(1), 79-94. https://doi.org/10.1016/j.ydbio.2007.08.019

Monier, B., Gettings, M., Gay, G., Mangeat, T., Schott, S., Guarner, A., & Suzanne, M. (2015). Apico-basal forces exerted by apoptotic cells drive epithelium folding. *Nature*, *518*(7538), 245-248. https://doi.org/10.1038/nature14152

Monks, J., Rosner, D., Geske, F. J., Lehman, L., Hanson, L., Neville, M. C., & Fadok, V. A. (2005). Epithelial cells as phagocytes: apoptotic epithelial cells are engulfed by mammary alveolar epithelial cells and repress inflammatory mediator release. *Cell Death and Differentiation*, *12*(2), 107-114. https://doi.org/10.1038/sj.cdd.4401517

Morgan, T. H. (1898). Experimental Studies of the Regeneration of Planaria maculata. *Roux's archives of developmental biology*, *7*, 364-397.

Nagata, S., Hanayama, R., & Kawane, K. (2010). Autoimmunity and the Clearance of Dead Cells. *Cell*, *140*(5), 619-630. https://doi.org/10.1016/j.cell.2010.02.014

Nakajima, Y., Kuranaga, E., Sugimura, K., Miyawaki, A., & Miura, M. (2011). Nonautonomous Apoptosis Is Triggered by Local Cell Cycle Progression during Epithelial Replacement in Drosophila. *Molecular and Cellular Biology*, *31*(12), 2499-2512. https://doi.org/10.1128/Mcb.01046-10

Newmark, P. A., & Alvarado, A. S. (2000). Bromodeoxyuridine specifically labels the

regenerative stem cells of planarians. *Developmental Biology*, *220*(2), 142-153. https://doi.org/10.1006/dbio.2000.9645

Nicholson, D. W., & Thornberry, N. A. (1997). Caspases: killer proteases. *Trends in Biochemical Sciences*, *22*(8), 299-306. https://doi.org/10.1016/S0968-0004(97)01085-2

Ninov, N., Chiarelli, D. A., & Martin-Blanco, E. (2007). Extrinsic and intrinsic mechanisms directing epithelial cell sheet replacement during Drosophila metamorphosis. *Development*, *134*(2), 367-379. https://doi.org/10.1242/dev.02728

Ohsawa, S., Vaughen, J., & Igaki, T. (2018). Cell Extrusion: A Stress-Responsive Force for Good or Evil in Epithelial Homeostasis. *Dev Cell*, *44*(4), 532. https://doi.org/10.1016/j.devcel.2018.02.007

Okamoto, K., Takeuchi, K., & Agata, K. (2005). Neural projections in planarian brain revealed by fluorescent dye tracing. *Zoolog Sci*, *22*(5), 535-546. https://doi.org/10.2108/zsj.22.535

Orii, H., Ito, H., & Watanabe, K. (2002). Anatomy of the planarian Dugesia japonica I. The muscular system revealed by antisera against myosin heavy chains. *Zoological Science*, *19*(10), 1123-1131. https://doi.org/10.2108/zsj.19.1123

Orii, H., Sakurai, T., & Watanabe, K. (2005). Distribution of the stem cells (neoblasts) in the planarian Dugesia japonica. *Development Genes and Evolution*, *215*(3), 143-157. https://doi.org/10.1007/s00427-004-0460-y

Orii, H., & Watanabe, K. (2007). Bone morphogenetic protein is required for dorso-ventral patterning in the planarian. *Development Growth & Differentiation*, *49*(4), 345-349. https://doi.org/10.1111/j.1440-169x.2007.00931.x

Park, D., Tosello-Trampont, A. C., Elliott, M. R., Lu, M. J., Haney, L. B., Ma, Z., Klibanov, A. L., Mandell, J. W., & Ravichandran, K. S. (2007). BAI1 is an engulfment receptor for apoptotic cells upstream of the ELMO/Dock180/Rac module. *Nature*, *450*(7168), 430-434. https://doi.org/10.1038/nature06329

Paskin, T. R., Jellies, J., Bacher, J., & Beane, W. S. (2014). Planarian Phototactic Assay Reveals Differential Behavioral Responses Based on Wavelength. *PLoS One*, *9*(12), e114708. https://doi.org/10.1371/journal.pone.0114708

Pastor-Pareja, J. C., Grawe, F., Martin-Blanco, E., & Garcia-Bellido, A. (2004). Invasive cell behavior during Drosophila imaginal disc eversion is mediated by the JNK signaling cascade. *Developmental Cell*, *7*(3), 387-399. https://doi.org/10.1016/j.devcel.2004.07.022

Pearson, B. J. (2022). Finding the potency in planarians. *Communications Biology*, *5*(1), 970. https://doi.org/10.1038/s42003-022-03905-9

Pearson, B. J., & Alvarado, A. S. (2010). A planarian p53 homolog regulates proliferation and self-renewal in adult stem cell lineages. *Development*, *137*(2), 213-221.

https://doi.org/10.1242/dev.044297

Pedersen, K. J. (1976). Scanning electron microscopical observations on epidermal wound healing in the PlanarianDugesia tigrina. *Wilehm Roux Arch Dev Biol*, *179*(4), 251-273. https://doi.org/10.1007/BF00848236

Pellettieri, J., & Alvarado, A. S. (2007). Cell turnover and adult tissue homeostasis: From humans to planarians. *Annual Review of Genetics*, *41*, 83-105. https://doi.org/10.1146/annurev.genet.41.110306.130244

Pellettieri, J., Fitzgerald, P., Watanabe, S., Mancuso, J., Green, D. R., & Sanchez Alvarado, A. (2010). Cell death and tissue remodeling in planarian regeneration. *Developmental Biology*, *338*(1), 76-85. https://doi.org/10.1016/j.ydbio.2009.09.015

Peña-Blanco, A., & García-Sáez, A. J. (2018). Bax, Bak and beyond - mitochondrial performance in apoptosis. *Febs Journal*, *285*(3), 416-431. https://doi.org/10.1111/febs.14186

Peralta, X. G., Toyama, Y., Hutson, M. S., Montague, R., Venakides, S., Kiehart, D. P., & Edwards, G. S. (2007). Upregulation of forces and morphogenic asymmetries in dorsal closure during Drosophila development. *Biophys J*, *92*(7), 2583-2596. https://doi.org/10.1529/biophysj.106.094110

Petersen, C. P., & Reddien, P. W. (2009). A wound-induced Wnt expression program controls planarian regeneration polarity. *Proc Natl Acad Sci U S A*, *106*(40), 17061-17066. https://doi.org/10.1073/pnas.0906823106

Potten, C. S. (1992). The Significance of Spontaneous and Induced Apoptosis in the Gastrointestinal-Tract of Mice. *Cancer and Metastasis Reviews*, *11*(2), 179-195. https://doi.org/10.1007/Bf00048063

Potten, C. S. (1997). Epithelial cell growth and differentiation .2. Intestinal apoptosis. *American Journal of Physiology-Gastrointestinal and Liver Physiology*, *273*(2), G253-G257. https://doi.org/10.1152/ajpgi.1997.273.2.G253

Raz, A. A., Wurtzel, O., & Reddien, P. W. (2021). Planarian stem cells specify fate yet retain potency during the cell cycle. *Cell Stem Cell*, *28*(7), 1307-1322 e1305. https://doi.org/10.1016/j.stem.2021.03.021

Reddien, P. W., & Alvarado, A. S. (2004). Fundamentals of planarian regeneration. *Annual Review of Cell and Developmental Biology*, *20*, 725-757. https://doi.org/10.1146/annurev.cellbio.20.010403.095114

Reddien, P. W., Bermange, A. L., Murfitt, K. J., Jennings, J. R., & Sanchez Alvarado, A. (2005). Identification of genes needed for regeneration, stem cell function, and tissue homeostasis by systematic gene perturbation in planaria. *Dev Cell*, *8*(5), 635-649. https://doi.org/10.1016/j.devcel.2005.02.014

Reddien, P. W., Oviedo, N. J., Jennings, J. R., Jenkin, J. C., & Alvarado, A. S. (2005). SMEDWI-2 is a PIWI-like protein that regulates planarian stem cells. *Science*, *310*(5752), 1327-

1330. https://doi.org/10.1126/science.1116110

Redza-Dutordoir, M., & Averill-Bates, D. A. (2016). Activation of apoptosis signalling pathways by reactive oxygen species. *Biochim Biophys Acta*, *1863*(12), 2977-2992. https://doi.org/10.1016/j.bbamcr.2016.09.012

Reiter, S., Crescenzi, M., Galliot, B., & Buzgariu, W. (2012). Hydra, a versatile model to study the homeostatic and developmental functions of cell death. *International Journal of Developmental Biology*, *56*(6-8), 593-604. https://doi.org/10.1387/ijdb.123499sr

Reuter, H., Marz, M., Vogg, M. C., Eccles, D., Grifol-Boldu, L., Wehner, D., Owlarn, S., Adell, T., Weidinger, G., & Bartscherer, K. (2015). Beta-catenin-dependent control of positional information along the AP body axis in planarians involves a teashirt family member. *Cell Rep*, *10*(2), 253-265. https://doi.org/10.1016/j.celrep.2014.12.018

Rink, J. C. (2013). Stem cell systems and regeneration in planaria. *Development Genes and Evolution*, *223*(1-2), 67-84. https://doi.org/10.1007/s00427-012-0426-4

Rink, J. C., Gurley, K. A., Elliott, S. A., & Sanchez Alvarado, A. (2009). Planarian Hh signaling regulates regeneration polarity and links Hh pathway evolution to cilia. *Science*, *326*(5958), 1406-1410. https://doi.org/10.1126/science.1178712

Rink, J. C., Vu, H. T., & Sanchez Alvarado, A. (2011). The maintenance and regeneration of the planarian excretory system are regulated by EGFR signaling. *Development*, *138*(17), 3769-3780. https://doi.org/10.1242/dev.066852

Rompolas, P., Azimzadeh, J., Marshall, W. F., & King, S. M. (2013). Analysis of ciliary assembly and function in planaria. *Methods Enzymol*, *525*, 245-264. https://doi.org/10.1016/B978-0-12-397944-5.00012-2

Rompolas, P., Patel-King, R. S., & King, S. M. (2010). An Outer Arm Dynein Conformational Switch Is Required for Metachronal Synchrony of Motile Cilia in Planaria. *Molecular Biology of the Cell*, *21*(21), 3669-3679. https://doi.org/10.1091/mbc.E10-04-0373

Rosenblatt, J., Raff, M. C., & Cramer, L. P. (2001). An epithelial cell destined for apoptosis signals its neighbors to extrude it by an actin- and myosin-dependent mechanism. *Curr Biol*, *11*(23), 1847-1857. https://doi.org/10.1016/s0960-9822(01)00587-5

Rumore, P. M., & Steinman, C. R. (1990). Endogenous circulating DNA in systemic lupus erythematosus. Occurrence as multimeric complexes bound to histone. *J Clin Invest*, *86*(1), 69-74. https://doi.org/10.1172/JCI114716

Saelens, X., Festjens, N., Vande Walle, L., van Gurp, M., van Loo, G., & Vandenabeele, P. (2004). Toxic proteins released from mitochondria in cell death. *Oncogene*, *23*(16), 2861-2874. https://doi.org/10.1038/sj.onc.1207523

Saló, E. (2006). The power of regeneration and the stem-cell kingdom:: freshwater planarians (platyhelminthes). *Bioessays*, *28*(5), 546-559. https://doi.org/10.1002/bies.20416

Schindelin, J., Arganda-Carreras, I., Frise, E., Kaynig, V., Longair, M., Pietzsch, T., Preibisch, S., Rueden, C., Saalfeld, S., Schmid, B., Tinevez, J. Y., White, D. J., Hartenstein, V., Eliceiri,

K., Tomancak, P., & Cardona, A. (2012). Fiji: an open-source platform for biological-image analysis. *Nature Methods*, *9*(7), 676-682. https://doi.org/10.1038/Nmeth.2019

Schlesinger, P. H., Krogstad, D. J., & Herwaldt, B. L. (1988). Antimalarial Agents - Mechanisms of Action. *Antimicrobial Agents and Chemotherapy*, *32*(6), 793-798. https://doi.org/10.1128/Aac.32.6.793

Schmidt, U., Weigert, M., Broaddus, C., & Myers, G. (2018). Cell Detection with Star-Convex Polygons. *Medical Image Computing and Computer Assisted Intervention - Miccai 2018, Pt Ii*, *11071*, 265-273. https://doi.org/10.1007/978-3-030-00934-2_30

Scimone, M. L., Meisel, J., & Reddien, P. W. (2010). The Mi-2-like Smed-CHD4 gene is required for stem cell differentiation in the planarian Schmidtea mediterranea. *Development*, *137*(8), 1231-1241. https://doi.org/10.1242/dev.042051

Scimone, M. L., Wurtzel, O., Malecek, K., Fincher, C. T., Oderberg, I. M., Kravarik, K. M., & Reddien, P. W. (2018). foxF-1 Controls Specification of Non-body Wall Muscle and Phagocytic Cells in Planarians. *Curr Biol*, *28*(23), 3787-3801 e3786. https://doi.org/10.1016/j.cub.2018.10.030

Sender, R., & Milo, R. (2021). The distribution of cellular turnover in the human body. *Nat Med*, *27*(1), 45-48. https://doi.org/10.1038/s41591-020-01182-9

Shettigar, N., Joshi, A., Dalmeida, R., Gopalkrishna, R., Chakravarthy, A., Patnaik, S., Mathew, M., Palakodeti, D., & Gulyani, A. (2017). Hierarchies in light sensing and dynamic interactions between ocular and extraocular sensory networks in a flatworm. *Science Advances*, *3*(7). https://doi.org/10.1126/sciadv.1603025

Slattum, G., Gu, Y. P., Sabbadini, R., & Rosenblatt, J. (2014). Autophagy in Oncogenic K-Ras Promotes Basal Extrusion of Epithelial Cells by Degrading S1P. *Current Biology*, *24*(1), 19-28. https://doi.org/10.1016/j.cub.2013.11.029

Slattum, G., McGee, K. M., & Rosenblatt, J. (2009). P115 RhoGEF and microtubules decide the direction apoptotic cells extrude from an epithelium. *J Cell Biol*, *186*(5), 693-702. https://doi.org/10.1083/jcb.200903079

Slattum, G. M., & Rosenblatt, J. (2014). Tumour cell invasion: an emerging role for basal epithelial cell extrusion. *Nat Rev Cancer*, *14*(7), 495-501. https://doi.org/10.1038/nrc3767

Slee, E. A., Adrain, C., & Martin, S. J. (2001). Executioner caspase-3, -6, and -7 perform distinct, non-redundant roles during the demolition phase of apoptosis. *J Biol Chem*, *276*(10), 7320-7326. https://doi.org/10.1074/jbc.M008363200

Stubenhaus, B. M., Dustin, J. P., Neverett, E. R., Beaudry, M. S., Nadeau, L. E., Burk-McCoy, E., He, X., Pearson, B. J., & Pellettieri, J. (2016). Light-induced depigmentation in planarians models the pathophysiology of acute porphyrias. *Elife*, *5*. https://doi.org/10.7554/eLife.14175

Sun, Y. J., Huang, Y. D., Hao, Z. T., Zhang, S. T., & Tian, Q. N. (2023). *MRLC* controls apoptotic

cell death and functions to regulate epidermal development during planarian regeneration and homeostasis. *Cell Proliferation*. https://doi.org/10.1111/cpr.13524

Teng, X., Qin, L., Le Borgne, R., & Toyama, Y. (2017). Remodeling of adhesion and modulation of mechanical tensile forces during apoptosis in Drosophila epithelium. *Development*, *144*(1), 95-105. https://doi.org/10.1242/dev.139865

Thommen, A., Werner, S., Frank, O., Philipp, J., Knittelfelder, O., Quek, Y., Fahmy, K., Shevchenko, A., Friedrich, B. M., Julicher, F., & Rink, J. C. (2019). Body size-dependent energy storage causes Kleiber's law scaling of the metabolic rate in planarians. *Elife*, *8*. https://doi.org/10.7554/eLife.38187

Toyama, Y., Peralta, X. G., Wells, A. R., Kiehart, D. P., & Edwards, G. S. (2008). Apoptotic force and tissue dynamics during Drosophila embryogenesis. *Science*, *321*(5896), 1683-1686. https://doi.org/10.1126/science.1157052

Tu, K. C., Cheng, L. C., Vu, H. T. K., Lange, J. J., McKinney, S. A., Seidel, C. W., & Alvarado, A. S. (2015). Egr-5 is a post-mitotic regulator of planarian epidermal differentiation. *Elife*, *4*. https://doi.org/10.7554/eLife.10501

van Wolfswinkel, J. C., Wagner, D. E., & Reddien, P. W. (2014). Single-cell analysis reveals functionally distinct classes within the planarian stem cell compartment. *Cell Stem Cell*, *15*(3), 326-339. https://doi.org/10.1016/j.stem.2014.06.007

Varley, A., Horkan, H. R., McMahon, E. T., Krasovec, G., & Frank, U. (2023). Pluripotent, germ cell competent adult stem cells underlie cnidarian regenerative ability and clonal growth. *Curr Biol*, *33*(10), 1883-1892 e1883. https://doi.org/10.1016/j.cub.2023.03.039

Vu, H. T. K., Mansour, S., Kucken, M., Blasse, C., Basquin, C., Azimzadeh, J., Myers, E. W., Brusch, L., & Rink, J. C. (2019). Dynamic Polarization of the Multiciliated Planarian Epidermis between Body Plan Landmarks. *Developmental Cell*, *51*(4), 526-542.e526. https://doi.org/10.1016/j.devcel.2019.10.022

Vu, H. T. K., Rink, J. C., McKinney, S. A., McClain, M., Lakshmanaperumal, N., Alexander, R., & Alvarado, A. S. (2015). Stem cells and fluid flow drive cyst formation in an invertebrate excretory organ. *Elife*, *4*. https://doi.org/10.7554/eLife.07405

Wagner, D. E., Wang, I. E., & Reddien, P. W. (2011). Clonogenic Neoblasts Are Pluripotent Adult Stem Cells That Underlie Planarian Regeneration. *Science*, *332*(6031), 811-816. https://doi.org/10.1126/science.1203983

Watt, F. M. (1998). Epidermal stem cells: markers, patterning and the control of stem cell fate. *Philos Trans R Soc Lond B Biol Sci*, *353*(1370), 831-837. https://doi.org/10.1098/rstb.1998.0247

Weigert, M., Schmidt, U., Boothe, T., Muller, A., Dibrov, A., Jain, A., Wilhelm, B., Schmidt, D., Broaddus, C., Culley, S., Rocha-Martins, M., Segovia-Miranda, F., Norden, C., Henriques, R., Zerial, M., Solimena, M., Rink, J., Tomancak, P., Royer, L., . . . Myers, E.

W. (2018). Content-aware image restoration: pushing the limits of fluorescence microscopy. *Nature Methods*, *15*(12), 1090-1097. https://doi.org/10.1038/s41592-018-0216-7

Wenemoser, D., & Reddien, P. W. (2010). Planarian regeneration involves distinct stem cell responses to wounds and tissue absence. *Developmental Biology*, *344*(2), 979-991. https://doi.org/10.1016/j.ydbio.2010.06.017

Willier, B. H., Hyman, L. H., & Rifenburgh, S. A. (1925). A histochemical study of intracellular digestion in triclad flatworms. *Journal of Morphology and Physiology*, *40*(2), 299-340. https://doi.org/10.1002/jmor.1050400205

Wolff, E., & Dubois, F. (1947). Sur Les Facteurs Qui Declenchent La Migration Des Cellules De Regeneration Chez Les Planaires. *Comptes Rendus Des Seances De La Societe De Biologie Et De Ses Filiales*, *141*(9), 906-909.

Wurtzel, O., Oderberg, I. M., & Reddien, P. W. (2017). Planarian Epidermal Stem Cells Respond to Positional Cues to Promote Cell-Type Diversity. *Developmental Cell*, *40*(5), 491-504. https://doi.org/10.1016/j.devcel.2017.02.008

Zeng, A., Li, H., Guo, L. H., Gao, X., McKinney, S., Wang, Y. F., Yu, Z. L., Park, J., Semerad, C., Ross, E., Cheng, L. C., Davies, E., Lei, K., Wang, W., Perera, A., Hall, K., Peak, A., Box, A., & Alvarado, A. S. (2018). Prospectively Isolated Tetraspanin Neoblasts Are Adult Pluripotent Stem Cells Underlying Planaria Regeneration. *Cell*, *173*(7), 1593-1608. https://doi.org/10.1016/j.cell.2018.05.006

Zheng, H. X., Liu, H. B., Xu, Q., Wang, W. J., Li, L. F., Ye, G., Wen, X. M., Chen, F. L., & Yu, Y. (2021). PI3K Plays an Essential Role in Planarian Regeneration and Tissue Maintenance. *Frontiers in Cell and Developmental Biology*, *9*. https://doi.org/10.3389/fcell.2021.649656

Zhu, S. J., Hallows, S. E., Currie, K. W., Xu, C. J., & Pearson, B. J. (2015). A mex3 homolog is required for differentiation during planarian stem cell lineage development. *Elife*, *4*. https://doi.org/10.7554/eLife.07025

Zhu, S. J., & Pearson, B. J. (2018). Smed-myb-1 Specifies Early Temporal Identity during Planarian Epidermal Differentiation. *Cell Reports*, *25*(1), 38-46. https://doi.org/10.1016/j.celrep.2018.09.011

Zhu, Y. L., Crowley, S. C., Latimer, A. J., Lewis, G. M., Nash, R., & Kucenas, S. (2019). Migratory Neural Crest Cells Phagocytose Dead Cells in the Developing Nervous System. *Cell*, *179*(1), 74-89. https://doi.org/10.1016/j.cell.2019.08.001

Zulueta-Coarasa, T., & Rosenblatt, J. (2022). The role of tissue maturity and mechanical state in controlling cell extrusion. *Curr Opin Genet Dev*, *72*, 1-7. https://doi.org/10.1016/j.gde.2021.09.003